This publication should be cited as follows:

Plass, Simon: Cellular MC-CDMA Downlink Systems – Coordination, Cancellation, and Use of Inter-Cell Interference. Fortschr.-Ber.VDI Reihe 10 Nr. 788. Dusseldorf: VDI-Verlag 2008. ISBN 978-3-18-378810-1, ISSN 0178-9627

Contents

Chapter 1

Introduction

The use of wireless equipment and standards for mobile communications has steadily increased worldwide. The anticipated migration from the current era of mobile communications towards the era of mobile computing require highly flexible data rates. Simultaneously, future users expect mobile services at any time and anywhere with full reliability for future cellular systems. Therefore, high data rates combined with entire coverage have to be guaranteed.

High data rates can be achieved by a simple extension of the bandwidth. Unfortunately, it is very difficult to find continuous large segments of spectrum. Instead, the spectral efficiency of future transmission techniques have to increase significantly compared to the systems in use today. The goal of a next generation system can be highlighted by the need of high spectral efficiency in combination with high packet data flexibility to guarantee throughput rates of more than $100\ \mathrm{MBit/s}$ outdoor and even $1\ \mathrm{GBit/s}$ for indoor applications [THS06].

Recent studies showed that generalized multi-carrier (GMC) transmission schemes provide flexible adaptive packet data traffic [WG00]. The orthogonal frequency division multiplexing (OFDM) [WE71] as the base technology for the GMC approach uses efficiently the available spectrum and is very robust in typical mobile radio multi-path environments. OFDM can be realized in less complex receivers and offers simple digital realization because the orthogonal basis functions can be readily obtained from the fast Fourier transformation (FFT). Additionally, spread spectrum, namely code division multiple access (CDMA), offers high flexibility, robustness, and frequency diversity gains. These benefits are combined in the multi-carrier code division multiple access (MC-CDMA) transmission scheme [FK03].

The MC-CDMA principle was simultaneously introduced by Fazel *et al.* [FP93] and Yee *et al.* [YLF93] in 1993. During the following decade a new research field emerged and was in the focus of several research projects, e.g., IST-4MORE [ISTa], IST-WINNER [ISTb, ISTc]. MC-CDMA is also a candidate for next generation transmission scenarios. The feasibility of using an MC-CDMA based next generation system was shown by field tests of Japanese NTT DoCoMo where already rates of 5 GBit/s were achieved [NTT07].

A further consequential step towards an efficient usage of the available spectrum is the reuse of the whole spectrum in each served cell which corresponds to a frequency reuse factor of one. By applying the same frequency band in neighboring cells, the cell border areas are prone to inter-cell interference. This causes severe performance degradation or even connection loss. The basic principle is illustrated in Figure 1.1 where a desired mobile station is influenced by neighboring base stations.

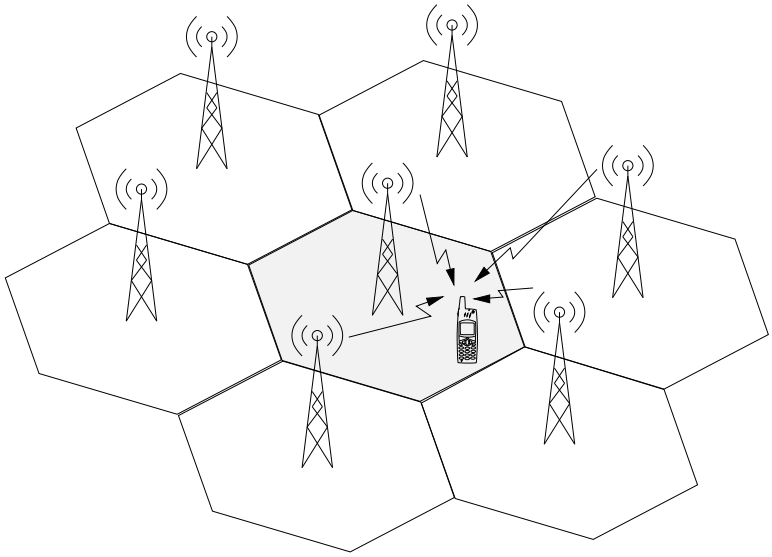

Figure 1.1: Cellular environment

Current mobile communications systems approach the problem of potential inter-cell interference in different ways, which is often a compromise between inter-cell interference occurrence and efficient usage of the available spectrum. In the global system for mobile communications (GSM) [ETS] the reuse of the same frequency band within adjacent cells is avoided, which results in an inefficient allocation of available frequency resources. In the universal mobile telecommunications system (UMTS) a frequency reuse factor of one is employed. Due to the specification of wideband CDMA, the so-called processing gain provides the robustness against interference [UMT98]. However, at the same time the near-far problems exists, i.e., one user's signal blocking other users' communications. This has to be avoided by tight and fast power controlling [HT04].

The challenge for future GMC technologies is to develop and to assess concepts both at the base station and at the mobile station to handle inter-cell interference. Only this will provide a reliable and acceptable system performance throughout the whole cell/sector site. With respect to inter-cell interference, four main objectives exist:

- determining the influence and characteristics of the existing inter-cell interference;
- developing interference coordination strategies to support universal coverage;
- investigating and assessing methods to cancel inter-cell interference at the mobile station in order to increase data rates of the desired user;
- using and benefiting from the inter-cell interference setup by developing cellular diversity schemes to offer high and reliable quality-of-service at cell borders.

Since 1993 the focus in the field of MC-CDMA was based on a single-cell layout. Therefore, the MC-CDMA system was investigated intensively how its behavior is influenced by a mobile radio channel environment and the occurring intra-cell interference on the link layer, e.g., multiple access interference (MAI). However, it is necessary to extend the investigations to more realistic scenarios, i.e., cellular structures. Already in 1998 a first attempt of studying a cellular environment has been made [NSR+98] which represents an overloaded single-cell downlink not a cellular system unfortunately. First results regarding the influence and properties of downlink inter-cell interference in

MC-CDMA were given in [ASDK04, BHWD05, DL05, BNG06]. These investigations on the link level are based on a single interfering cell. Further investigations of a single-cell-interference environment were based on basic cancellation principles [DL07, CHL07].

This thesis develops and assesses concepts both at the base station and at the mobile station for the coordination, cancellation, and use of inter-cell interference. The knowledge of inter-cell interference characteristics on the link level, also called physical layer, is necessary to investigate and assess new methods for mitigation schemes of inter-cell interference. The goal is to investigate the four main objective of inter-cell interference for an MC-CDMA downlink system on the link level in a multi-cell environment.

Cellular MC-CDMA downlink systems have been intensively studied by the author [1-21]. The findings and recommendations of these publications are compiled in the following five chapters. A summary of the main investigations is highlighted below:

- The cellular setup with its propagation environment including the used channel models is introduced in Chapter 2. Furthermore, the basic assumptions are given for the transmitter and receiver based on the multi-carrier transmission.

- Chapter 3 investigates the influences on the desired signal of the multi-cell environment. At this stage, a sectorized system is also studied. The nature of the cellular MC-CDMA signal is determined and a model for the overall signal is derived.

- The coordination of available orthogonal resources within a cellular system are in the focus of Chapter 4. First, the orthogonal frequency resources are coordinated to avoid or mitigate inter-cell interference. This study is extended to an OFDM access scheme which provides a challenging comparative transmission technique for MC-CDMA. A second orthogonal resource is given by the used spreading codes in MC-CDMA. Thus, a coordination scheme of spreading codes for a cellular system is investigated.

- Inter-cell interference cancellation at the mobile station avoids large management schemes at the network side. Due to the spreading codes in MC-CDMA, the built-in redundancy can be used for detecting the different signals at the mobile station. Chapter 5 introduces different concepts of inter-cell interference cancellation for a cellular MC-CDMA system. These concepts show large performance gains over the whole cell border area. Since one of the investigated cancellation concepts is based on an iterative process by exchanging extrinsic information, the extrinsic information is evaluated, also with the use of extrinsic information transfer (EXIT) charts.

- Methods are presented to take advantage of the constellation of neighboring base stations serving the same area, namely their cell borders by applying cellular diversity schemes within this broadcasted regions. In Chapter 6, cellular diversity techniques are introduced based on transmit diversity schemes, i.e., cyclic delay diversity and Alamouti coding. Investigations show that reliable performances are assured throughout the whole broadcasted areas, the severe cell border areas respectively.

Notation Remarks

Throughout this thesis, the time and sub-carrier indices are denoted by the subscripts l and i. Furthermore, the superscript m in parentheses describes the used base station. The signal description is given in time discrete signals. The frequency domain symbol is represented by capital letters, e.g., $X_{l,i}^{(m)}$ and the time domain symbol by lower case letters. The symbols $(\cdot)^*$, $(\cdot)^{\mathrm{T}}$, and $(\cdot)^{\mathrm{H}}$ denote the complex conjugation, transpose, and the Hermitian transpose operations.

Since the world of mobile communications is based on many abbreviations and symbols, a list of the used abbreviations and variables within this thesis can be found in Appendix D.

Chapter 2

Cellular MC-CDMA

In this chapter, the setup of a cellular downlink environment is introduced. Furthermore, the existing propagation behavior and a description of the mobile radio channel are given. Then, the basic principles of the orthogonal frequency division multiplexing (OFDM) modulation are briefly explained. The system design of the multi-carrier transmission is described for the transmitter and receiver.

2.1 Cellular Environment

Basic Assumptions

In a simplified approach, a cellular setup can be displayed as a hexagonal grid of cells. A desired cell surrounded by one tier of 6 neighboring or interfering cells with equal cell sizes is illustrated in Figure 2.1. Throughout this thesis, the cellular system is assumed to be centralized, i.e., the cells are coordinated by a central unit. Furthermore, the cellular downlink system is considered to be synchronized in time and frequency for simplicity. Since a simultaneously transmission of the signals in the downlink for all cells is assumed, the system characteristics are independent of the used duplex mode, i.e., frequency division duplex or time division duplex. Unless otherwise noted, all cells use the same system parameter settings as the desired cell. In all cellular system designs a cell identification scheme is provided to guarantee the cell specific signaling information of the desired signal at the mobile station (MS) in the whole cell area, i.e., also at the severe cell edge [KKH05]. Therefore, all N_{BS} cell specific information from the base stations (BSs) are assumed to be perfectly available at the MS. This also includes the perfect knowledge of the channel state information and signal strength at the receiver. On the other hand, there is no feedback or *a priori* information of the channel at the transmitter assumed, unless otherwise noted. Finally, the cells belongs to the same operator in our investigations.

In the following, an appropriate geographical reference system for defining the location of the MS is introduced. As depicted in Figure 2.1 the MS moves towards the border along a straight line from $\mathrm{BS}^{(0)}$ to an arbitrary point of the current cell. This line forms an angle α with the line connecting $\mathrm{BS}^{(0)}$ and $\mathrm{BS}^{(\mathrm{I},1)}$. The distance between the desired BS and MS is denoted as d_0, and the cell radius r is normalized to 1. For example, the mobile device may be situated along a line from the desired BS to the intersection of the desired cell and two interfering cells ($\mathrm{BS}^{(\mathrm{I},1)}$ and $\mathrm{BS}^{(\mathrm{I},2)}$). In this case, the angle α is 30°.

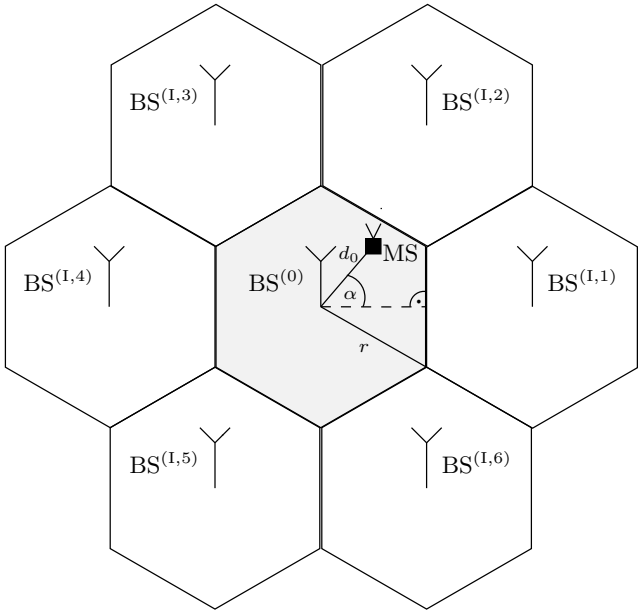

Figure 2.1: Cellular environment

2.1.1 Propagation Environment

A propagation loss model is assumed to calculate the received signal power P_m from BS m [Stü02]. The slowly varying signal power attenuation due to path loss is generally modeled as the product of the ρth power of distance and a log-normal component representing shadowing losses. Shadow variations are caused by large terrain obstacles between the BS and MS such as buildings and hills [Par92]. Since fast multi-path fading is modeled by the channel transfer function and detection mitigates the more rapidly varying Rayleigh fading loss and other channel distortions, such as multiple access interference (MAI), the fast multi-path fading process is not included in the propagation model [TC03]. Hence, the signal power from the mth BS received by the MS is

$$P_m \;=\; P_{\mathrm{t},m} \cdot d_m^{-\rho} \cdot 10^{\eta_m/10\mathrm{dB}}\,, \tag{2.1}$$

where $P_{\mathrm{t},m}$ is the transmitted signal power from the mth BS, ρ is the path loss factor, and d_m is the distance between the MS and the mth BS. Furthermore, the shadowing factor η_m is a Gaussian distributed random variable with zero mean and standard deviation σ_η and is given in dB. Within this thesis $\sigma_\eta = 8\ \mathrm{dB}$. Thus, the attenuation factor for the signal from BS m can be given by

$$\alpha_{\mathrm{att}}^{(m)} = \;\; d_m^{-\rho} \cdot 10^{\eta_m/10\mathrm{dB}}\,. \tag{2.2}$$

In a multi-cell environment, comparison of path losses among two or more BSs is necessary. Since the path loss from one BS to the MS correlates with the path loss from another BS to the MS, the interaction of the combined path losses is included in the model [VVZ94]. The shadowing factor can be split into two components: first, a near-field component ζ which is common to all BSs; second, a component ζ_m with regard to the received signal at the MS which is independent of the individual BS. Since the single path losses are Gaussian, a joint Gaussian probability density is assumed for the path losses when receiving from two or more BSs.

The random component of the dB loss for the mth BS can be expressed as

$$\eta_m = a\zeta + b\zeta_m\,, \tag{2.3}$$

where $a^2 + b^2 = 1$, $E\{\eta_m\} = E\{\zeta\} = E\{\zeta_m\} = 0$, $\sigma_\eta^2 = \mathrm{Var}\{\eta_m\} = \mathrm{Var}\{\zeta\} = \mathrm{Var}\{\zeta_m\}$ for all m, $E\{\zeta\zeta_m\} = 0$ for all m, and $E\{\zeta_m\zeta_n\} = 0$ for all m and n with $m \neq n$. The correlation coefficient is defined as the normalized covariance

$$E\{\eta_m\eta_n\}/\sigma_\eta^2 = a^2 = 1 - b^2\,. \tag{2.4}$$

A reasonable correlation coefficient of 0.5 is assumed because the near field and the BS specific propagation uncertainties have equal standard deviations [VVZ94].

2.1.2 Channel Models

For the investigations in this thesis, two different channel models are used. The first channel model represents the modeling of a realistic mobile radio channel, described by a tap-delay channel model. Additionally, a channel model is chosen for investigating different correlation properties by using a correlated Rayleigh fading channel.

Tap-Delay Channel Model

The mobile radio channel is assumed to be a time-variant, frequency-selective fading channel, which is modeled by a tapped delay-line with Q_0 non-zero taps [Pro95]. The Q_0 channel taps are mutually uncorrelated and all tap delays are in the range $[0, \tau_{\max}]$, where $\tau_{\max}$ represents the maximum delay spread. The channel impulse response (CIR) can be expressed as

$$h^{(m)}(\tau, t) = \sum_{q=0}^{Q_0-1} h_q^{(m)}(t) \cdot \delta(\tau - \tau_q^{(m)})\,, \tag{2.5}$$

where $h_q^{(m)}(t)$ and $\tau_q^{(m)}$ are the complex amplitude and delay of the qth channel tap for the signal from BS m. $\delta(\cdot)$ denotes the Dirac delta function. The Doppler effect, resulting from the motion of the mobile station, causes $h_q^{(m)}(t)$ to be time-variant. Furthermore, the maximum Doppler frequency $f_{\mathrm{D,max}}$ leads to a band-limited CIR. The coherence time of the channel defines the duration over which the channel characteristics can be considered as time-invariant. It can be approximated by

$$(\Delta t)_{\mathrm{c}} \approx \frac{1}{f_{\mathrm{D,max}}}\,. \tag{2.6}$$

Furthermore, the coherence bandwidth is the bandwidth over which the signal propagation characteristics are correlated. It can be approximated by

$$(\Delta f)_{\mathrm{c}} \approx \frac{1}{\tau_{\max}}\,. \tag{2.7}$$

The channel is assumed to be a wide-sense stationary random process, i.e., the channel has a fading statistic that remains constant over short periods of time or small spatial distances [Hoe92]. Therefore, the CIR needs to be constant during one symbol. Thus, $h_{l,q}^{(m)} = h_q^{(m)}(lT_{\mathrm{s}}')$, where T_{s}' is the overall symbol time including a guard time.

For the channel model the fading processes are normalized such that the averaged impulse response energy equals one. Therefore, the averaged energy of $h_{l,q}^{(m)}$ is given by

$$\sum_{q=0}^{Q_0-1} E\{|h_{l,q}^{(m)}|^2\} = 1\,. \tag{2.8}$$

Equivalently, the channel can be characterized by the channel transfer function $H(f,t)^{(m)}$, which is the Fourier transform of the CIR in (2.5). After sampling the transform at time $t = lT'_{\mathrm{s}}$ and at frequency $f = i/T_{\mathrm{s}}$, given the sole symbol duration T_{s}, the channel transfer function (CTF) is given by

$$H_{l,i}^{(m)} = H^{(m)}(i/T_{\mathrm{s}}, lT'_{\mathrm{s}}) = \sum_{q=0}^{Q_0-1} h_{l,q}^{(m)} e^{-\mathrm{j}2\pi\tau_q^{(m)} i/T_{\mathrm{s}}} \,. \tag{2.9}$$

Correlated Rayleigh Fading Channel Model

To investigate the influence of different correlation properties a correlated Rayleigh fading channel model is described in the following. The channel on each sub-carrier is assumed to be a slowly-varying frequency-non-selective Rayleigh channel. Let α_i, $i = 0, \ldots, N_{\mathrm{c}} - 1$, denote the fade amplitude variable on the ith sub-carrier out of N_{c} sub-carriers. The Rayleigh random variables α_i have zero mean and unit variance, $\mathrm{E}\{|\alpha_i|^2\} = 1$, and uniform random variables over $[0, 2\pi)$. The fading correlation property between sub-carriers j and k can be described by the correlation coefficient

$$\rho_{j,k} = \frac{\mathrm{Cov}\{\alpha_j, \alpha_k\}}{\sqrt{\mathrm{Var}\{\alpha_j\}\mathrm{Var}\{\alpha_k\}}}, \qquad 0 \leq |\rho_{j,k}| < 1 \,, \tag{2.10}$$

where the covariance is defined by [LG94]

$$\mathrm{Cov}\{\alpha_j \alpha_k\} = \mathrm{E}\{(\alpha_j - \mathrm{E}\{\alpha_j\})(\alpha_k - \mathrm{E}\{\alpha_k\})^*\} \,. \tag{2.11}$$

The sub-carriers are said to be

$$\text{uncorrelated if:} \quad \rho_{j,k} = 0 \,, \quad \text{totally correlated if:} \quad |\rho_{j,k}| = 1 \,. \tag{2.12}$$

For the investigations, the correlation factor remains constant over all sub-carriers, and therefore, $\rho_{\mathrm{c}} = \rho_{j,k}$. Thus, the channel and its correlation properties can be described by one parameter ρ_{c}.

2.2 MC-CDMA System

In this chapter, the basic principles of the underlying OFDM modulation in multi-carrier code division multiple access (MC-CDMA) are briefly described. A more detailed description can be found in [FK03] or [vNP00] for example. The general transmitter is described in the following. The receiver for an MC-CDMA transmission scheme is also introduced including the additional needs and aspects within a cellular setup. For comparison, the basic multiple access scheme orthogonal frequency division multiplex access (OFDMA) [SK98] is also described where the differences to MC-CDMA are pointed out.

2.2.1 OFDM Principles

During the last decades the OFDM modulation scheme has emerged as a robust and spectral efficient multi-carrier scheme for multi-path propagation channels [Bin90]. OFDM is already widely used in several communications standard, e.g., terrestrial digital video broadcasting (DVB-T) [DVB04], digital audio broadcasting (DAB) [DAB00], and wireless local area network (WLAN) [IEE03]. The

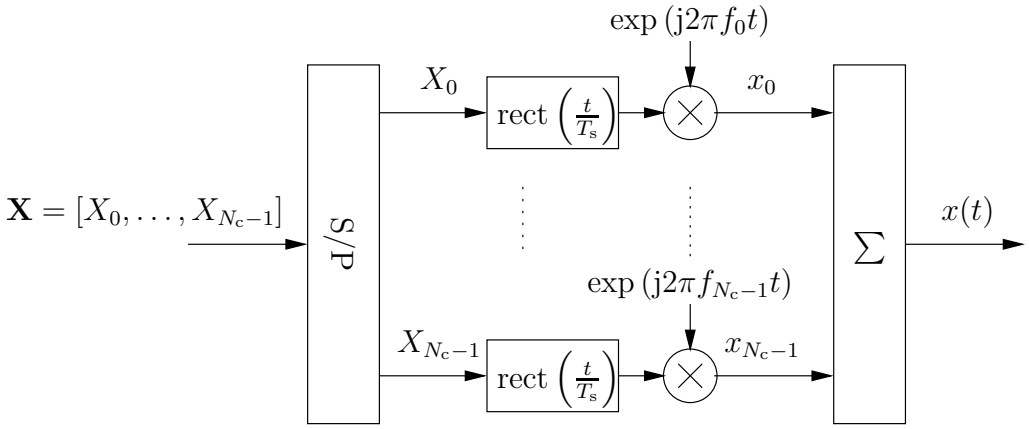

Figure 2.2: OFDM principle with rectangular pulse shaping

principle of OFDM is to superimpose N_c orthogonal signals $x_0(t), \ldots, x_{N_\mathrm{c}-1}(t)$, which are located on equidistant center frequencies $f_0, \ldots, f_{N_\mathrm{c}-1}$, by using rectangular pulse shaping. These center frequencies are commonly called sub-carriers. To achieve the orthogonality between the signals, the sub-carrier spacing is

$$F_\mathrm{s} = \frac{1}{T_\mathrm{s}} \tag{2.13}$$

which represents the inverse of the OFDM symbol duration T_s with $f_i = F_\mathrm{s} \cdot i$. Without loss of generality the time index l and base station index m are skipped in the following of this section.

After serial-to-parallel conversion of a stream of N_c complex-valued symbols X_i, rectangular pulse shaping, and modulating on the sub-carrier frequency (cf. Figure 2.2), the OFDM signal has the form

$$x(t) = \sum_{i=0}^{N_\mathrm{c}-1} X_i \,\mathrm{rect}\left(\frac{t}{T_\mathrm{s}}\right) e^{\mathrm{j}2\pi f_i t} \,. \tag{2.14}$$

By sampling the OFDM signal $x(t)$ with rate $N_\mathrm{c}/T_\mathrm{s}$, the resulting sampled sequence is

$$x(k \cdot \frac{T_\mathrm{s}}{N_\mathrm{c}}) = x_k = \sum_{i=0}^{N_\mathrm{c}-1} X_i e^{\mathrm{j}\frac{2\pi}{N_\mathrm{c}} ik} \,. \tag{2.15}$$

The inverse discrete Fourier transformation (DFT) with N_DFT samples is comprised in the representation of the sampled OFDM sequence, except its normalization factor $1/\sqrt{N_\mathrm{DFT}}$, by

$$\text{inverse DFT}: \qquad x_\nu = \frac{1}{\sqrt{N_\mathrm{DFT}}} \sum_{\mu=0}^{N_\mathrm{DFT}-1} X_\mu e^{\mathrm{j}\frac{2\pi}{N_\mathrm{DFT}}\mu\nu} \,, \tag{2.16}$$

$$\text{DFT}: \qquad X_\mu = \frac{1}{\sqrt{N_\mathrm{DFT}}} \sum_{\nu=0}^{N_\mathrm{DFT}-1} x_\nu e^{-\mathrm{j}\frac{2\pi}{N_\mathrm{DFT}}\nu\mu} \,. \tag{2.17}$$

For the sake of completeness the DFT is also presented. The benefit of OFDM is the possibility to implement the multi-carrier modulation in the discrete domain by using an inverse DFT. For a further reduction of complexity the inverse fast Fourier transformation (FFT) with N_FFT samples can be applied. Using the normalized (balanced) form of the inverse DFT or inverse FFT results in equal

averaged signal powers of the time and frequency signals which is given by Parseval's theorem:

$$\sum_{\mu=0}^{N_{\mathrm{DFT}}-1} |X_\mu|^2 = \sum_{\nu=0}^{N_{\mathrm{DFT}}-1} |x_\nu|^2 \,. \tag{2.18}$$

By transmitting the OFDM signal in a mobile communication environment, the signal undergoes the influence of a multi-path channel. Two main effects on the signal can be highlighted: First, due to reflections and scattering, adjacent signals overlap and interfere because of different delays of their propagation paths. The maximum delay spread $\tau_{\max}$ of the channel describes the highest delay of this property and it can result inter-symbol interference (ISI). Second, variations on amplitude and phase of the received signal are caused by moving the receiver entity, the so-called Doppler spread. The effect of the Doppler spread on adjacent sub-carriers results in inter-carrier interference (ICI) and its influence is defined by the maximum Doppler spread $f_{\mathrm{D,max}}$.

To avoid ICI, the sub-carrier spacing has to be chosen much larger than the range of the Doppler power spectrum, i.e., $F_{\mathrm{s}} \gg 2f_{\mathrm{D,max}}$ [FK03]. A guard interval (GI) has to be added to the OFDM signal to maintain the orthogonality between the signals on the sub-carriers, which eliminates the effects of ISI. A cyclic prefix of each OFDM symbol is taken with length

$$T_{\mathrm{GI}} \geq \tau_{\max} \tag{2.19}$$

and the overall length of the resulting OFDM symbol is

$$T_{\mathrm{s}}' = T_{\mathrm{s}} + T_{\mathrm{GI}} \,. \tag{2.20}$$

The sample time is given by $T_{\mathrm{samp}} = T_{\mathrm{s}}/N_{\mathrm{FFT}}$. With this setup for the design of the OFDM modulation, the well-known representation of the frequency domain OFDM model can be given. Since ICI and ISI can be avoided by applying the guard interval, each sub-carrier is influenced by a separate sub-channel. This results in the received symbol

$$Y_i = X_i H_i + N_i \,, \tag{2.21}$$

which includes the transmitted symbol X_i, the channel transfer function H_i (cf. (2.9)), and the noise term N_i. The noise is assumed to be additive white Gaussian noise (AWGN) with variance

$$\sigma^2 = E\{|N_i|^2\} \,. \tag{2.22}$$

This simplifies the OFDM multi-carrier modulation to a discrete time and frequency transmission system with N_{c} different complex-valued attenuations H_i and Gaussian channels in parallel. Figure 2.3 shows the simplified transmission system. Furthermore, an OFDM symbol can be described in a time/frequency representation. Figure 2.4 illustrates an OFDM symbol and an OFDM frame, i.e., a set of N_{s} OFDM symbols.

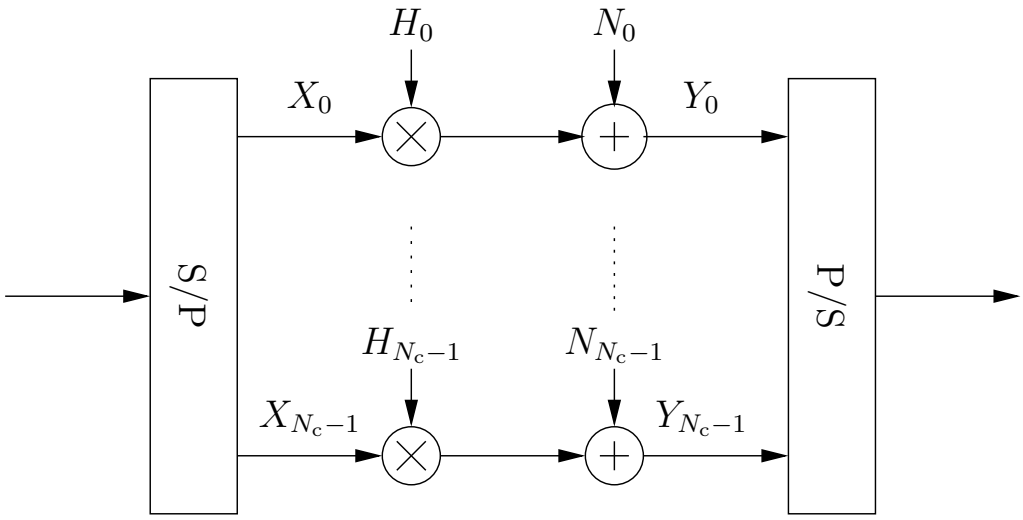

Figure 2.3: Simplified OFDM multi-carrier modulation

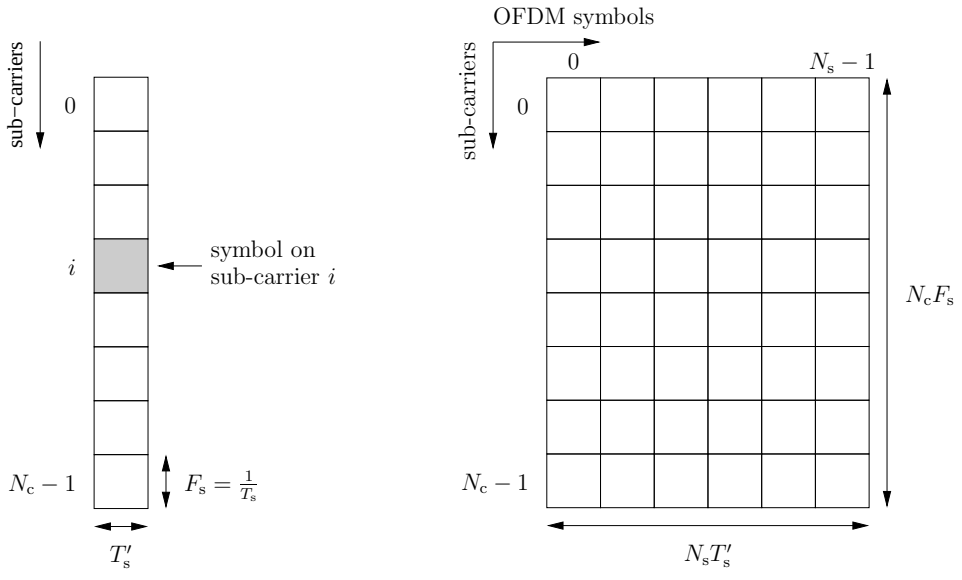

(a) OFDM symbol (b) OFDM frame

Figure 2.4: OFDM symbol and OFDM frame in time-frequency representation

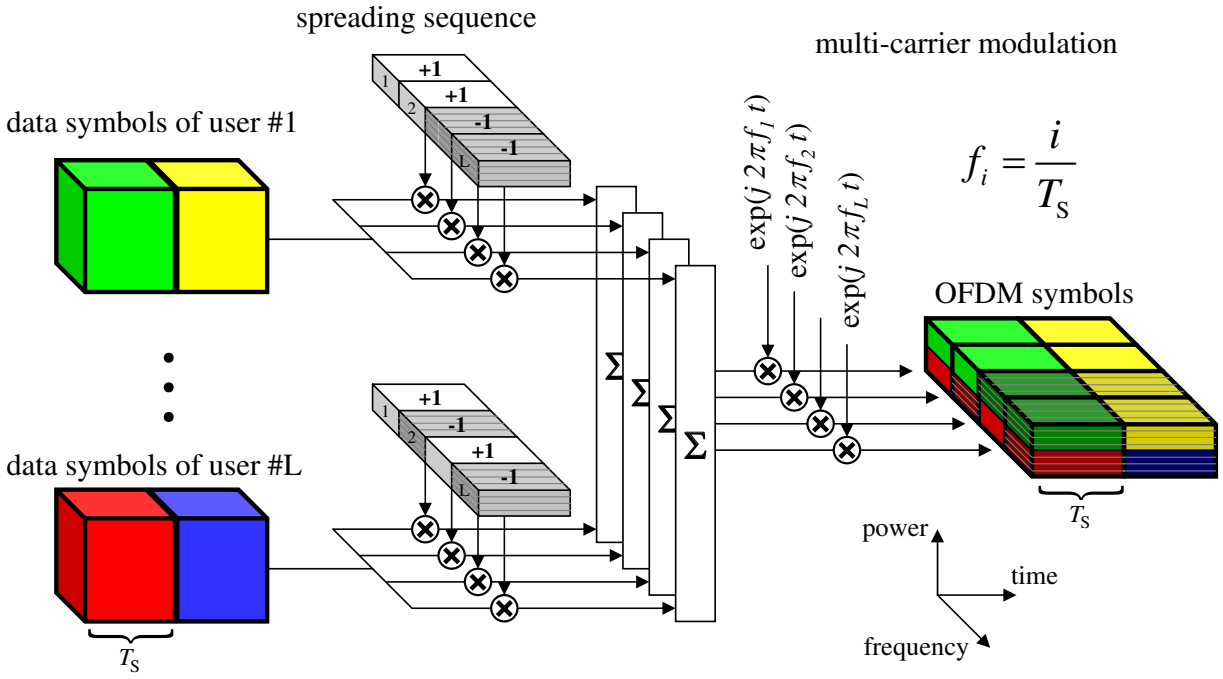

Figure 2.5: Principle of MC-CDMA

2.2.2 Transmitter

The basic principle of an MC-CDMA transmitter is shown in Figure 2.5. The use of spreading codes merges several users onto one chip. The chips of this CDMA signal are transmitted in parallel over OFDM modulated sub-carriers. At the receiver side, due to orthogonal spreading codes, the users can be recovered. Since one user is spread over several sub-carriers (it is also possible to spread them over several OFDM symbols or both), the receiver can collect a higher frequency diversity at the decoding process. It was shown that the MC-CDMA transmission can be also seen as a special case of multi-level coding [BSB04, Bos05]. Furthermore, due to the spread users' data which are superimposed on the transmitted chips, the broadcast principle [Cov72] is inherently included in MC-CDMA.

Multiple access transmission schemes based on the OFDM modulation can be commonly described as generalized multi-carrier (GMC) [WG00]. MC-CDMA is within this GMC principle by introducing the spreading component. Without the spreading component the OFDMA [SK98] scheme is given as the basic GMC access scheme.

At the transmitter the MC-CDMA and OFDMA transmission schemes differ in the sub-carrier allocation and the additional spreading component for MC-CDMA. In the following, the terminology, notation, and description is identical for both systems, and the differences are pointed out in this section.

The GMC transmitter is shown in Figure 2.6. The system contains N_c sub-carriers for N_u users. The system can serve maximal $N_\mathrm{u,max}$ users. A channel-coder encodes the information bit stream $\mathbf{i}^{(n)}$ of each user n with a coding rate

$$R = \frac{k_\mathrm{cod}}{n_\mathrm{cod}}\,, \tag{2.23}$$

where k_cod and n_cod represent the information length and the code length. The encoded bits are interleaved by the outer interleaver Π_out and the interleaved code bits $\mathbf{c}^{(n)}$ are passed to the symbol modulator. With respect to different modulation alphabets (e.g., phase-shift keying (PSK) or quadra-

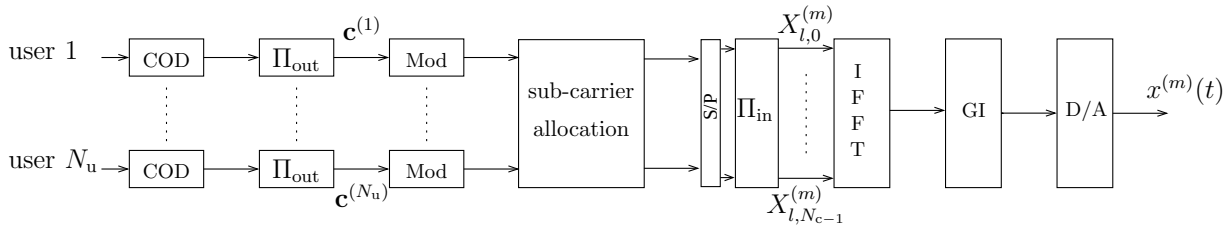

Figure 2.6: GMC transmitter of the mth base station

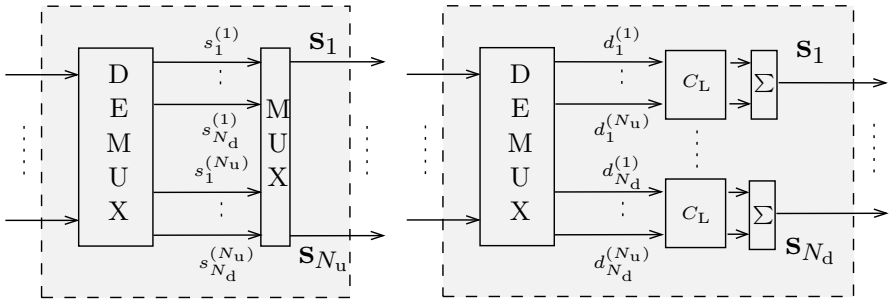

(a) OFDMA (b) MC-CDMA

Figure 2.7: Sub-carrier allocation

ture amplitude modulation (QAM)), the bits are modulated to complex-valued data symbols with the chosen cardinality. A sub-carrier allocation block arranges the symbols with respect to each transmission scheme in the following way:

- **OFDMA:** The allocation of sub-carriers for OFDMA is shown in Figure 2.7(a). The demultiplexer (DEMUX) arranges the passed data symbols from the mapper to $N_{\text{d}} = N_{\text{c}}/N_{\text{u,max}}$ parallel symbols per user. These symbols can be multiplexed (MUX), i.e., combined to a block $\mathbf{s} = [\mathbf{s}_1, \ldots, \mathbf{s}_{N_{\text{u}}}]^T$, where $\mathbf{s}_k = [s_1^{(k)}, \ldots, s_{N_{\text{d}}}^{(k)}]$. In the case of $N_{\text{u}} < N_{\text{u,max}}$, the remaining sub-carriers are set to zero. For $N_{\text{u}} = N_{\text{u,max}}$, all sub-carriers are allocated, i.e., the system is fully loaded.

- **MC-CDMA:** Figure 2.7(b) shows the MC-CDMA sub-carrier allocation including the spreading component. Before each modulated signal can be spread with a sequence out of a set of orthogonal Walsh-Hadamard sequences of length

$$L = N_{\text{u,max}} \geq N_{\text{u}} \tag{2.24}$$

  a DEMUX arranges the signals to $N_{\text{d}} \leq N_{\text{c}}/L$ parallel data symbols per user. For the case that $N_{\text{d}} = N_{\text{c}}/L$, the data stream is distributed over all available sub-carriers. On the other hand, if $N_{\text{d}} < N_{\text{c}}/L$, other data streams are assigned to the remaining sub-carriers, which are named user groups [FK03] and are independent from the aforementioned data stream. This guarantees equally loaded sub-carriers. Furthermore, an equal transmission power P_{s} is assumed in all data sub-carriers, i.e., the same second moment $E\{|d_k^{(n)}|^2\}$ per user. The kth symbol of all users, $\mathbf{d}_k = [d_k^{(1)}, \ldots, d_k^{(N_{\text{u}})}]^T$, is multiplied with a $L \times N_{\text{u}}$ spreading matrix $\mathbf{C}_{\text{L}}$ resulting in

$$\mathbf{s}_k = \mathbf{C}_{\text{L}}\mathbf{d}_k\,,\ \mathbf{s}_k \in \mathbb{C}\,, 1 \leq k \leq N_{\text{d}}\,. \tag{2.25}$$

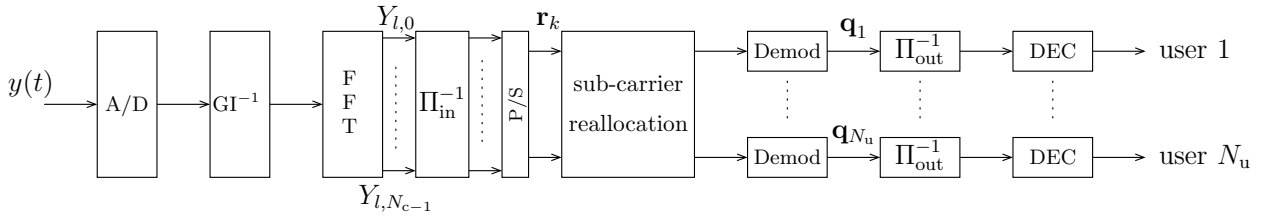

Figure 2.8: Cellular GMC receiver

Due to the equal-loaded sub-carriers in MC-CDMA, there exists the relation

$$E\{|\mathbf{s}_k|^2\} = \frac{N_{\mathrm{u}}}{L} \cdot P_{\mathrm{s}} \tag{2.26}$$

and $\mathbf{s}_k$ can also be combined to a block $\mathbf{s} = [\mathbf{s}_1, \ldots, \mathbf{s}_{N_{\mathrm{d}}}]^T$.

For maximizing the diversity gain, the block $\mathbf{s}$ is frequency-interleaved by the inner interleaver Π_{in}. By taking into account a whole OFDM frame the interleaving can be done in two dimension, i.e., time and frequency. An OFDM modulation is performed on each block. First, an inverse FFT (IFFT) with $N_{\mathrm{FFT}} \geq N_{\mathrm{c}}$ points is done. Then, the guard interval is inserted having N_{GI} samples. The front-end digital to analog (D/A) converts the signal, up-converts it to the appropriate frequency bands, and $x^{(m)}(t)$ is obtained.

2.2.3 Cellular Receiver

Over the last decades, GMC downlink systems like OFDMA or MC-CDMA have been studied intensively. However, it is necessary to extend the investigations to more realistic scenarios, i.e., cellular structures. The receiver design has to take into account the cellular setup. Therefore, in the following a cellular downlink receiver is described including the needed definitions within a cellular environment.

Figure 2.8 depicts the receiver structure of the GMC system. The signals $x^{(m)}(t)$ from the m BSs are transmitted over a mobile radio channel and $y(t)$ is received. Then the inverse OFDM is performed including the removing of the guard interval and the FFT. For the channel fading a quasi-static fading process is assumed, i.e., the fading is constant for the duration of one OFDM frame. With this quasi-static channel assumption the well-known description of OFDM in the frequency domain is given (cf. (2.21)).

After OFDM demodulation of the OFDM symbol, the received signal in a cellular environment is

$$Y_{l,i} = \underbrace{X_{l,i}^{(0)} H_{l,i}^{(0)}}_{\text{desired signal}} + \underbrace{\sum_{m=1}^{N_{\mathrm{BS}}-1} X_{l,i}^{(m)} H_{l,i}^{(m)}}_{\text{interfering signal}} + N_{l,i}\,, \tag{2.27}$$

where the received powers from all BSs are assumed to be equal in this representation.

The inner deinterleaver Π_{in}^{-1} and a parallel-to-serial converter arranges the received signal to the block $\mathbf{r}_k$. The re-allocation process of the symbols is applied as follows and also depicted in Figure 2.9.

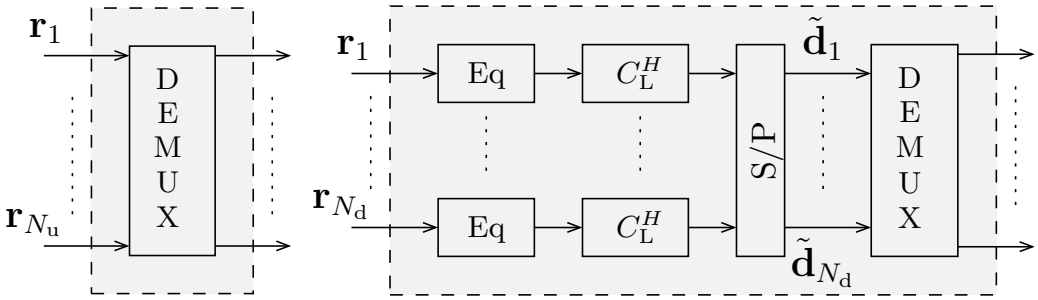

(a) OFDMA (b) MC-CDMA

Figure 2.9: Sub-carrier re-allocation

- **OFDMA:** The block $\mathbf{r}_k$ is demultiplexed in such a way that the data symbols are assigned to the corresponding user. With the knowledge of $H_{l,i}^{(0)}$, the data symbols can be directly demodulated including the equalization process, i.e., correcting the distortions of the channel by multiplying each sub-carrier with $1/H_{l,i}^{(0)}$.
- **MC-CDMA:** The N_d data symbol streams are passed to the equalizers. In MC-CDMA, due to different fading coefficients on each sub-channel the orthogonality between the spreading codes is lost and MAI occurs, if $N_\mathrm{u} > 1$. This can be compensated by restoring the orthogonality by equalization. An efficient compromise between reducing MAI and noise enhancement is the minimum mean square error (MMSE) equalizer detector for the single-user detection [FK03]. The data symbols for the demodulator process results in

$$\tilde{\mathbf{d}}_k = \mathbf{C}_\mathrm{L}^H \mathbf{G} \mathbf{r}_k = [\tilde{d}_k^{(1)}, \ldots, \tilde{d}_k^{(N_\mathrm{u})}]^T \,, \tag{2.28}$$

  where $\mathbf{G}$ represents the diagonal equalization matrix.

In this these, the knowledge of $H_{l,i}^{(m)}$ at the receiver is assumed to be perfect. All symbols of the desired user $\tilde{d}_k^{(1)}$ are combined to a serial data stream. The symbol and user indices k and n are skipped for notational convenience in the following. By using the maximum *a posteriori* probability (MAP) criterion [Pro95], the symbol demodulator demaps the data symbols to real valued log-likelihood ratios (LLRs) [HOP96b] for each code bit c by

$$L(c) = \log \frac{P(c=0)}{P(c=1)} \,. \tag{2.29}$$

The sign of $L(c)$ is the hard decision and the magnitude $|L(c)|$ is the reliability of the decision. The code bits are deinterleaved and decoded using the MAX-Log-MAP algorithm [RVH95] which generates an approximation of the LLR for the code bit sequence $\mathbf{q} = [q_0 \ldots q_{n_\mathrm{cod}-1}]$ by

$$L(c|\mathbf{q}) = \log \frac{P(c=0|\mathbf{q})}{P(c=1|\mathbf{q})} \,. \tag{2.30}$$

In contrast to (2.29) the LLR value $L(c|\mathbf{q})$ is the estimate of all bits in the coded sequence $\mathbf{q}$ [KH97].

Another degree of reliability of the decoder output can be given by the expectation of $E\{c|\mathbf{q}\}$, the so-called soft bits [KH97, Bos04] which are defined by

$$\begin{aligned} \lambda(c|\mathbf{q}) &= (+1) \cdot P(c=0|\mathbf{q}) + (-1) \cdot P(c=1|\mathbf{q}) \\ &= \tanh(L(c|\mathbf{q})/2) \,. \end{aligned} \tag{2.31}$$

These soft bits are in the range of

$$-1 \leq \lambda(c|\mathbf{q}) \leq 1\,. \tag{2.32}$$

The closer to the minimum or maximum the more reliable the decoded bits are. Therefore, $\lambda(c|\mathbf{q}) = 0$ represents equal probable bits.

Finally, after a correct decoding process, the sent information bit stream $\mathbf{i}$ is recovered.

Resource Load

For the multi-carrier schemes a resource load (RL) can be defined. For the OFDMA system, the RL is the ratio of the number of assigned sub-carriers to the total number of available sub-carriers. This corresponds directly to the RL of the MC-CDMA system, which is defined by the ratio of the number of active users to the number of maximum users. Note that in terms of total transmitted signal power $\sum_{i=0}^{N_\mathrm{c}-1} E\{|X_i^{(m)}|^2\}$ per OFDM symbol, the following relation holds:

$$\mathrm{RL} = \mathrm{RL}_{\mathrm{OFDMA}} = \frac{N_\mathrm{d} N_\mathrm{u}}{N_\mathrm{c}} = \mathrm{RL}_{\mathrm{MC-CDMA}} = \frac{N_\mathrm{u}}{L}\,. \tag{2.33}$$

Signal-to-Noise Ratio

At the input of the receiver, the averaged signal-to-noise ratio (SNR) on the ith sub-carrier can be defined. The SNR describes the ratio of the desired received signal power to the arising noise. Therefore, the signal powers of the interfering BSs are not taking into account. The time index l and BS index m are omitted due to the same averaged SNRs for different l and m. Using the OFDM modulation as illustrated in Figure 2.3 the averaged SNR on the ith sub-carrier in the frequency domain is defined as

$$\gamma_i = \frac{E\{|Y_i|^2\}}{\sigma^2}\,. \tag{2.34}$$

The data and channel fading are statistical independent one another due to the frequency domain model. Furthermore, by assuming equal transmission power in all data sub-carriers the SNR yields

$$\gamma_i = \frac{E\{|X_i|^2\} \cdot E\{|H_i|^2\}}{\sigma^2} \overset{(2.8)}{=} \left.\frac{E\{|X|^2\}}{\sigma^2}\right|_{E\{|H_i|^2\}=1}\,. \tag{2.35}$$

If the transmitted signal power P_s is normalized to one, i.e., $P_\mathrm{s} = E\{|d_k^{(n)}|^2\} = 1$ the SNR is given by

$$\gamma_i = \mathrm{RL} \cdot \left.\frac{1}{\sigma^2}\right|_{P_\mathrm{s}=1} \tag{2.36}$$

due to the relation in (2.26) and the definition of the resource load in (2.33). In general, the SNR is represented in decibel (dB) by

$$\gamma_{i,\mathrm{dB}} = 10 \cdot \log_{10} \gamma_i \quad [\mathrm{dB}]\,. \tag{2.37}$$

In this thesis, the knowledge of the SNR at the receiver is assumed to be perfect.

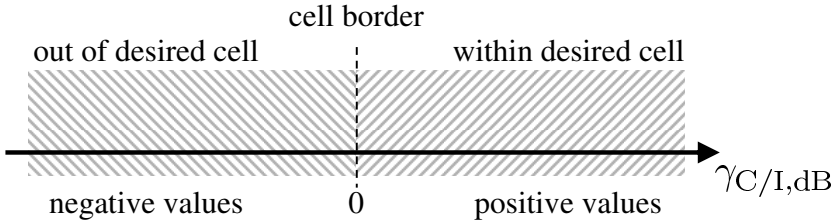

Figure 2.10: Quality of C/I values for a two-cell environment

Carrier-to-Interference-and-Noise Ratio

In contrast to the SNR definition, the interfering signal variance (respectively the power) from the neighboring cell sites

$$\sigma_{\mathrm{int}}^2 = \sum_{m=1}^{N_{\mathrm{BS}}-1} E\{|X_i^{(m)} \cdot H_i^{(m)} \cdot \alpha_{\mathrm{att}}^{(m)}|^2\} \tag{2.38}$$

are taking into account for the carrier-to-interference-and-noise ratio (CINR) depending on the position of the MS (cf. (2.2)). The CINR definition can be also seen as the *3GPP geometry factor* [3GP06], i.e., averaged power received from the desired BS to total received averaged inter-cell interference plus noise. The CINR is consequentially

$$\gamma_{\mathrm{CINR}} = \frac{E\{|X_i^{(0)} \cdot H_i^{(0)} \cdot \alpha_{\mathrm{att}}^{(0)}|^2\}}{\sigma_{\mathrm{int}}^2 + \sigma^2}\,. \tag{2.39}$$

Carrier-to-Interference Ratio

In the case of an interference-limited cellular system, a more appropriate measure can be given by the carrier-to-interference ratio (C/I). The C/I is defined by

$$\gamma_{\mathrm{C/I}} = \frac{E\{|X_i^{(0)} \cdot H_i^{(0)} \cdot \alpha_{\mathrm{att}}^{(0)}|^2\}}{\sigma_{\mathrm{int}}^2}\,. \tag{2.40}$$

Using the same assumptions as in (2.35), the C/I can be expressed by

$$\gamma_{\mathrm{C/I}} = \sum_{m=1}^{N_{\mathrm{BS}}-1} \frac{E\{|X^{(0)}|^2\}}{E\{|X^{(m)}|^2\}} \cdot \left(\frac{d_0}{d_m}\right)^{-\rho} \cdot \left.\frac{E\{|10^{\eta_0/10\mathrm{dB}}|^2\}}{E\{|10^{\eta_m/10\mathrm{dB}}|^2\}}\right|_{E\{|H_i|^2\}=1}\,. \tag{2.41}$$

Since an equal transmission power on all sub-carriers in the MC-CDMA transmitter is assumed, the C/I and CINR do not depend on the resource load for MC-CDMA. The decibel representation

$$\gamma_{\mathrm{C/I,dB}} = 10 \cdot \log_{10} \gamma_{\mathrm{C/I}} \tag{2.42}$$

permits a clear interpretation of the MS position for a two-cell environment, see Figure 2.10. For $\gamma_{\mathrm{C/I,dB}} = 0$ dB the MS is directly located at the cell border. For positive $\gamma_{\mathrm{C/I,dB}}$ values the MS is allocated within the desired cell. On the other side, the MS is outside of the desired cell for negative $\gamma_{\mathrm{C/I,dB}}$ values. For more than one interfering cell the areas are shifted to the left, i.e., to higher negative values.

Chapter 3

Characteristics of Inter-Cell Interference

Before any kind of technique can be developed to handle the influence of inter-cell interference, the main characteristics of the arising inter-cell interference have to be determined. Therefore, this chapter investigates the quantity, impact, and quality of the emerging inter-cell interference within a cellular MC-CDMA system.

Additionally, a large complexity reduction exists for multi-cell simulations on the link level if an appropriate modeling of the inter-cell interference can be given. Especially the generation of the channel coefficients demands a high computational complexity for each simulated cellular link.

In this chapter, the influence of the overall received inter-cell interference on the MS for different scenarios is investigated [21, 12, 1]. These studies are extended to sectorized cellular system to get a general idea of the inter-cell interference effect [17]. The nature of the resulting cellular MC-CDMA signal is derived [12]. Following these results a model for the inter-cell interference is investigated based on a Gaussian approximation of the inter-cell interference [21]. This also leads to a modified MMSE equalizer for a cellular MC-CDMA system [12]. All simulations are based on the system parameters of *System A* (cf. Appendix C.1) unless otherwise stated.

3.1 Influence of Inter-Cell Interference

A first step for the investigations of the inter-cell interference characteristics in an MC-CDMA downlink system is to determine the most significant contributing interfering base stations to the interference experienced by the mobile station. The influence of the inter-cell interference can be described by the resulting distributions of the carrier-to-interference-and-noise ratio (CINR) (cf. (2.39)) for different interference scenarios. In the following, these CINR values are determined for a varying number of interfering BSs. For the simulations, the first BS is the closest to the desired MS, the second BS the second closest, etc. The maximal number of interfering cells is 18 which represents two tiers of interfering cells in a hexagonal cellular structure, see Figure 2.1. A comparison of the CINRs produced by different numbers of interfering base stations indicates which of the BSs are the most significant contributors to the inter-cell interference experienced by the MS.

The resulting CINR at the MS is depicted versus the number of interferers in Figure 3.1. Two MS positions are chosen: *inner cell* represents the MS close to the desired BS with $\alpha = 30°, d_0 = 0.2$; *cell border* describes the MS position directly at the cell border with $\alpha = 30°, d_0 = 1.0$. The simulation results show that the strongest influence is generated by the two closest interfering BSs to the desired MS. For higher numbers of interfering BSs the additional influence is minimal. For both

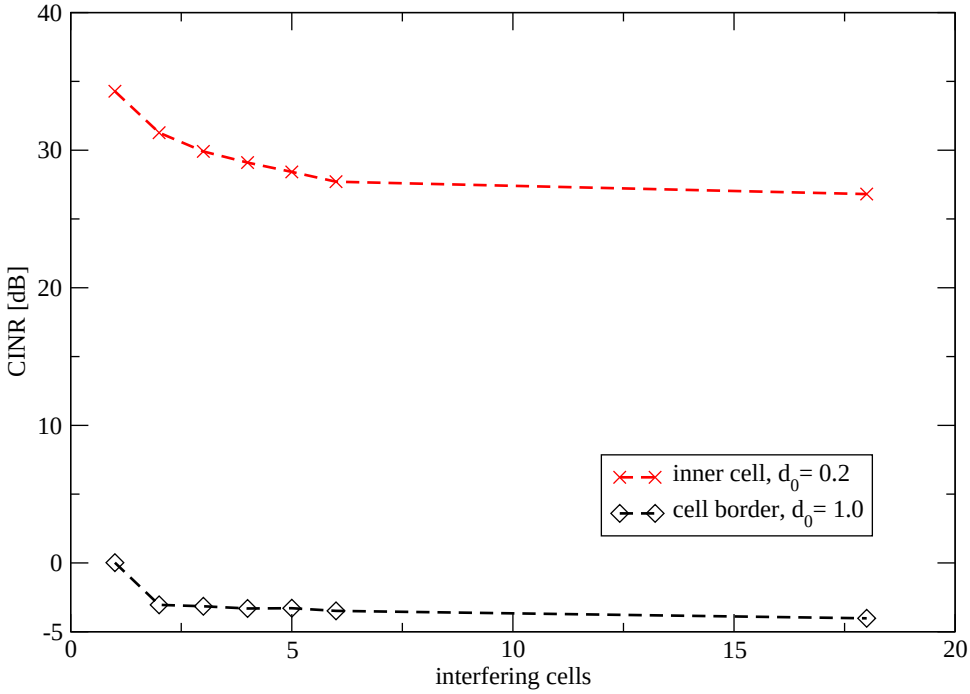

Figure 3.1: CINR versus number of interfering base stations

scenarios the strongest influence is generated by the two closest interfering base stations. In the inner cell, the CINR difference between 3 and 6 cells is only $1\ \mathrm{dB}$ and the MS is already in a very high CINR region of around $30\ \mathrm{dB}$. In contrast, the CINR difference between the first and second BS is $3\ \mathrm{dB}$; and between the second and third: $1.4\ \mathrm{dB}$. For the position of the MT at the cell border, the CINR is consequently worse for a higher number of interfering cells. There is a CINR difference between first and second BS of $3\ \mathrm{dB}$; between second and third: $0.25\ \mathrm{dB}$; and between the third and sixth: $0.25\ \mathrm{dB}$. This second scenario confirms the results of the first scenario in the inner part of the desired cell. For the case of one interfering BS the CINR is close to $0\ \mathrm{dB}$. For this scenario the received signal powers from both BSs are the same. Furthermore, the noise does not have a large influence to the overall inter-cell interference situation. Therefore, the MC-CDMA cellular environment is an interference-limited system, i.e., the interference dominates the noise. Consequently, the carrier-to-interference ratio (C/I) (cf. (2.40)) is used in the following.

Figure 3.2 shows the received C/I ratio at the mobile station for different locations within the cellular setup for a varying number of interfering cells. The MS moves along a straight line between the cell center and the outer part of the desired cell centered between two interfering BSs, i.e., $\alpha = 30°$. At the position $d_0 = 1.0$, the MS receives the same signal power from the desired BS and the two closest interfering BSs. For these simulations the order of interfering BSs are chosen by their decreasing distance to the MS. The closest interfering BS is the first and an SNR of $10\ \mathrm{dB}$ is given within all cells.

The simulation results for one interfering BS show at $d_0 = 1.0$ the expected C/I ratio of $0\ \mathrm{dB}$ because both signals are received with the same power at this location. By increasing the number of interfering BSs a degradation of the C/I ratio over all MS positions is given. In the outer regions of the desired cell ($d_0 \geq 0.8$) there is no influence on the C/I ratio for more than two interfering BSs. In the inner part of the desired cell a small influence of the number of interfering cells is visible because the MS is nearly equidistant to all surrounding BSs. These results show that the main contribution of the inter-cell interference in a cellular downlink MC-CDMA system is generated constantly over the

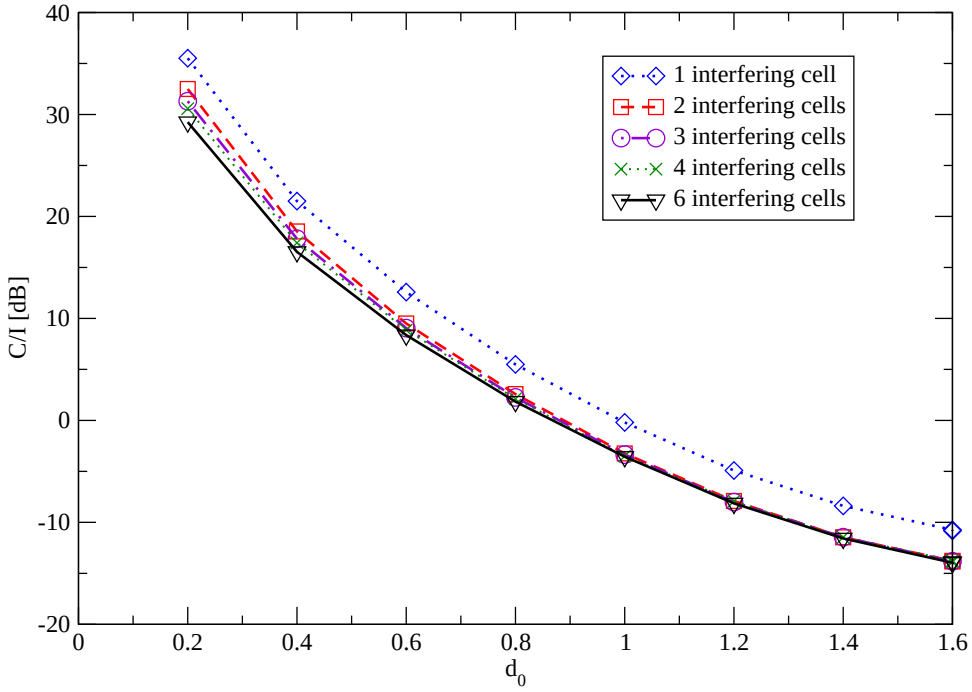

Figure 3.2: Influence of varying number of interfering cells on the C/I ratios at different MS positions

whole cell area by the two closest interfering BSs. Therefore, it is appropriate and sufficient to take into account only the two strongest interfering signals.

A better view on the influence of the inter-cell interference can be given by the investigations of the resulting bit error rate (BER) performances. These investigation can determine in which cell areas the influence of the inter-cell interference is dominant. Figure 3.3 depicts the BER versus the distance d_0 of the MS to the desired BS for different number of cells. For these simulations, the system is half loaded and the SNR is set to $10\ \mathrm{dB}$. A lower bound of the system, displayed by the unmarked dashed line, is defined by the performance without any inter-cell interference, i.e., no interfering cells. A BER performance of approximately 10^{-5} is reached. For distances smaller than $d_0 = 0.3$, all performances of the multi-cell environment approach the lower bound of the system. By increasing the number of interfering cells from one to two, a large performance loss can be seen. Since the MS moves directly towards the cell boundary, the second interference cell $\mathrm{BS}^{(\mathrm{I},2)}$ strongly interferes with the desired signal. Further increase to an even higher number of interfering cells does not entail large performance losses. The remaining interfering cells are farther away and disturb the signal less. The influence of the adjacent cells is limited and consequently restricted to the peripheral area of the desired cell. A severe performance degradation can be identified for $d_0 > 0.5$. Obviously, the influence of the inter-cell interference concentrates on the peripheral cell areas.

Sectorized Cellular System

In a cellular system, cell sectorization can increase the capacity of the total communications system, but also raises the need of a higher hardware complexity. In the following, inter-sector and intra-sector interference is investigated to determine if the main characteristics differ from pure inter-cell interference. In a sectorized system, the cells are divided into radial sectors with wide-beam directional BS

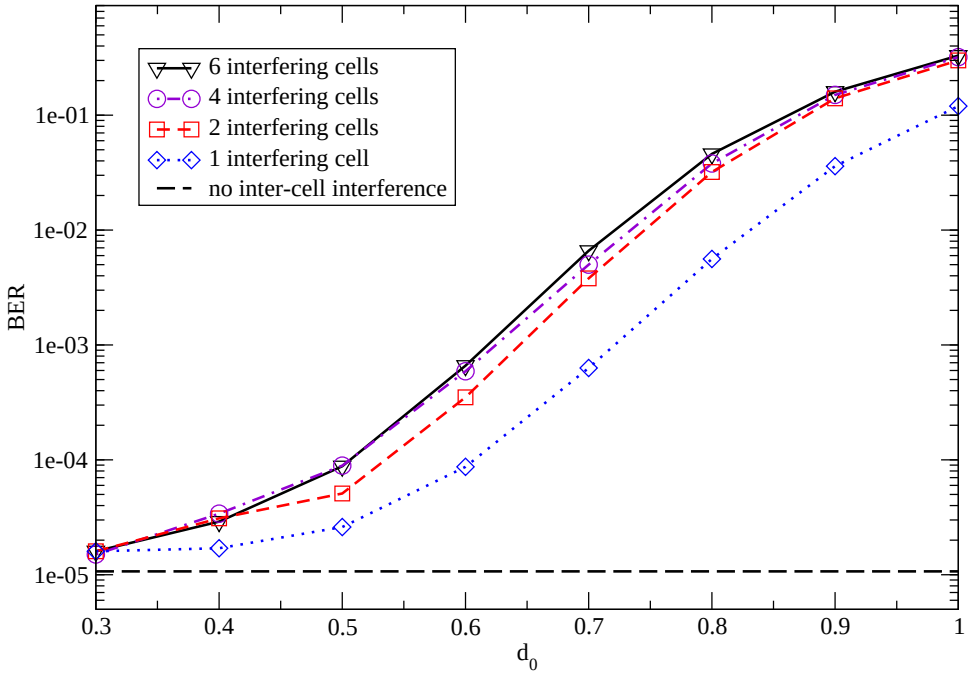

Figure 3.3: BER versus distance d_0 for different number of interfering cells; half loaded, $\gamma_{i,\mathrm{dB}} = 10$ dB

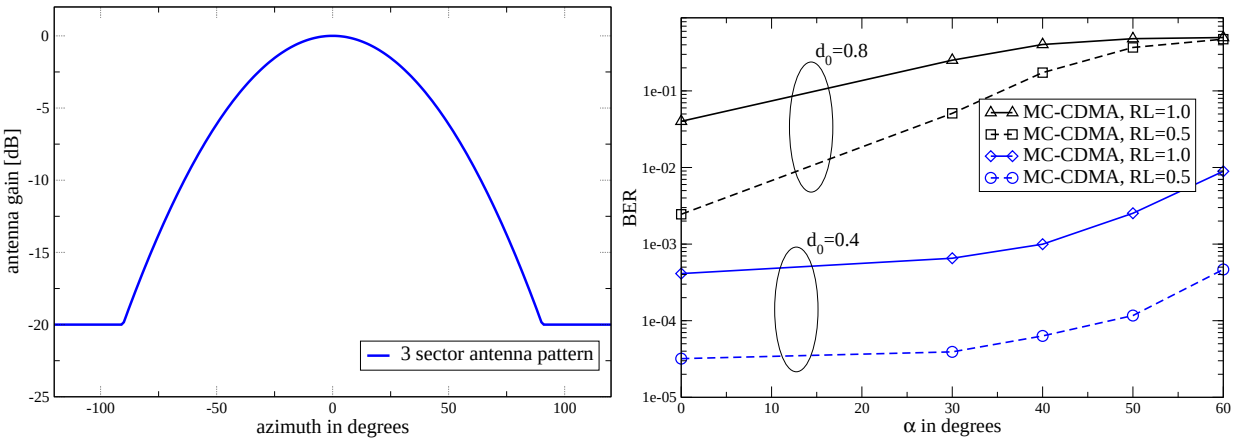

(a) Sector antenna gain pattern

(b) BER versus α for two different d_0

Figure 3.4: Influence of sectorized cell structure to cellular MC-CDMA system

antennas. Each sector has an antenna gain pattern which is defined by

$$A(\beta) = -\min\left[12\left(\frac{\beta}{\beta_{3\mathrm{dB}}}\right)^2, A_{\mathrm{m}}\right], \tag{3.1}$$

where $-180° \leq \beta \leq 180°$. The boresight of the antenna is the direction with the maximum antenna gain. In the above equation, the angle between the direction of interest and the boresight of the antenna is given by β, the $3\,\mathrm{dB}$ beamwidth $\beta_{3\mathrm{dB}} = 70°$, and the maximum attenuation A_{m} is $20\,\mathrm{dB}$ [UMT98]. The antenna gain pattern is shown in Figure 3.4(a).

In Figure 3.4(b) two different distances to the desired BS of the MS in one sector are investigated regarding the BER in a one-tier cellular environment with an SNR of $10\,\mathrm{dB}$. The sectors are arranged in such a way that $\alpha = \beta$. The MS position varies in the angle α, and therefore, moves from the boresight of the antenna to the lateral edge of the sector. There exists a large degradation for higher RLs due to the increased MAI. But the nature of the performance behaviors is similar for a half-loaded or fully-loaded system. The core of the desired cell ($d_0 \leq 0.4$) obtains a minimum of interference which is known from the previous investigations. Therefore, the same BER of $3 \cdot 10^{-5}$ as in Figure 3.3 is reached for $\alpha = 30°$. Furthermore, the degradation of the performance for $\alpha > 30°$ results only from the influence of the directly neighbored sector. This intra-sector interference can be directly mapped onto the antenna gains pattern in (cf. (3.1)). In the peripheral area ($d_0 = 0.8$), the performance shows a large degradation from surrounding sector, generating inter-sector interference and an additionally weakening by the intra-sector interference for $\alpha > 30°$.

Consequently, the influence of the directly adjacent sector of the same cell has to be taken into account by closer investigations of a sectorized cellular system. The amount of interference is increased within the whole intra-sector border.

3.2 Modeling of Inter-Cell Interference

Simulations of a cellular system on the link level are highly complexity consuming. Not only the transmitting signal of each active base station has to be generated, also the channel realization of each transmitted signal consumes most of the simulation complexity. At the receiver, the simulation complexity depends on the applied cellular signal processing algorithms. Therefore, the main complexity of a basic cellular downlink link level simulation increases linearly by the number of simulated cells.

By modeling the inter-cell interference, i.e., the impinging signals from the neighboring BSs appropriately, the complexity would be significantly reduced. In this section, the character of the elementary MC-CDMA signal is investigated. Furthermore, the resulting assumption of an Gaussian approximation (GA) for the inter-cell interference is analyzed and validated.

3.2.1 Nature of the Cellular MC-CDMA Signal

One approach to determine the nature of the received superimposed MC-CDMA signals is based on the signal's power density function (PDF) [DL05]. In the first step, the transmitted signal is investigated without the influence of the mobile radio channel. The generated discrete signal at the transmitter can be characterized by its resulting PDF with random variable $\Omega = \vartheta_1 + \ldots \vartheta_L$. The discrete uniform random variables ϑ_j depend on the chosen modulation alphabet. Using the binary PSK (BPSK) modulation and the binomial theorem [Pro95] a closed form expression can be given

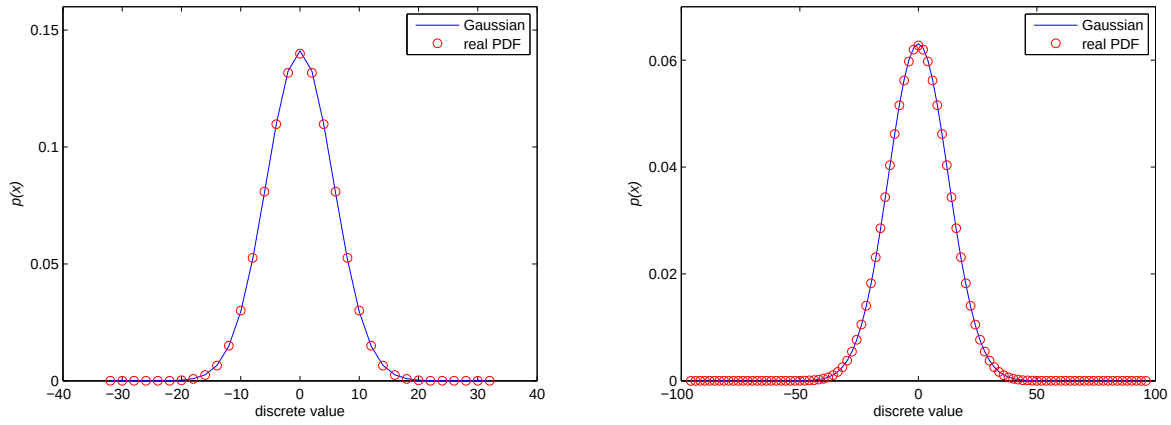

(a) BPSK (b) 16-QAM

Figure 3.5: PDF of transmitted symbols for different modulation alphabets and $L = 32$

for the PDF by

$$p_{\mathrm{BPSK}}(x) = \binom{L}{\frac{x+L}{2}} 0.5^L\,, \quad x = -L, -L+2, \ldots, L\,. \tag{3.2}$$

It is possible to approximate $p_{\mathrm{BPSK}}(x)$ by a Gaussian distribution with mean $\mu_{\mathrm{BSPK}} = L/2$ and variance $\sigma^2_{\mathrm{BPSK}} = L/4$. The discrete values are given by $\omega = x$, and therefore

$$P^{\mathrm{GA}}_{\mathrm{BPSK}}(\Omega = \omega) = \frac{1}{\sqrt{2\pi}\sigma^2_{\mathrm{BPSK}}} \, ^{-\frac{(\omega-\mu_{\mathrm{BPSK}})^2}{2\sigma^2_{\mathrm{BPSK}}}} \approx p_{\mathrm{BPSK}}(x)\,. \tag{3.3}$$

In the case of 16-QAM, the $L-1$ times convolution with the PDF of one discrete symbol, i.e., $[0.25, 0.25, 0.25, 0.25]$ determines the real PDF $p_{16-\mathrm{QAM}}(x)$. For 16-QAM the parameters of the Gaussian distribution $P^{\mathrm{GA}}_{16-\mathrm{QAM}}(\Omega = \omega)$ for the discrete values $\omega = \frac{x+3L}{2}$ with $x = -3L, -3L+2, \ldots, 3L$ can be set to

$$\mu_{16-\mathrm{QAM}} = 3L/2, \quad \sigma^2_{16-\mathrm{QAM}} = 5L/4\,. \tag{3.4}$$

For the overall picture, the 64-QAM distribution is defined by $\mathcal{N}(7L/2, 21L/4)$ with $\omega = \frac{x+7L}{2}$ and $x = -7L, -7L+2, \ldots, 7L$.

Figure 3.5 represents the PDF of the discrete signals for the two different modulation alphabets, i.e., BPSK, and 16-QAM. The parameters of the Gaussian distribution seems to fit very well the real PDFs. Therefore, the MC-CDMA signal looks Gaussian like and it is independent of the QAM modulation scheme.

In the following, a closer look will be taken on the absolute error between the real PDF and the Gaussian PDF, exemplarily for a 16-QAM modulation scheme. The real and the Gaussian approximation PDFs can take $3L+1$ discrete values. The error between the real and GA signal PDFs is defined by

$$\varepsilon(n) = p_{16-\mathrm{QAM}}(n) - P^{\mathrm{GA}}_{16-\mathrm{QAM}}(n)\,, \tag{3.5}$$

and the absolute error by

$$\varepsilon_{\mathrm{abs}}(n) = \left| p_{16-\mathrm{QAM}}(n) - P^{\mathrm{GA}}_{16-\mathrm{QAM}}(n) \right|\,, \tag{3.6}$$

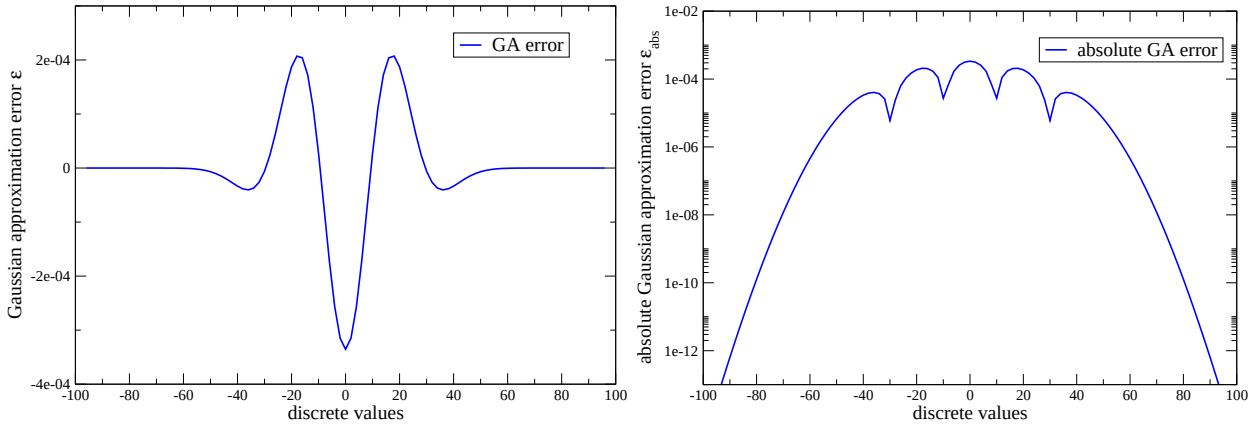

(a) $\varepsilon(n)$ (b) $\varepsilon_{\mathrm{abs}}(n)$

Figure 3.6: Gaussian approximation error; 16-QAM, full load, and $L = 32$

for $n = -3L, -3L+2, \ldots, 3L$. The errors $\varepsilon(n)$ and $\varepsilon_{\mathrm{abs}}(n)$ are plotted in Figure 3.6 for a fully-loaded system, i.e., $N_{\mathrm{u}} = L = 32$. The maximum error occurs for the most probable discrete values and is around $3.3 \cdot 10^{-4}$ which presents a tolerable error for the GA. For less probable values the error decreases, respectively almost vanishes.

Since a fully-loaded system ($\mathrm{RL} = 1.0$) was assumed, the overall absolute error in respect to the system load is investigated in the following. The overall error for a 16-QAM modulation is given by

$$\varepsilon_{\mathrm{total}}(N_{\mathrm{u}}) = \frac{1}{N_{\mathrm{u}}} \sum_{n=0}^{3N_{\mathrm{u}}} \varepsilon_{\mathrm{abs}}(2n - 3N_{\mathrm{u}}) \,, \quad \text{for} \quad N_{\mathrm{u}} = 1, \ldots, L \,. \tag{3.7}$$

Figure 3.7 depicts the fast decreasing total error of the GA for increasing number of users in the MC-CDMA system. For a system load higher than 10%, the error of the GA is negligible. The Central Limit Theorem [Pro95] also confirms this behavior because an increasing number of random process approximates better a Gaussian distribution. Therefore, the MC-CDMA signal at the transmitter is well represented by a Gaussian approximation.

3.2.2 Gaussian Approximation

At the transmitter the MC-CDMA signal can be well approximated by a Gaussian distribution. In a cellular setup, these random processes will superimpose and should increase the Gaussian character. On the other side the mobile radio channel influences each signal independently and the resulting superimposed signal at the receiver can behave differently. In this section, a simplified modeling of interferes in cellular MC-CDMA is investigated and verified by approximating the received inter-cell interference at the desired MS as a Gaussian noise.

Figure 3.8 shows the block diagram of a simulation setup for cellular MC-CDMA. Each cell has to be simulated by generating its transmit signal. Additionally, the transmitted signals are influenced by individual independent mobile radio channel realizations $H_{l,i}^{(m)}$ (cf. (2.9)) and their distance dependent propagation model (cf. (2.1)). The interfering signals powers are weighted with the factor

$$\Delta P_m = \frac{d_m^{-\rho} \cdot 10^{\eta_m/10\mathrm{dB}}}{d_0^{-\rho} \cdot 10^{\eta_0/10\mathrm{dB}}} \,, \tag{3.8}$$

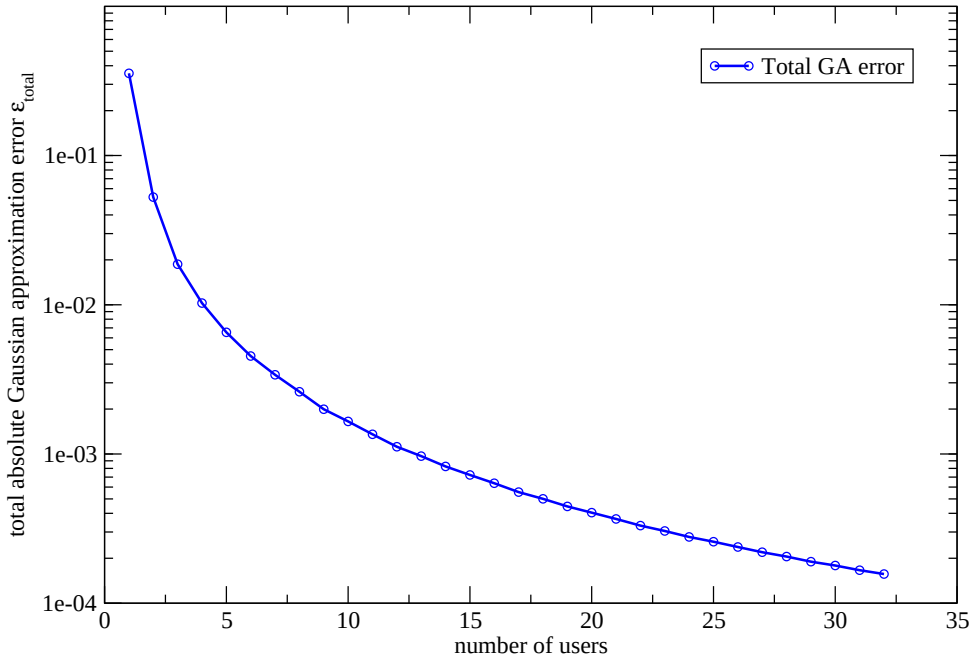

Figure 3.7: Total absolute Gaussian approximation error versus the number of users; 16-QAM, $L = 32$

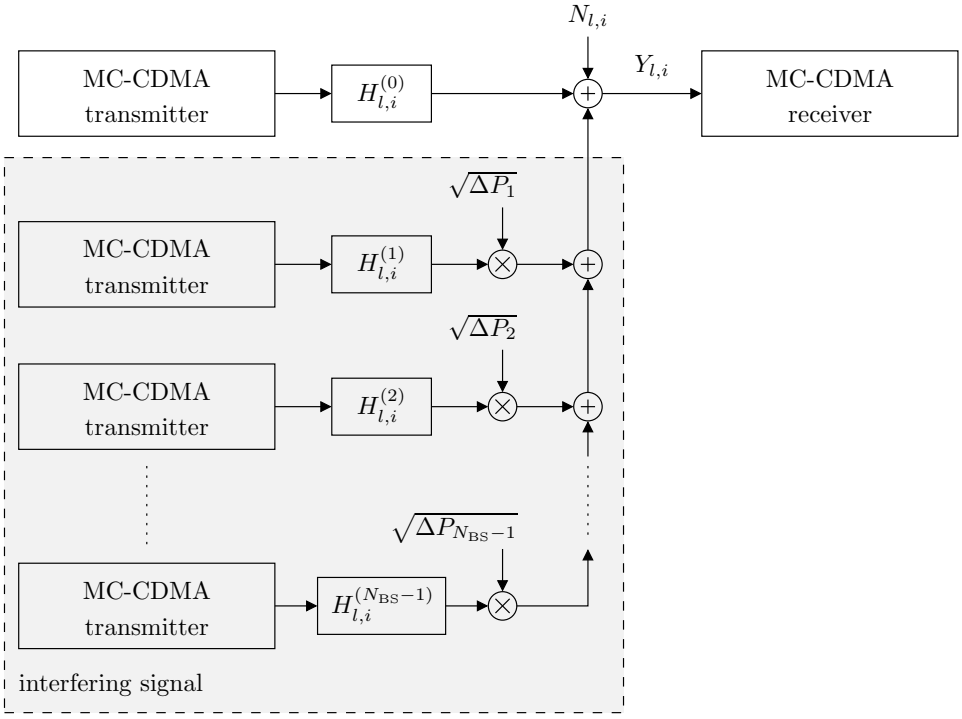

Figure 3.8: Model of the cellular MC-CDMA simulation setup

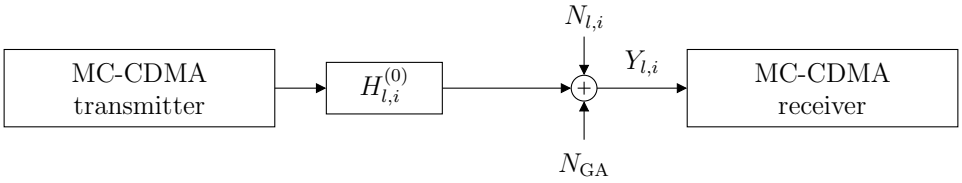

Figure 3.9: Model of simplified cellular simulation setup with Gaussian approximation

which are normalized to the desired signal. Therefore, the total received signal is

$$Y_{l,i} = X_{l,i}^{(0)} H_{l,i}^{(0)} + \sum_{m=1}^{N_{\mathrm{BS}}-1} \sqrt{\Delta P_m} X_{l,i}^{(m)} H_{l,i}^{(m)} + N_{l,i}\,. \tag{3.9}$$

Due to the results of the previous Section 3.2.1 the inter-cell interference is assumed to be an additional AWGN term at the receiver. This reduces significantly the simulation complexity. The new simulation structure for the GA of a cellular MC-CDMA system is illustrated in Figure 3.9. Thus, only the desired signal has to be generated, including its channel transfer functions and the Gaussian approximation noise term has to be added. Consequently, the received signal is

$$Y_{l,i} \approx X_{l,i}^{(0)} H_{l,i}^{(0)} + N_{\mathrm{GA}} + N_{l,i}\,, \tag{3.10}$$

where the variance of the GA term is set to

$$\sigma_{\mathrm{GA}}^2 = E\{|N_{\mathrm{GA}}|^2\} = \sum_{m=1}^{N_{\mathrm{BS}}-1} E\{|\sqrt{\Delta P_m} X_{l,i}^{(m)}|^2\} \overset{(2.26)}{=} \sum_{m=1}^{N_{\mathrm{BS}}-1} \Delta P_m \cdot \mathrm{RL} \cdot P_{\mathrm{s}}\,. \tag{3.11}$$

This approach decreases the number of signal and channel realizations to be simulated for a cellular environment by the factor $(N_{\mathrm{BS}} - 1)$.

Cellular MMSE Equalization

Within a cellular MC-CDMA environment the equalizer at the receiver has to take into account the additional received power from the interfering BSs. In the following the equalization coefficients $G_{i,i}$ of the applied MMSE (cf. Section 2.2.3) are derived for the cellular setup. For brevity, but without loss of generality, the OFDM symbol and sub-carrier indices l and i are omitted. Equalization according to the MMSE criterion minimizes the mean square value of the error

$$\varepsilon = X^{(0)} - GY \tag{3.12}$$

between the transmitted signal and the output of the equalizer. The mean square error $J = E\{|\varepsilon|^2\}$ can be minimized by applying the orthogonality principle [Pap91]. This principle states that the mean square error J is minimal if the equalizer coefficient G is selected such that the error ε is orthogonal to the received signal Y, that is,

$$E\{\varepsilon Y^*\} \overset{!}{=} 0 \tag{3.13}$$

and the modified MMSE coefficient (cf. (A.2) in Appendix A) is

$$G = \frac{H^{(0)*}}{|H^{(0)}|^2 + \frac{\sigma^2 + \sigma_{\mathrm{GA}}^2}{E\{|X^{(0)}|^2\}}}\,. \tag{3.14}$$

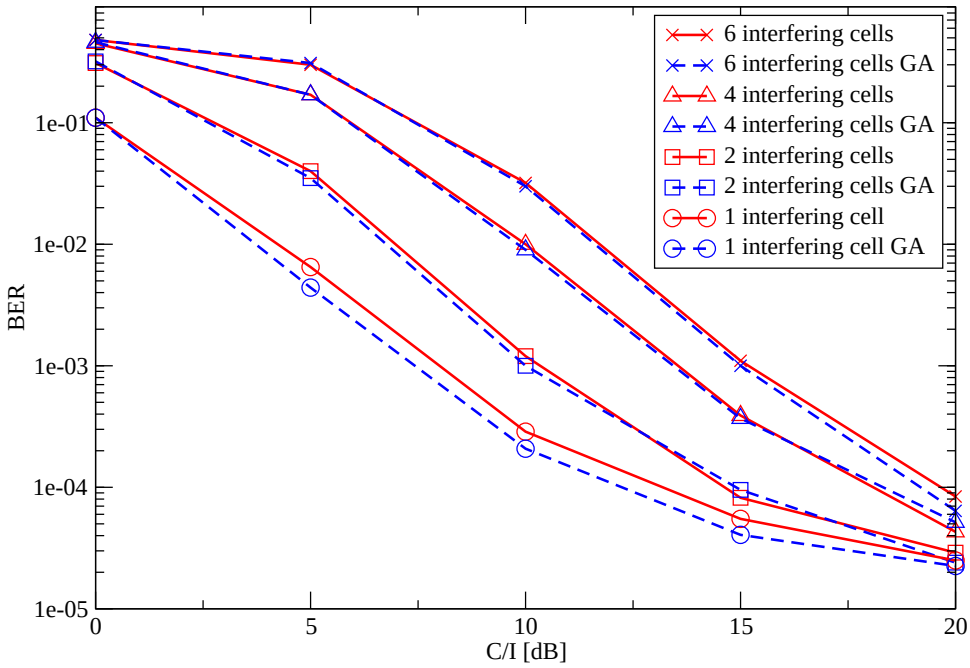

Figure 3.10: BER versus C/I for real cellular simulations and Gaussian approximation with different numbers of interfering cells; half loaded, $\gamma_{i,\mathrm{dB}} = 10$ dB

With the assumptions of (2.26) and (3.11) the last term in the denominator of G becomes

$$\frac{\sigma^2 + \sigma^2_{\mathrm{GA}}}{E\{|X^{(0)}|^2\}} = \frac{L}{N_\mathrm{u}} \cdot \frac{\sigma^2 + \sum\limits_{m=1}^{N_\mathrm{BS}-1} \frac{N_\mathrm{u}}{L} \Delta P_m P_\mathrm{s}}{P_\mathrm{s}} = \frac{L}{N_\mathrm{u} P_\mathrm{s}} \sigma^2 + \sum_{m=1}^{N_\mathrm{BS}-1} \Delta P_m \tag{3.15}$$

and the resulting modified MMSE coefficient is

$$G = \frac{H^{(0)*}}{|H^{(0)}|^2 + \frac{L}{N_\mathrm{u} P_\mathrm{s}} \sigma^2 + \sum\limits_{m=1}^{N_\mathrm{BS}-1} \Delta P_m} \,. \tag{3.16}$$

Therefore, the MMSE has to be scaled by the total simulated signal power from the desired and interfering BSs. In a real MC-CDMA cellular environment, the modified diagonal matrix entries for the MMSE for sub-carrier i has to be scaled by the total received signal power (cf. (2.35) and (2.38)), i.e.,

$$G_{i,i} = \frac{H_i^{(0)*}}{|H_i^{(0)}|^2 + (\frac{1}{\gamma_i} + \sigma^2_{\mathrm{int}})} \,. \tag{3.17}$$

Additionally, the MAP criterion in the demodulator is also influenced by the received signal power, and therefore, the demodulator has to take into account the overall received power $(1/\gamma_i + \sigma^2_{\mathrm{int}})$. If not a Gaussian like inter-cell interference signal can be assumed, e.g., due to a strong line-of-sight component, the MMSE coefficients are chosen accordingly to (A.5) in Appendix A.

In order to verify the Gaussian approximation in (3.10), Figure 3.10 shows simulation results of a half-loaded MC-CDMA system in the multi-cell environment of *System A*. The bit error rate is plotted as a function of the C/I ratio with the number of interfering cells as a parameter. The dashed curves represent the GA. For a scenario with one interfering cell the GA is too optimistic compared to the

performance of the cellular system. Since the MMSE equalizer is optimum for AWGN [Hay88], the GA results in a better performance compared to a non-Gaussian distributed interfering signal. For a higher number of interfering cells, more random signals will superimpose and with the law of great numbers approximate a Gaussian distribution more closely. Therefore, in this case the GA models accurately and is suitable for systems with a larger number of interfering cells and higher resource loads.

3.3 Summary

The characteristics of inter-cell interference in a cellular MC-CDMA transmission system are investigated in this chapter. Two main questions arise with regard to inter-cell interference: Where and from whom emerges the major inter-cell interference and can the inter-cell inference be modeled?

The knowledge of the influence of inter-cell interference to the overall received signal can ease the use of concepts for handling the additional disturbance by the neighboring cells. For example, coordinating or avoiding inter-cell interference can be done more appropriately. Only the cell areas which are influenced are taken into account for this kind of scheme which reduces the coordination complexity and increases the system efficiency.

By an appropriate modeling of the inter-cell interference, large simulation complexities can be avoided. This reduces significantly the computation times for link level simulation. Furthermore, link level investigations permit inter-cell interference to be studied from the mobile station perspective. The characteristics of inter-cell interference on the link level are necessary to investigate and assess new methods for mitigation schemes of inter-cell interference at the mobile station or base station.

A cellular MC-CDMA system represents an inter-cell interference limited environment, i.e., the inter-cell interference dominates the noise. Therefore, the use of the C/I ratio is an appropriate choice. The two closest interfering BSs affect the desired user most. This impact is constantly given over the whole desired cell area. Therefore, it is appropriate and sufficient to take into account only the two strongest interfering signals. Already for $d_0 > 0.5$ a performance degradation can be identified by using the same spectrum in each cell. Therefore, most of the cell area (more than 70%) is influenced by inter-cell interference. Severe performance degradations are concentrated on the peripheral cell areas. This confirms the importance not to neglect the cellular influence on the link level within a communications system.

With a sectorized design of the desired cell also intra-cell interference exists. The influence emerges in the intra-sector border areas. Consequently, the influence of the adjacent sector has to be taken into account by closer investigation of a sectorized cellular system. On the other side, intra-cell interference coordination or avoidance can be efficiently applied due to the direct communication possibilities within one cell.

The nature of cellular MC-CDMA signals show a very good match to a Gaussian approximation of the overall inter-cell interference signal. To adjust the receiver to a cellular environment, the MMSE equalization and MAP demodulation process has to be adapted to the overall received signal power. For higher system loads than 10%, the error between the real inter-cell interference signal and the Gaussian modeled are negligible. Therefore, the MC-CDMA signal at the transmitter is well represented by a Gaussian approximation. This is also confirmed by increasing the number of interfering cells in one-tier environment simulations. For more than two interfering signals the Gaussian approximation holds.

At last, it should be emphasized that the Gaussian approximation cannot be used if one interferer is highly dominating the received inter-cell interference (as there is no possible averaging effect anymore), nor when interference mitigation techniques take advantage of specific signal properties hidden by the Gaussian approximation. Among these techniques are interference cancellation schemes (which require the interferers being canceled to be modeled accurately) and smart antenna techniques (which require the spatial correlation of at least the dominant interfering signals to be modeled accurately). Nevertheless, the Gaussian approximation may be used in these cases to model the background interferers which reduces the number of signal and channel realizations to be simulated.

Chapter 4

Coordination of Inter-Cell Interference

In a cellular GMC transmission system several orthogonal resources are available, e.g., frequency, time, and spatial resources. For an MC-CDMA system the spreading codes are also an orthogonal resource. By coordinating these resources inter-cell interference can be reduced or even avoided. For a mobile communications system it is always desirable to attempt an efficient usage of all available resources. Therefore, inter-cell interference avoidance excludes shared resources within one cell. On the other side, inter-cell interference coordination takes a loss in performance due to shared resources but tries to guarantee best performance and maximum resource usage.

For avoidance or coordination schemes a certain amount of knowledge of the actual inter-cell interference has to be given. There has to be a communication between the BSs or within the network. On the other side, short-term assignment of orthogonal resources, e.g, set of sub-carriers, spreading codes, etc., can reduce the BS-to-BS communication complexity. This time-scale can be in the order of several OFDM frames. Long-term assignments can be used for coordinating fractional frequency reuse, i.e., there exist different frequency reuse patterns in the cellular setup [Hal83]. These assignments can be updated at a slow rate, in the order of minutes [3].

This chapter handles inter-cell interference coordination strategies for MC-CDMA by using orthogonal frequency resources and spreading codes. Since OFDMA has an easy handling of its sub-carrier resources, i.e., frequency resources, an idealized coordination scheme for OFDMA is introduced [20] and investigated for comparison with MC-CDMA [19, 16]. Both transmission schemes are compared to their BER and throughput performances for different scenarios. The frequency resource coordination is studied and a hybrid cellular partitioning concept is investigated [15, 4]. Finally, the concept of spreading code coordination for a cellular MC-CDMA system is investigated [18]. Unless otherwise stated, all simulations are based on the system parameters of *System A* (cf. Appendix C.1).

4.1 Frequency Resource Coordination

In an OFDMA system, each user has its own allocated sub-carriers. Therefore, an inter-cell interference coordination using sub-carrier allocations can be introduced for a cellular environment to enhance the performance of the managed users. This can not be done in MC-CDMA on sub-carrier basis due to the spreading component which superimpose the users onto chips on the sub-carriers. Another approach of coordination for both systems is the use of different frequency reuse factors. Since the frequency resources are scarce, the focus is on systems with a frequency reuse factor of 1. Nevertheless, higher frequency reuse factors can reduce the interference in the desired cell and no

complex coordination is needed to achieve reasonable performances. On the other hand, the overall spectral efficiency is reduced.

Frequency Reuse Factor

For all mobile radio systems, there is the possibility of a basic resource management system, namely static resource allocation [Lee97]. The available spectrum is divided into a number of sets. These sets are reused in a systematic fashion to cover all the hexagonal cells with a maximum possible separation between the same frequency sets. Instead of using the same frequency in all cells, which corresponds to a frequency reuse factor of $K = 1$, the inter-cell interference can be decreased by increasing the frequency reuse factor. On the other hand, the spectral efficiency of the system decreases by the factor K.

Sub-Carrier Allocation in OFDMA

A centralized coordination for assigning sub-carriers improves the performance in the case of OFDMA due to the exclusively used sub-carriers and the resulting avoidance of double allocated sub-carriers between neighboring cells. This coordination process is illustrated in Figure 4.1. There is no feedback information of the channel state information assumed to assign the sub-carriers adaptively depending on the user's best possible channels. If in a fully-synchronized system the knowledge of all sub-carrier allocations is available, it is possible to assign the sub-carriers per BS in such a way that no double allocation of sub-carriers between the managed BSs occurs. This can be guaranteed up to a resource load of

$$\mathrm{RL}_{\mathrm{free}} = 1/m_{\mathrm{coord}}\,, \tag{4.1}$$

where m_{coord} is the total number of coordinated cells. The managed m_{coord} BSs need the same inner interleaver Π_{in} after the sub-carrier allocation. In spite of coordination the frequency diversity of the OFDMA system is preserved. The uncoordinated cells use their own independent inner interleaver. See Figure 4.1(a) as an example of transmitted OFDM symbols of two uncoordinated BSs and two coordinated ones. By exceeding the RL of $1/m_{\mathrm{coord}}$, the succeeding assignment of sub-carriers is done in such a way that the assigned sub-carriers per additional active user are randomly distributed over the remaining sub-carriers. This is shown for user number 3 in Figure 4.1(b). Therefore, the probability that any user is entirely disturbed is reduced. This coordination scheme is called *smart* coordination in the following.

A randomized allocation of the sub-carriers can also be seen as a coordination and it is the simplest way to assign sub-carriers. In [NBZ97] the randomized allocation was investigated in terms of capacity. The occurrence of corrupted sub-carriers is investigated for both coordination strategies, namely the *randomized* coordination and the *smart* coordination.

Randomized coordination: Consider that there a N_{u} active users in the OFDMA system, the probability of an allocated sub-carrier is

$$p_{\mathrm{r}}(N_{\mathrm{u}}) = \frac{N_{\mathrm{d}} \cdot N_{\mathrm{u}}}{N_{\mathrm{c}}}\,. \tag{4.2}$$

If all N_{c} sub-carriers are considered, the probability that m_{int} managed interfering cells allocate the same sub-carrier out of all N_{c} is

$$p_{\mathrm{r}}(m_{\mathrm{int}}, N_{\mathrm{u}}) = \binom{m_{\mathrm{coord}} - 1}{m_{\mathrm{int}}} p_{\mathrm{r}}(N_{\mathrm{u}})^{m_{\mathrm{int}}} \left(1 - p_{\mathrm{r}}(N_{\mathrm{u}})\right)^{m_{\mathrm{coord}}-1-m_{\mathrm{int}}}\,. \tag{4.3}$$

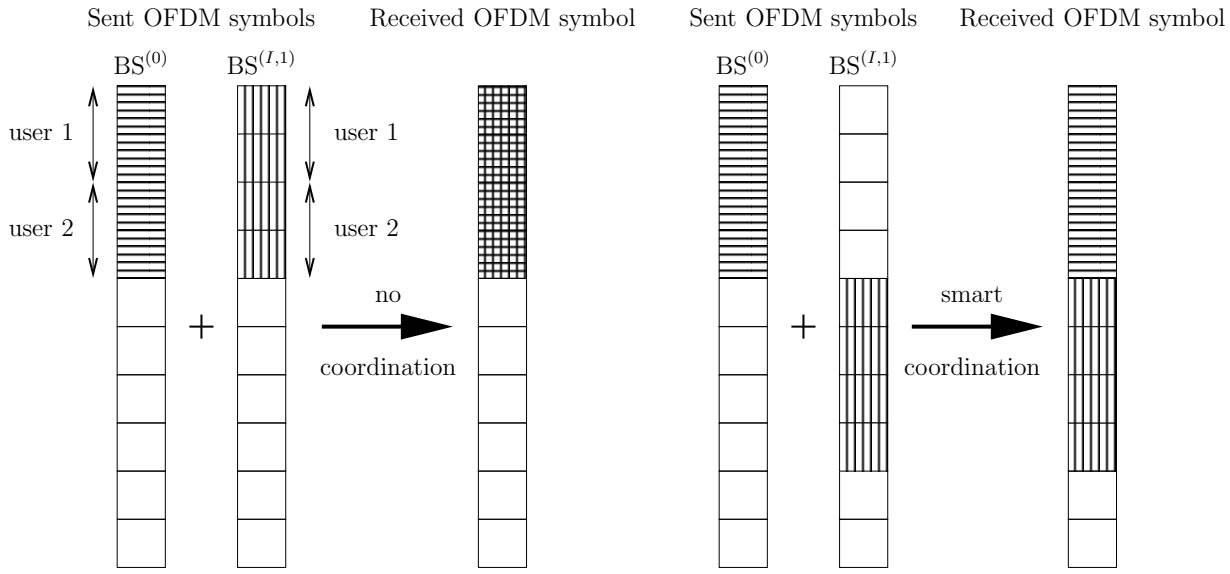

(a) Received symbol of 2 active users per BS

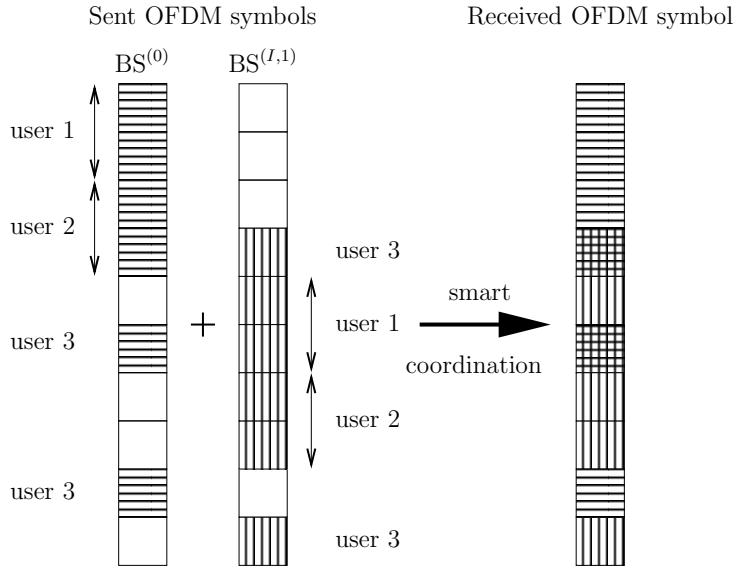

(b) Received symbol of 3 active users per BS

Figure 4.1: Coordination of sub-carriers with $m_{\text{coord}} = 2$ for OFDMA

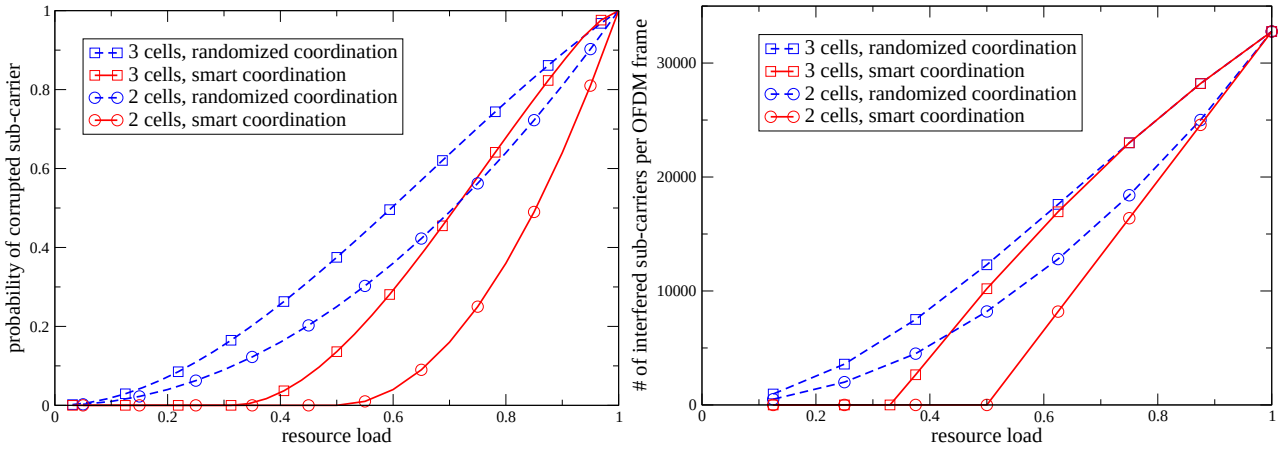

(a) Theoretical probability of a corrupted sub-carrier

(b) Interfered sub-carriers per simulated OFDMA frame in cellular environment

Figure 4.2: Corrupted sub-carrier distributions for *smart* and *randomized* coordination for 2 and 3 coordinated cells depending on the resource load in OFDMA

The probability that an assigned sub-carrier in the desired cell is corrupted by an interfering sub-carrier is

$$p_{\text{rand}}(m_{\text{int}}, N_{\text{u}}) = p_{\text{r}}(N_{\text{u}})\,(1 - p_{\text{r}}(0, N_{\text{u}}))\ . \tag{4.4}$$

Smart coordination: Since this coordination scheme uses knowledge for the sub-carrier allocation, the sub-carriers of users N_{u} up to

$$N_{\text{u,M}} = \lfloor (N_{\text{c}}/m_{\text{coord}})/N_{\text{d}} \rfloor \tag{4.5}$$

are allocated in such a way that no sub-carrier is corrupted in the system. The residual sub-carriers are randomly allocated for the remaining users. The probability of a random allocated sub-carrier for the residual user $N_{\text{u,R}}$ becomes

$$p_{\text{s}}(N_{\text{u,R}}) = \frac{N_{\text{d}} \cdot N_{\text{u,R}}}{N_{\text{c}}(m_{\text{coord}} - 1)/m_{\text{coord}}}\,, \quad \text{for } 1 \le N_{\text{u,R}} \le N_{\text{u,max}} - N_{\text{u,M}}\,. \tag{4.6}$$

The probability for the same allocated sub-carrier of m_{int} managed interfering cells is given by

$$p_{\text{s}}(m_{\text{int}}, N_{\text{u,R}}) = \binom{m_{\text{coord}} - 1}{m_{\text{int}}} p_{\text{s}}(N_{\text{u,R}})^{m_{\text{int}}}\,(1 - p_{\text{s}}(N_{\text{u,R}}))^{m_{\text{coord}}-1-m_{\text{int}}}\ . \tag{4.7}$$

Finally, for $0 \le N_{\text{u}} \le N_{\text{u,max}}$ the probability of a corrupted sub-carrier which was allocated in the desired cell is

$$p_{\text{smart}}(m_{\text{int}}, N_{\text{u}}) = \begin{cases} 0 & \text{for } 0 \le N_{\text{u}} \le N_{\text{u,M}} \\ p_{\text{s}}(N_{\text{u,R}})\,(1 - p_{\text{s}}(0, N_{\text{u,R}})) & \text{for } N_{\text{u,R}} \end{cases}\,, \tag{4.8}$$

where $1 \le N_{\text{u,R}} \le N_{\text{u,max}} - N_{\text{u,M}}$ and $N_{\text{u}} = N_{\text{u,M}} + N_{\text{u,R}}$.

Figure 4.2(a) shows the probability of a corrupted sub-carrier by increasing the resource load of an arbitrary OFDMA system using both coordination schemes. These results are validated by simulations of a two-cell and three-cell OFDMA environment in Figure 4.2(b). As assumed, the *smart* coordination can avoid double allocations of sub-carriers up to RL_{free} in contrast to the performance of the

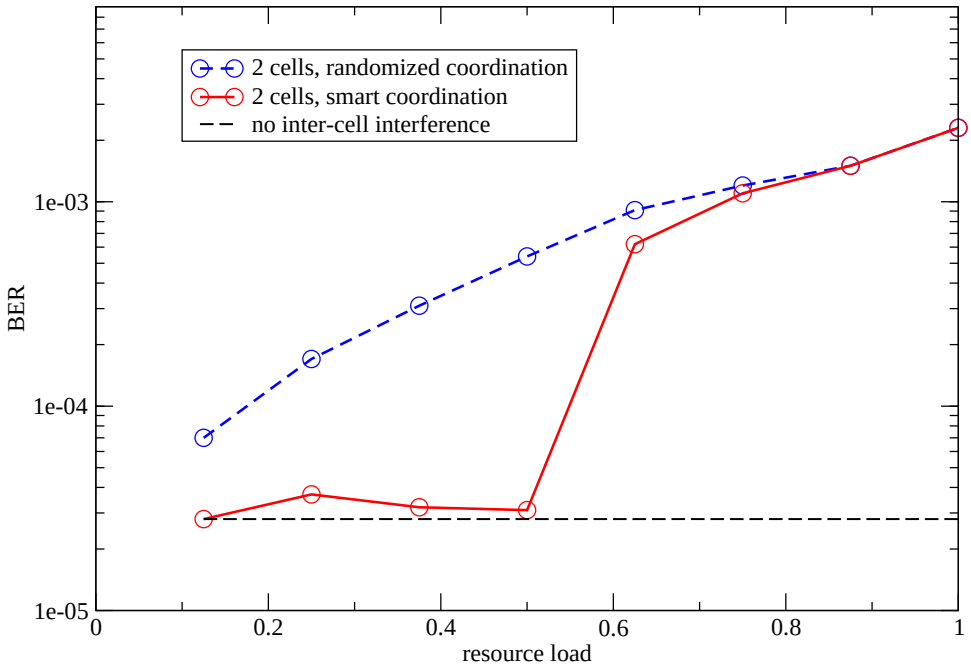

Figure 4.3: BER versus resource load using sub-carrier coordination schemes in a two-cell OFDMA environment; $\gamma_{i,\mathrm{dB}} = 10$ dB, $C/I = 10$ dB

randomized coordination. Consequently, all sub-carriers are interfered by a fully-loaded scenario. The *smart* coordination scheme should improve the performance of an cellular OFDMA system for RLs smaller than $1/m_{\mathrm{coord}}$.

As an example of the performance behavior by applying the sub-carrier coordination schemes, Figure 4.3 shows results of an OFDMA system in a two-cell environment applying *System A*. The BER is plotted as a function of the RL for the two coordination schemes. As expected from the results in Figure 4.2, the *smart* coordination can ensure the maximum performance up to a half-loaded system in each cell. Furthermore, the randomized assignment for higher RLs prevents a direct adaptation to the *randomized* coordination performance. The performance of the system without any interfering cell represents the maximum performance, and therefore, a lower bound of the system.

In the following, the *randomized* coordination is not considered as a coordination component for the OFDMA system design because this sub-carrier allocation technique needs no additional knowledge from neighboring cells. Therefore, using the term coordination represents the *smart* coordination scheme.

4.1.1 Comparing MC-CDMA and OFDMA

In contrast to OFDMA, MC-CDMA averages the total transmitted signal power over all used sub-carriers. Therefore, the inter-cell interference is averaged at the desired receiver. On the other hand, the sub-carrier coordination approaches for OFDMA also try to avoid burst sub-carrier interference. Furthermore, the spreading component in MC-CDMA guarantees an exploitation of frequency diversity but MAI causes performance degradations. These main characteristics will influence the overall cellular performances. In the following the two GMC based transmission schemes are investigated in terms of BER and throughput performances for different scenarios.

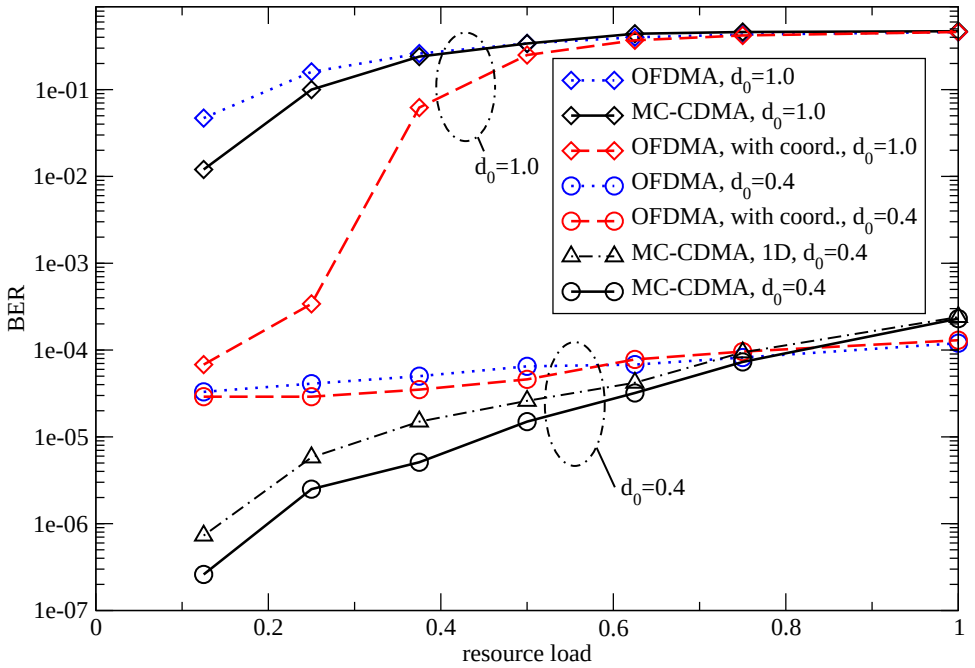

Figure 4.4: BER versus resource load for MC-CDMA and OFDMA in a cellular environment for two different d_0; $\gamma_{i,\mathrm{dB}} = 10$ dB, $N_{\mathrm{BS}} = 7$

A first direct comparison between OFDMA and MC-CDMA in a cellular environment (*System A*) is shown in Figure 4.4, where the BER versus the RL is presented. Since the number of active users, the maximum number of users, the data symbols per user, and the frame size are equal, the comparison of the systems is fair. Two scenarios are illustrated.

First scenario, $d_0 = 0.4$: Since the interference is negligible for $d_0 \leq 0.4$ (cf. Figure 3.3), the coordination does not enhance the OFDMA performance. And in spite of the increasing C/I for lower RLs, the OFDMA performance keeps almost constant by increasing the RL in contrast to the performance of MC-CDMA. For small RLs, MC-CDMA outperforms OFDMA by far because MC-CDMA can utilize the whole diversity of all assigned sub-carriers. The benefit of MC-CDMA reduces with increasing RL because the MAI increases for higher RLs.

Second scenario, $d_0 = 1.0$: The MS is at the cell boundary, where two interfering BS are at the same distance as the desired BS. Thus, the cellular interference is maximal. Only in a small region of lower RLs MC-CDMA gains in comparison to pure OFDMA without coordination. For a RL of $3/8$, the performances are equal. OFDMA with coordination has a huge performance gain up to a $\mathrm{RL} = 3/8$. The sub-carrier coordination can avoid any collision with the major interfering signals from the neighboring cells up to a $\mathrm{RL} = 1/3$.

In Figure 4.4 it is shown that also in a cellular environment an additional diversity gain can be given by using an random interleaving over the whole transmitted frame. This is represented by the performance loss using a 1D interleaving for Π_{in} (cf. Section 2.2.2), instead of a 2D interleaving for the $d_0 = 0.4$ scenario. The additional diversity gain, due to 2D interleaving, is more significant when the MAI decreases for lower RLs. For higher RLs, the performances for 1D and 2D interleaving merge.

A strong disturbance by the adjacent interfering cells exists in the peripheral area of the desired cell (cf. Section 3.1). In contrast, the core of the desired cell ($d_0 \leq 0.4$) obtains a minimum of interference. Therefore, a huge performance degradation between the two scenarios $d_0 = 0.4$ and $d_0 = 1.0$ is existent in Figure 4.4. In the same way, the performances of Figure 4.5 are influenced.

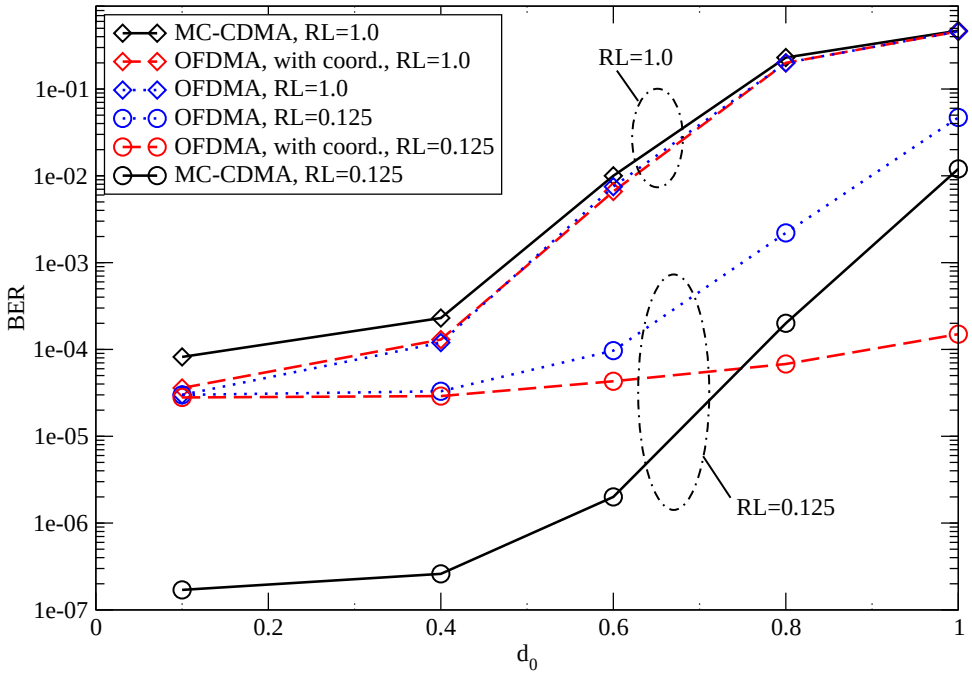

Figure 4.5: BER versus d_0 for MC-CDMA and OFDMA in a cellular environment for two different resource loads; $\gamma_{i,\mathrm{dB}} = 10$ dB, $N_{\mathrm{BS}} = 7$

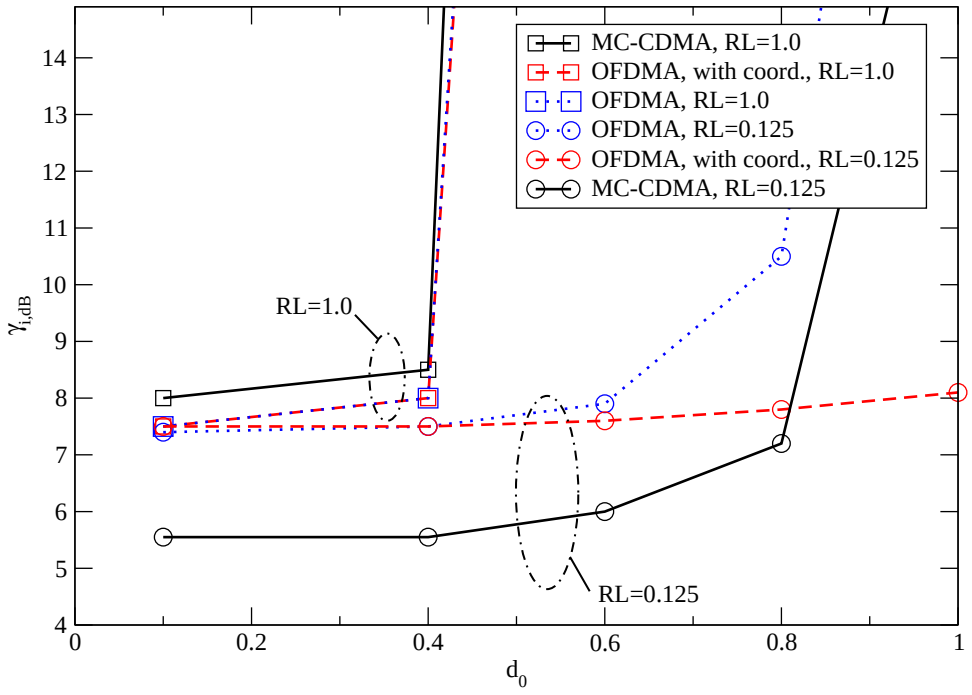

Figure 4.6: SNR $\gamma_{i,\mathrm{dB}}$ versus d_0 for a target BER of $P_{\mathrm{b}} = 10^{-3}$ for MC-CDMA and OFDMA in a cellular environment for two different resource loads

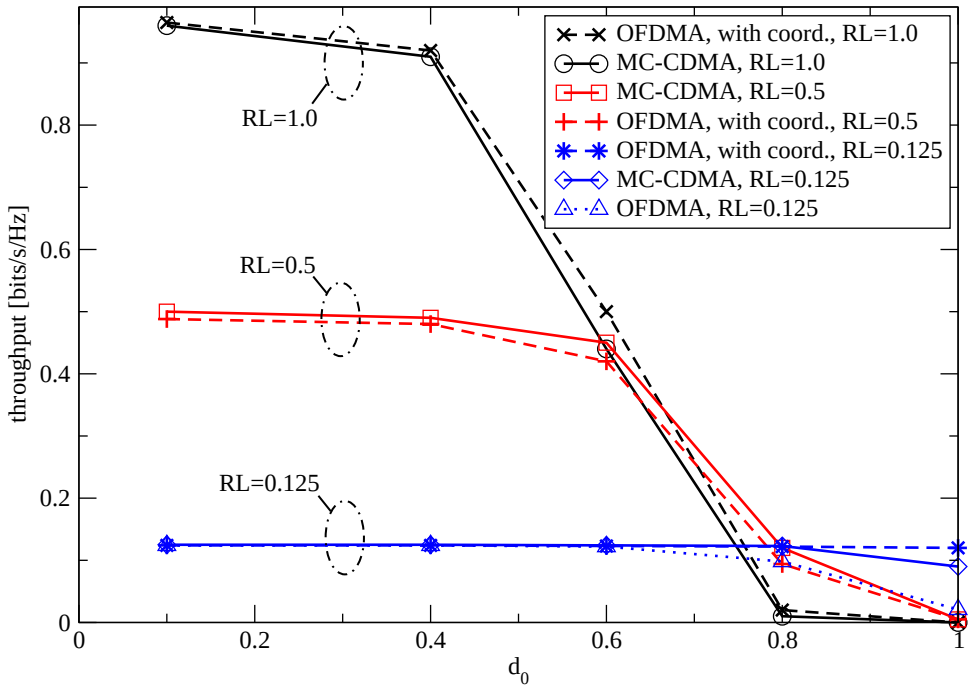

Figure 4.7: Throughput versus d_0 for MC-CDMA and OFDMA with coordination for three different resource loads; $\gamma_{i,\mathrm{dB}} = 10\ \mathrm{dB}$, QPSK

The BER is plotted as a function of the distance d_0 for different transmission schemes in the same multi-cell environment. The performances show a distinctively steeper slope for $d_0 > 0.4$.

The performance for OFDMA with coordination and an $\mathrm{RL} = 1/8$ in Figure 4.5 keeps roughly constant because no sub-carriers are doubly allocated due to the coordination scheme. A small performance loss exists, resulting from the higher inter-cell interference. Again, MC-CDMA outperforms OFDMA for $\mathrm{RL} = 1/8$ in the inner cell area up to $d_0 = 0.75$. In contrast, OFDMA slightly exceeds the MC-CDMA performance in the fully-loaded scenario because the MAI is the major degradation factor of MC-CDMA. Since all sub-carriers are allocated in the fully-loaded case, there is no difference between OFDMA with and without coordination.

Figure 4.6 shows performances of the two systems in terms of the required SNR $\gamma_{i,\mathrm{dB}}$ in all cells for achieving a target BER of $P_\mathrm{b} = 10^{-3}$ for different resource loads. The performances are illustrated for $\gamma_{i,\mathrm{dB}}$ versus the position of the MS. The fully-loaded scenario shows that only in the core of the cell the target BER can be reached by an $\gamma_{i,\mathrm{dB}}$ between $7.5\ \mathrm{dB}$ and $8\ \mathrm{dB}$ for OFDMA. MC-CDMA looses $0.5\ \mathrm{dB}$ versus OFDMA because of the high MAI.

In the case of $\mathrm{RL} = 1/8$, the target BER can be achieved in the whole cell for OFDMA with coordination. At the edge of the cell, MC-CDMA and pure OFDMA cannot provide the BER. OFDMA with coordination needs a higher $\gamma_{i,\mathrm{dB}}$ up to $d_0 = 0.8$ than MC-CDMA. Furthermore, OFDMA has the same SNR level as in the fully-loaded case. In contrast, MC-CDMA can gain up to $2\ \mathrm{dB}$ compared to OFDMA.

Finally, we investigate the throughput of the systems and compare MC-CDMA with OFDMA including the sub-carrier coordination scheme. The investigations are limited to the higher medium access control (MAC) layer automatic-repeat-request (ARQ) scheme [LCM84]. The fully-loaded *System A* has a maximum throughput of

$$\eta_{\max} = M_{\mathrm{mod}} \cdot R \cdot N_\mathrm{c}/T_\mathrm{s}/B\,, \tag{4.9}$$

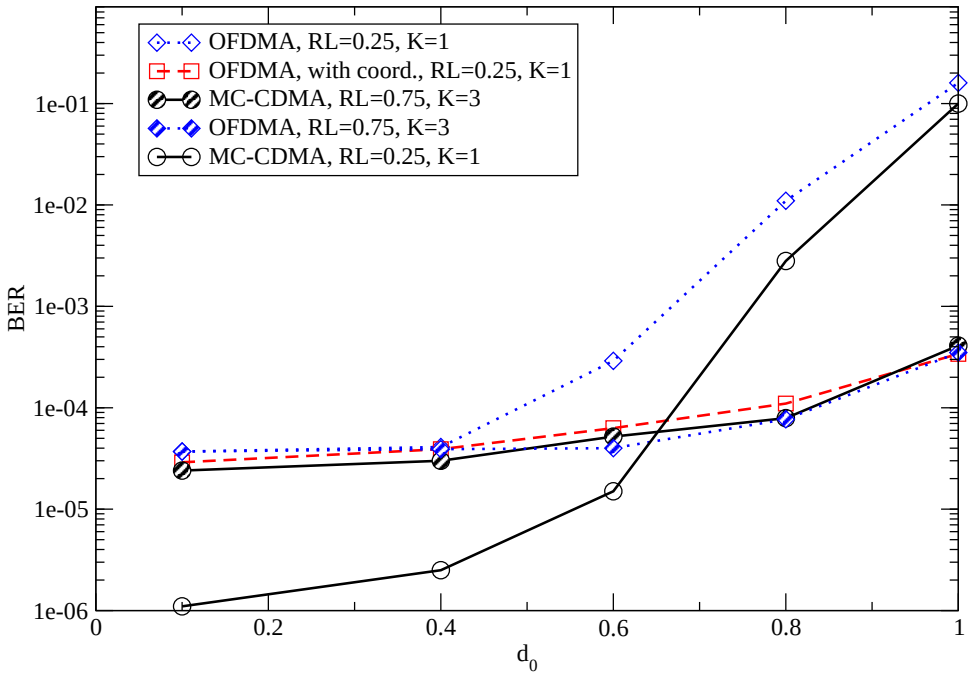

Figure 4.8: BER versus d_0 for MC-CDMA and OFDMA in a cellular environment for two different frequency reuse factors K; $\gamma_{i,\mathrm{dB}} = 10$ dB

which is approximately $\eta_{\max} = 1\,\mathrm{bits/s/Hz}$ by using QPSK with cardinality $M_{\mathrm{mod}} = 2$, a code rate of $R = 1/2$, $N_{\mathrm{c}} = 768$ sub-carriers, an OFDM symbol duration of $T_{\mathrm{s}} = 7.58\ \mu\mathrm{s}$, and a used broadband bandwidth of $B = 101.25$ MHz. Since the total number of sub-carriers is equally distributed to the maximum number of users per cell, each user has a maximum throughput of $\eta_{\max}$. The throughput η of the system, by using the probability $P(k)$ of the first correct frame transmission after $k-1$ failed retransmissions, is given by

$$\eta = \sum_{k=0}^{\infty} \frac{\eta_{\max}}{k+1} P(k) \geq \eta_{\max}(1 - \mathrm{FER})\,. \tag{4.10}$$

A lower bound of the system is given by the right hand side of (4.10) by only considering $k = 0$ and the frame error rate (FER). This lower bound is illustrated in Figure 4.7. The throughputs of both systems have similar performances and match the characteristics of the above-mentioned investigations for $\mathrm{RL} = 1/2$ and $\mathrm{RL} = 1$. Due to the exploitation of the frequency diversity, MC-CDMA with $\mathrm{RL} = 1/8$ can provide the maximal effective throughput, except at the cell border. OFDMA can also achieve the maximum effective throughput but only by using the coordination scheme. Without coordination, the throughput of OFDMA degrades almost to zero in the peripheral area of the cell.

4.1.2 Hybrid Cell Partitioning Concept

The large performance degradation at the cell border can be circumvented by introducing a larger frequency reuse factor K than 1. This will avoid the inter-cell interference but also reduces the overall spectral efficiency of the system. In the following, the concept of different frequency reuse factors is investigated by comparing MC-CDMA and OFDMA.

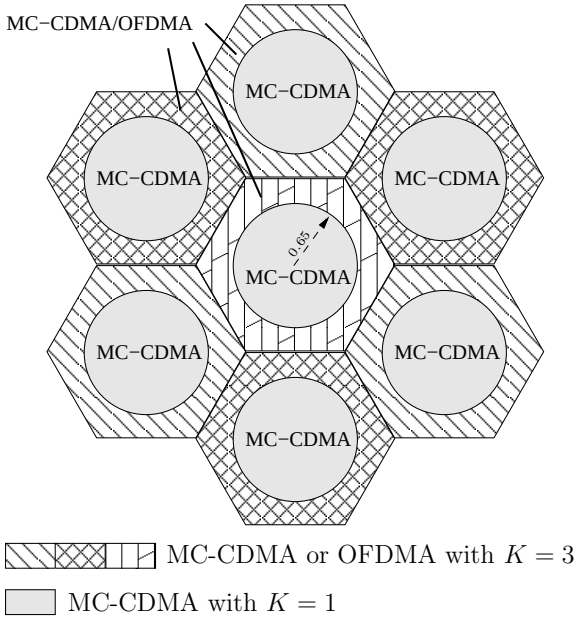

Figure 4.9: Hybrid partitioned cellular structure for MC-CDMA and OFDMA

Performances for two different frequency reuse factors K are shown in Figure 4.8. To provide the same spectral efficiency in the cellular radio systems, $\mathrm{RL} = 1/4$ for $K = 1$ and $\mathrm{RL} = 3/4$ for $K = 3$ are chosen. For $K = 1$, MC-CDMA exploits the whole sub-carrier diversity, and therefore, it outperforms pure OFDMA and also OFDMA with coordination in the inner cell up to $d_0 = 0.65$. Since the RL for $K = 3$ is higher than $\mathrm{RL}_{\mathrm{free}} = 1/3$, no coordination scheme is assumed in the OFDMA system. Due to the trade-off between sub-carrier diversity and increased MAI for higher RLs, the performance of MC-CDMA almost match the pure OFDMA performance for $K = 3$. The two performances show a small degradation towards the cell edge through the increasing inter-cell interference. Furthermore, OFDMA with coordination for $K = 1$ can avoid inter-cell interference and performs equal to $K = 3$.

For future cellular systems, there will always be the trade-off between spectral efficiency and performance as seen in these results. For achieving the best error performance, a partitioning of the cell in two zones is proposed with respect to the lower bounds of the system performance. Therefore, a hybrid structure is obtained: an inner zone with bandwidth B_1 and an outer zone with bandwidth B_2. The inner zone should be served with $K = 1$ and MC-CDMA. To reduce inter-cell interference for $d_0 \geq 0.65$, the outer zone shares B_2 among the other cells with a frequency reuse factor of 3. The partitioning pattern is illustrated in Figure 4.9. Therefore, the spectral efficiency for the total bandwidth B is reduced by a factor of $(B_1 + 1/3 \cdot B_2)/B$. The outer zones can be served by OFDMA or MC-CDMA.

It has to be stated, that OFDMA can only outperform significantly MC-CDMA by applying a sub-carrier coordination scheme. The performance degradation of MC-CDMA in the fully-loaded case is minimal. Nevertheless, the coordination schemes demand a large communication complexity between the centralized coordination unit of the affected BSs. In contrast, MC-CDMA does not rely upon a coordination scheme. Furthermore, MC-CDMA generates a beneficial averaged inter-cell interference without bursting single sub-carriers. MC-CDMA also provides redundancy due to the spreading component, and therefore, it supports the possibility to cancel the arising inter-cell interference at the cell border which is discussed in Chapter 5.

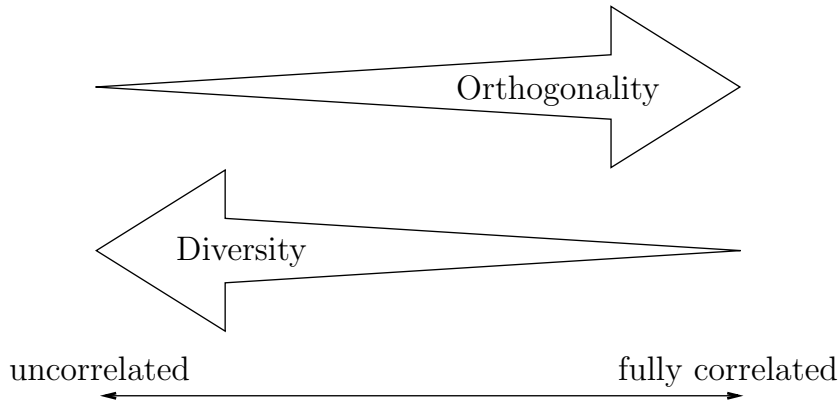

Figure 4.10: Contrariness of diversity and orthogonality regarding the correlation properties

4.2 Spreading Code Coordination

The MC-CDMA transmission scheme provides an additional orthogonal resource, i.e., the orthogonal set of used spreading codes. Therefore, the idea of a coordination scheme for MC-CDMA is using different spreading codes to avoid inter-cell interference in the managed cells.

On the one hand, at the receiver the orthogonality between used user-specific Walsh-Hadamard spreading codes is not preserved by uncorrelated fading properties but frequency diversity is given. On the other hand, if the channel fading coefficients are correlated, the orthogonality is preserved [Pro95]. Real channel scenarios show correlations in time and frequency direction. There exist two extreme situations:

- The channel coefficients in an OFDM frame are uncorrelated in time and frequency:
  This provides maximal diversity but destroys the orthogonality between spreading codes of different cells. Without any pre-equalization this orthogonality cannot be recovered by equalization methods. Coordinating the resources between neighboring cells by using different spreading codes in different cells does not improve the performance for that reason.
- The channel coefficients in an OFDM frame are fully correlated (flat) in time and frequency:
  This provides minimal diversity, but maintains orthogonality, even between cells and a coordination over different spreading codes can be used.

Both orthogonality and diversity increase the system performance if they are increasing. However, with respect to multi-path channel fading correlation orthogonality and diversity are counteracting (see the two extreme situations mentioned above and Figure 4.10). Therefore, it is interesting to investigate the system performance for channel scenarios, showing different correlation properties. For these investigations, an academic Rayleigh fading channel with adjustable correlation properties is used (cf. Section 2.1.2). Performance results are also given including a realistic channel model which is partly correlated.

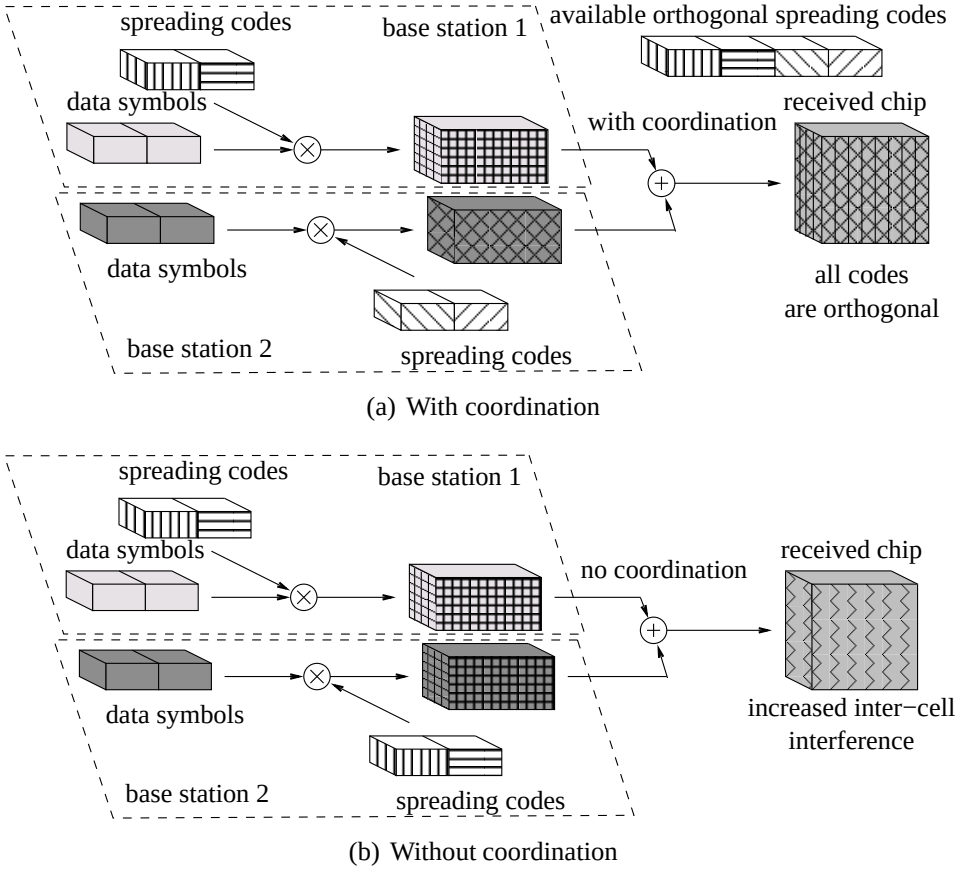

Figure 4.11: Coordination over spreading codes with $m_{\mathrm{coord}} = 2$ for MC-CDMA

4.2.1 Coordination Management over Spreading Codes

In the following, the coordination strategy over the used spreading codes with in the coordinated cells m_{coord} is given. As in the case of the sub-carrier allocation coordination for OFDMA, perfect knowledge about the available and allocated spreading codes for MC-CDMA in the coordinated cells is assumed. Each managed cell can assign up to

$$L_{\mathrm{free}} = \lfloor L/m_{\mathrm{coord}} \rfloor \tag{4.11}$$

spreading codes to N_{u} active users without allocating the same spreading code to different users. These users can transmit within the coordinated cells without disturbing each other if the orthogonality of the spreading codes at the receiver is preserved. By exceeding this number of spreading codes, the succeeding assignment of spreading codes is done randomly. Therefore, a total disturbance of one user is avoided. The procedure of using the available orthogonal spreading codes in different cells for the spreading code coordination scheme is shown in Figure 4.11(a) for the case of two managed cells. In contrast, Figure 4.11(b) shows a scenario without any coordination. Here, the codes of the superimposed received chips disturb each other Therefore, the spreading codes of the different cells are not orthogonal anymore and the inter-cell interference is increased.

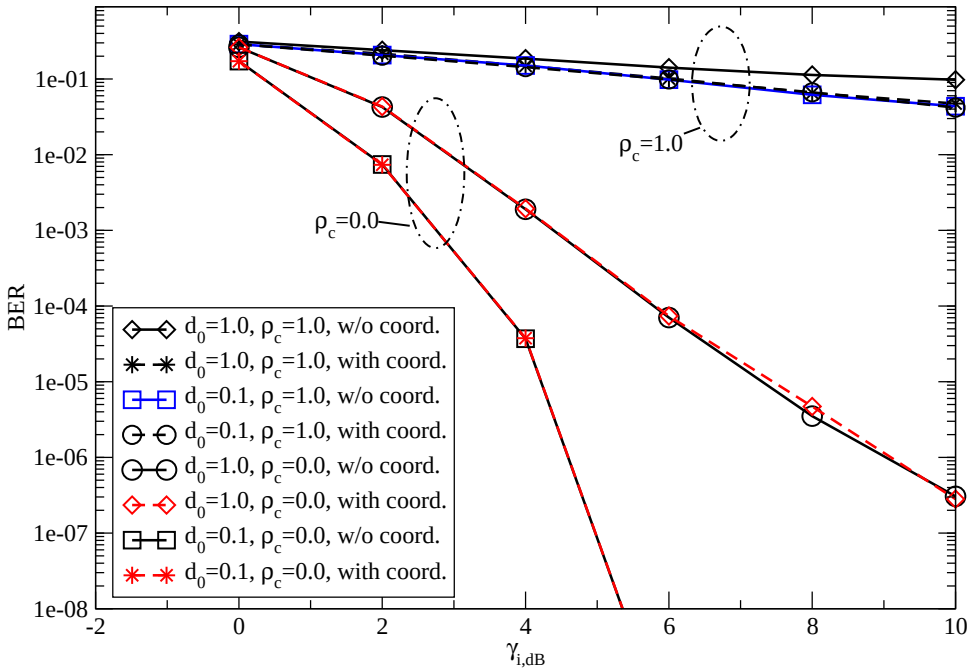

Figure 4.12: BER versus SNR $\gamma_{i,\mathrm{dB}}$ for varying MS locations and ρ_c; $\mathrm{RL} = 1/16$

4.2.2 Impact of Spreading Code Coordination

The influence on the diversity losses and gains due to the correlation properties for using the spreading code coordination is investigated for a cellular setup with one tier of interfering cells. The two closest interfering cells to the desired MS are coordination with the desired BS, i.e., $m_\mathrm{coord} = 3$. The residual cells of the interfering cellular structure are not taken into account for coordination due to their negligible influence on the overall performance (cf. Section 3.1). If the channel is fully correlated, the coordination scheme should guarantee inter-cell interference free transmission up to a resource load of $1/3$. The *System A* parameter setup is chosen for the simulations with a spreading length $L = 16$. For the first investigations, the correlated Rayleigh fading channel is taken (cf. Section 2.1.2).

Figure 4.12 shows results regarding the bit error rate performance versus the SNR $\gamma_{i,\mathrm{dB}}$ for the single-user case ($\mathrm{RL} = 1/16$). In the case of fully-correlated Rayleigh fading channels ($\rho_\mathrm{c} = 1.0$), the coordination scheme enables to enhance the performance by approximately $2\ \mathrm{dB}$ at the cell edge ($d_0 = 1.0$). Since the inter-cell interference in the inner area ($d_0 = 0.1$) of the desired cell is negligible (cf. Section 3.1), the performances with and without spreading code coordination are equal and the performance at the cell edge with managed spreading codes matches the non-interfered case of the inner cell. For the uncorrelated channels, there is no difference between the coordinated system and the non-coordinated one due to the lost orthogonality. For all scenarios without coordination, the performances degrade for higher correlation factors because of less diversity.

This can be also seen in Figure 4.13 where the figure shows the BER versus the correlation factor ρ_c. Furthermore, all three scenarios with different RLs ($\mathrm{RL} = [1/16, 3/16, 5/16]$) show a gain by using the coordination scheme for higher correlated Rayleigh fading channels. The performances can be enhanced for $\rho_\mathrm{c} > 0.2$. Obviously, a higher RL degrades the performances because the desired spreading code is corrupted by the other active spreading codes including the codes from the interfering cells. In the case of $\mathrm{RL} = 5/16$ inter-cell interference can be still avoided, and therefore, the coordination improves the performance up to the single-user scenario for fully-correlated Rayleigh

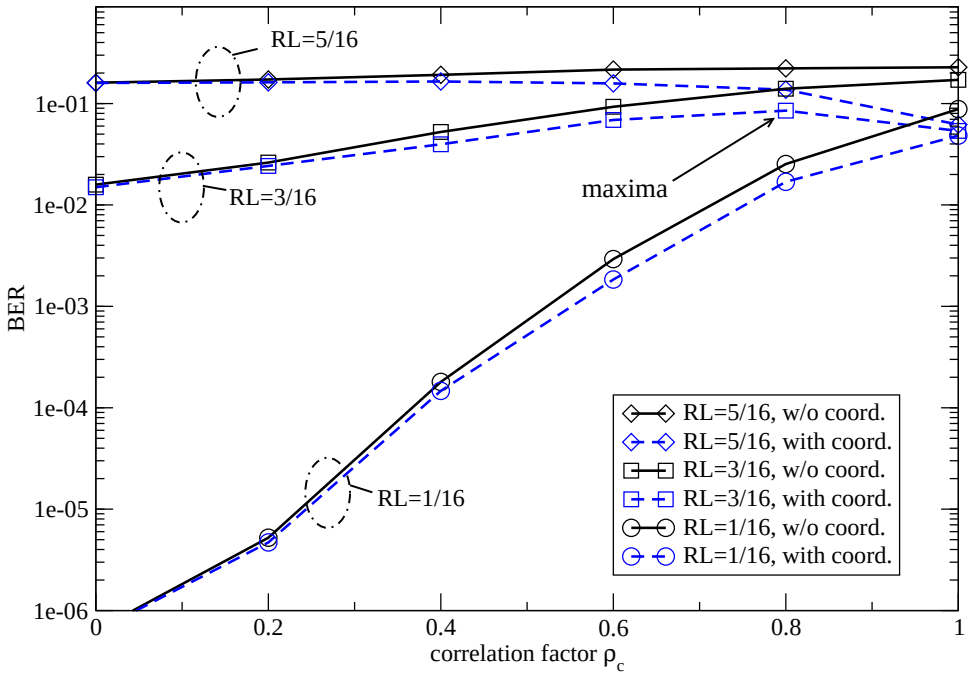

Figure 4.13: BER versus ρ_c for different RLs; $\gamma_{i,\mathrm{dB}} = 10\,\mathrm{dB}$, $d_0 = 1.0$

fading channels. The contrariness of diversity and orthogonality is well visible at the local maxima of the spreading code coordination performance for $\mathrm{RL} = 3/16$. For less correlated scenarios, the frequency diversity is beneficial for the performance and for higher correlated scenarios, the orthogonality can avoid performance degradation due to inter-cell interference.

The simulation results in Figure 4.14 show the BER versus the RL. Two different scenarios are investigated, namely with $\rho_\mathrm{c} = 0.5$ and $\rho_\mathrm{c} = 1.0$. It is obvious that the performances with or without spreading code coordination are close-by for a less correlated Rayleigh fading channel ($\rho_\mathrm{c} = 0.5$). In contrast, the coordination scheme can ensure the maximum performance up to a $1/3$-loaded system in each cell. Furthermore, the randomized assignment of spreading codes for higher RLs prevents a direct adaptation to the performance without coordination.

The academic approach by artificially varying of the channel correlation properties show the capabilities of the coordination scheme using the orthogonal spreading codes within a cellular setup. If the full orthogonality between the coordinated resources is given, the inter-cell interference can be avoided for maximal L_free spreading codes. Since in realistic mobile radio channel the neighboring sub-carriers are not fully correlated or even totally uncorrelated, the benefits of the spreading code coordination are investigated for a real scenario in the following.

For the simulations in Figure 4.15 the parameters of *System A* and the IEEE channel 802.11n Model C of *System B* are chosen. Three different positions of the MS show the influence of the BER versus the resource load. Obviously, the higher the resource load the larger the performance degradation due to the increased MAI. For resource loads smaller than $1/m_\mathrm{coord}$ a performance gain is given for the MC-CDMA system with coordination over the used spreading codes. Due to the increased inter-cell interference for larger d_0, the coordination scheme gains more in peripheral cell areas. It is also visible that a small benefit is given for larger RL than $1/m_\mathrm{coord}$. On the other side, the performance gains of the spreading code coordination scheme in a realistic scenario are not dramatic. The real channel does not provide the extreme and beneficial case of fully correlated sub-carriers, and therefore, the coordination scheme cannot significantly improve the overall performance.

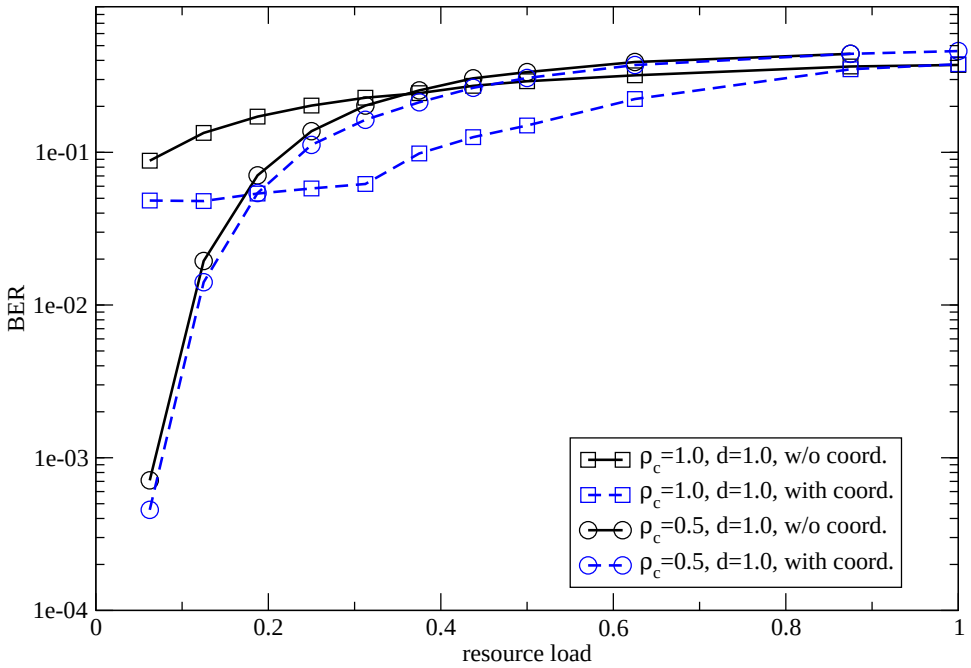

Figure 4.14: BER versus RL for varying ρ_{c}; $\gamma_{i,\mathrm{dB}} = 10$ dB, $d_0 = 1.0$

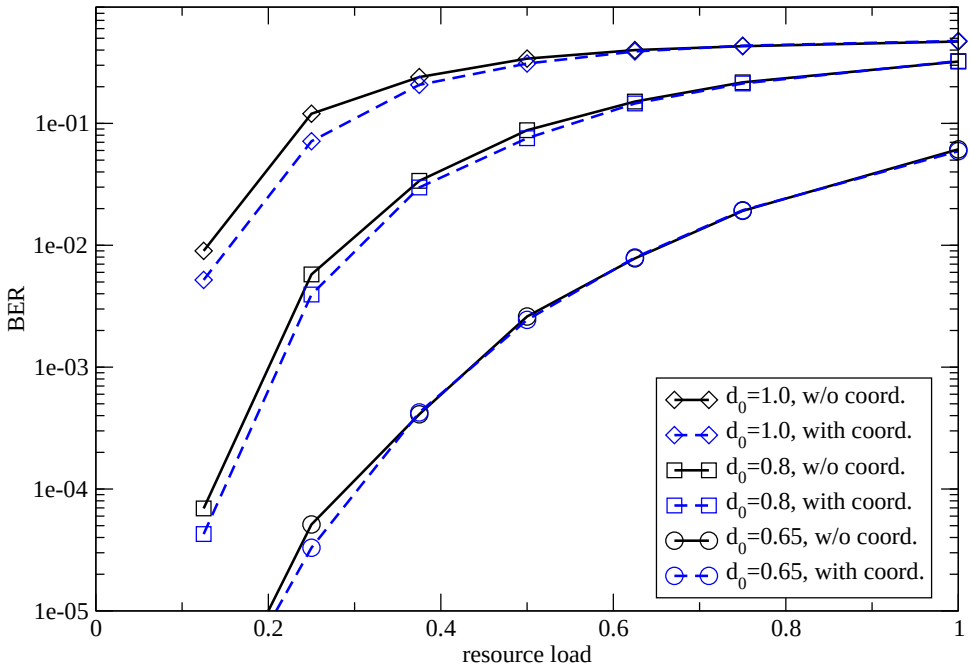

Figure 4.15: BER versus RL for different MS locations; $\gamma_{i,\mathrm{dB}} = 10$ dB

4.3 Summary

Two main orthogonal resources of cellular MC-CDMA are investigated to coordinate and avoid inter-cell interference in this chapter. The first is based on frequency coordination between the neighboring cells to avoid inter-cell interference. The other scheme utilizes the given orthogonal set of spreading codes in MC-CDMA.

Since the elementary GMC scheme, namely OFDMA, provides a simple and flexible allocation of the orthogonal sub-carrier resources, OFDMA is taken as a challenging comparative transmission system for MC-CDMA. Therefore, a *smart* sub-carrier coordination scheme for OFDMA is introduced which has the perfect knowledge of the allocated sub-carriers in the cellular system but does not take into account *a priori* information of the channel at the transmitter. The scheme tries to avoid burst inter-cell interference, but cannot entirely circumvent it. In contrast, MC-CDMA cannot coordinate on sub-carrier basis the frequency resources due to the spreading component. Therefore, MC-CDMA averages the influence of the inter-cell interference and excludes burst interference characteristics. On the other side, MC-CDMA suffers from MAI.

The simulations show that MC-CDMA can outperform ordinary OFDMA in the case of varying resource loads. In the core of the cell, MC-CDMA exploits the whole sub-carrier diversity and outperforms OFDMA for resource loads smaller than $3/4$. The use of the coordination scheme for OFDMA can highly enhance the OFDMA performance in the peripheral cell area and OFDMA surpasses the MC-CDMA performance. Regarding the SNR behavior at a target BER of $P_\mathrm{b} = 10^{-3}$, the simulation results present a $0.5\ \mathrm{dB}$ gain for OFDMA compared to MC-CDMA in a fully-loaded system. In contrast, MC-CDMA can gain up to $2\ \mathrm{dB}$ in a lower-loaded system. Pure OFDMA cannot provide any considerable throughput at the cell border in a cellular environment in contrast to MC-CDMA. To summarize, MC-CDMA outperforms pure OFDMA in most of the scenarios and in some cases even OFDMA with the *smart* coordination scheme. However, the coordination scheme for OFDMA demands a large communication complexity between the affected BSs. The MC-CDMA system does not rely upon a coordination scheme.

In contrast to a frequency reuse of one, inter-cell interference can be avoided in the outer parts of the cell by using a frequency reuse of three. In exchange, this concept has to put up with spectral loss. Therefore, a hybrid partitioning for the cell structure can achieve a maximum performance for the systems. The inner part of each cell is served by an MC-CDMA system with frequency reuse of one and the outer parts by OFDMA or MC-CDMA with frequency reuse of three.

A second source of orthogonal resources in a cellular MC-CDMA system are the spreading codes. Therefore, these codes can be coordinated within a cellular setup to avoid inter-cell interference. The investigations show the capability of the coordination scheme using orthogonal spreading codes. The degree of orthogonality depends directly on the correlation properties of the existing channels. Consequently, there exists a trade-off between diversity and orthogonality due to correlation characteristics. The benefit of using this coordination scheme for MC-CDMA depends directly on the degree of correlation within the channel characteristics of the cellular system.

Chapter 5

Cancellation of Inter-Cell Interference

Theoretically, gains from using inter-cell interference avoidance schemes are large [KFV06], but maximum gains would require fast and tight inter-cell coordination. For example, frequency partitioning in cellular networks on a slower time-scale [KN96] as well as the use of power control [FMM04], dynamic channel assignment, and channel borrowing has for a long period received interest. Note that the packet-switched channel-aware scheduled transmissions which will take place in future systems complicates the use of many of the previously suggested schemes for inter-cell interference avoidance or coordination (cf. Chapter 4). It is not, without additional side information, possible to conclude that the interference power in a set of sub-carriers is likely to be higher/lower than average just because it is measured as high/low at present. Therefore, due to the orthogonally spread data symbols and the resulting redundancy in the transmission the spread spectrum technique MC-CDMA provides the possibility to iteratively remove the inter-cell interference at the receiver side without the need of high complex inter-cell interference management schemes from the network side. Therefore, in this chapter, inter-cell interference cancellation (ICIC) concepts are introduced.

Due to the larger complexity of the ICIC concept, this technique can be applied at receivers with the available processing capabilities. This provides a unique selling point for MS vendors. Furthermore, ICIC techniques avoid large configurations at the transmitter side, namely, the base stations and network. By applying ICIC the resulting performance improvement can be utilized requesting a higher coding-and-modulation scheme, and therefore, to the user's benefit the data throughput will be increased.

Two main approaches of general interference cancellation exist: first, successive interference cancellation (SIC) [RLJ00]; second, parallel interference cancellation (PIC) [DSR98]. For MC-CDMA, these concepts focused on single-cell environments in the past, and therefore, the goal was to reduce or to cancel iteratively the MAI [KH97, FK03]. A high latency is given for SIC schemes and error propagation effects can occur if initial user estimates are erroneous. On the other side, PIC schemes require higher memory and a large signal processing in parallel. Since the storage capacities are not so critical nowadays and a low latency is preferred, the PIC principles are applied for the following ICIC concepts. These ICIC techniques do not take into account the MAI but the inter-cell interference. The MAI could be removed as described in [KH97] afterwards.

For ICIC concepts at the receiver, the signaling information of the neighboring cells has to be given. Since a user requires the signaling from its desired BS over the whole desired cell area, an orthogonal signaling design is provided in a cellular system. Different interleavers in cellular MC-CDMA can also feature a cell-specific sub-carrier assignment for cell separation like the scrambling code for UMTS [HT04]. Note that the less Gaussian a signal is, the better the signal can be detected and

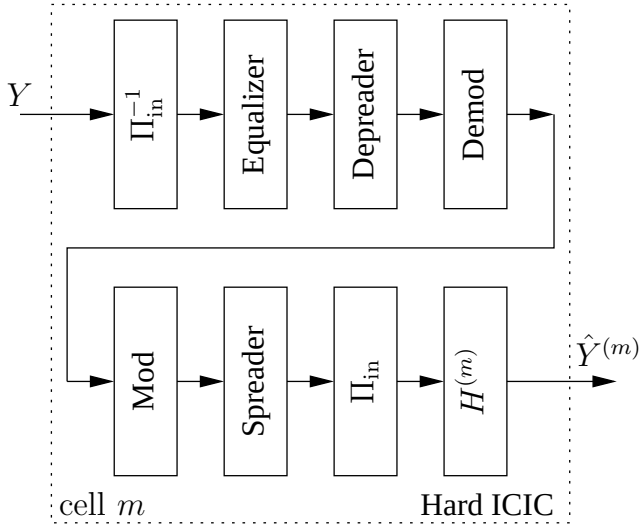

Figure 5.1: Concept of the hard ICIC

canceled [Ver98]. The major inter-cell interference is generated by the two closest interfering cells and the overall impinged signal is Gaussian-like for more than two cells (cf. Chapter 3). Therefore, a cellular MC-CDMA system satisfies the general demands of ICIC concepts.

In this chapter, different approaches of ICIC techniques are given and investigated. First, the hard decisions from the demodulator are used for the *hard* ICIC process. Varying combinations of hard ICICs are studied where the information of the received interfering signal power is included. Additional, an iterative ICIC technique based on soft values is presented in more detail which is named *soft* ICIC [9, 1]. The impact on the performance is investigated and the choice of interfering cells to be canceled [5]. The extrinsic information of the decoding process is considered as a degree of reliability for the soft ICIC process [1]. Further, the mutual information exchange between the inner and outer decoder is investigated with extrinsic information transfer (EXIT) charts [8] to analyze the convergence behavior [7]. The performance of the different ICIC schemes is compared by means of simulations within the cellular environment of *System A*.

5.1 Hard Iterative Cancellation Techniques

A first approach of ICIC is based on the use of the hard output of the demodulator at the receiver to reproduce the interfering or desired signals $\hat{Y}^{(m)}$. This process is named *hard* ICIC. In [DL07] three different combinations of the hard ICIC are proposed. Simplified block diagrams of the hard ICIC and its combinations are shown in Figure 5.1 and Figure 5.2. Without loss of generality the sub-carrier and time indices l and i are skipped for notational convenience in the following. The proposed hard ICIC concepts in [DL07] are extended to more than one interfering cell. This is done by parallel processing of the reconstruction of the interfering signals ($m \neq 0$). All blocks are set up with their specific cell parameters. First, the *direct* hard ICIC (D-ICIC) with output

$$\hat{Y}_{\text{D}} = Y - \sum_{m=1}^{N_{\text{BS}}-1} \hat{Y}^{(m)} \tag{5.1}$$

can be seen as the basic concept block. Note that for the D-ICIC the processing of the interfering cells ($m \neq 0$) is used. The *indirect* hard ICIC (I-ICIC) tries to reconstruct the desired signal first and then

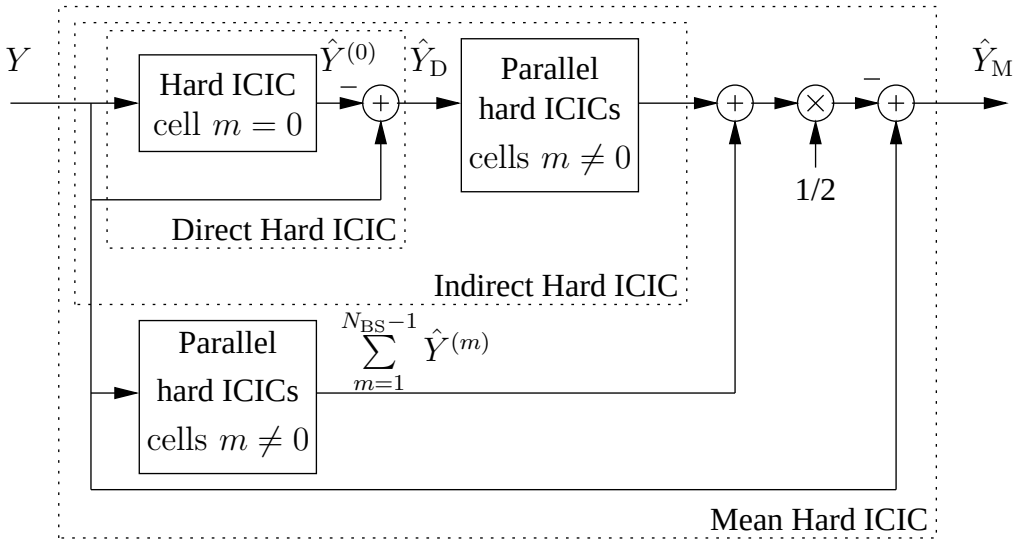

Figure 5.2: Combinations of hard ICICs

the interfering signals. It should be mentioned that the estimated interfering signals will be subtracted in the final step from the received signal Y in contrast to Figure 5.2. Therefore, the I-ICIC calculates

$$\hat{Y}_{\mathrm{I}} = Y - \sum_{m=1}^{N_{\mathrm{BS}}-1} \hat{Y}^{(m)}_{\hat{Y}^{(0)}}\,, \tag{5.2}$$

where $\hat{Y}^{(m)}_{\hat{Y}^{(0)}}$ represents the estimates depending on the first estimate $\hat{Y}^{(0)} = Y - \hat{Y}^{(0)}$. The *mean* hard ICIC (M-ICIC) combines the D-ICIC and I-ICIC concepts by

$$\hat{Y}_{\mathrm{M}} = Y - 0.5 \left(\sum_{m=1}^{N_{\mathrm{BS}}-1} \hat{Y}^{(m)}_{\hat{Y}^{(0)}} + \sum_{m=1}^{N_{\mathrm{BS}}-1} \hat{Y}^{(m)} \right). \tag{5.3}$$

All three concepts try to remove the inter-cell interference signals from the desired signal. In the final step the output of the hard ICIC is taken to be demodulated and decoded.

5.1.1 Combinations of Hard ICIC

In the following the results in [DL07] are verified by using the proposed hard ICIC concepts as described in Section 5.1. These hard ICIC techniques do not take into account the possible available signal powers for the equalization process. Figure 5.3 presents the BER performance versus the C/I ratio. The simulations are carried out with an SNR of $10\ \mathrm{dB}$ and within a two cell environment using the setup of *System A* where each cell is half loaded. Therefore, the low C/I values represent the outer part of the desired cell, $C/I = 0\ \mathrm{dB}$ is the cell border, and positive C/I values are given in the inner cell area.

All three hard ICIC concepts can increase the BER performance for low C/I values and at the cell border compared to the non-ICIC performance. The combination of D-ICIC and I-ICIC, namely M-ICIC can benefit from their performance behavior and provides the best performance. Only for $C/I \leq -5\ \mathrm{dB}$ M-ICIC performs worse than D-ICIC because the first component in the I-ICIC generates wrong estimates of the recovered signal. This is caused by the weak desired signal and the

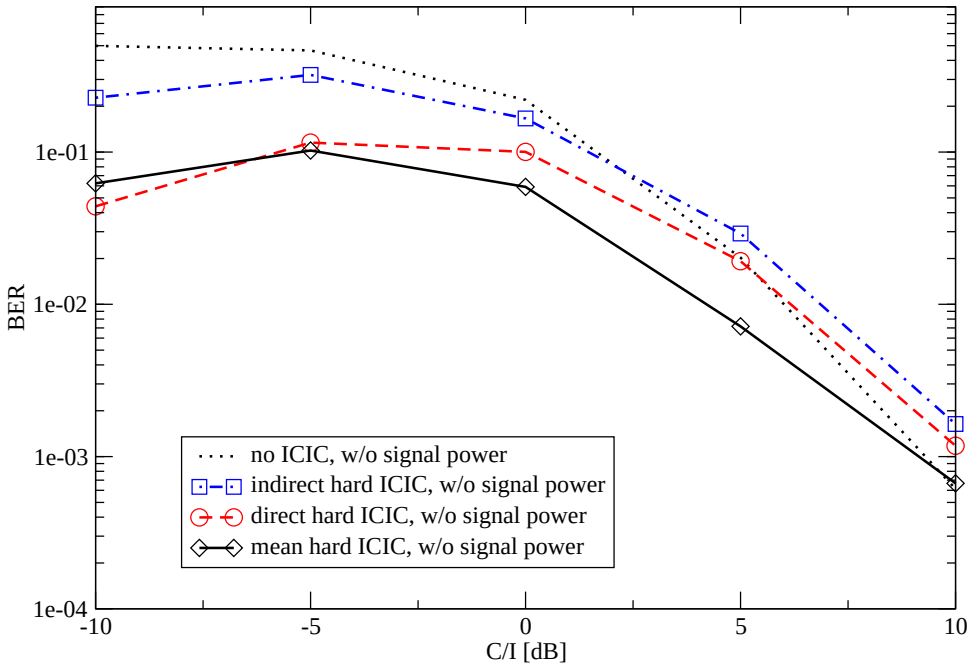

Figure 5.3: Performance of half-loaded system with different hard ICIC concepts in the cell border area, $\gamma_{\mathrm{C/I,dB}} = 10\ \mathrm{dB}$, without signal power knowledge

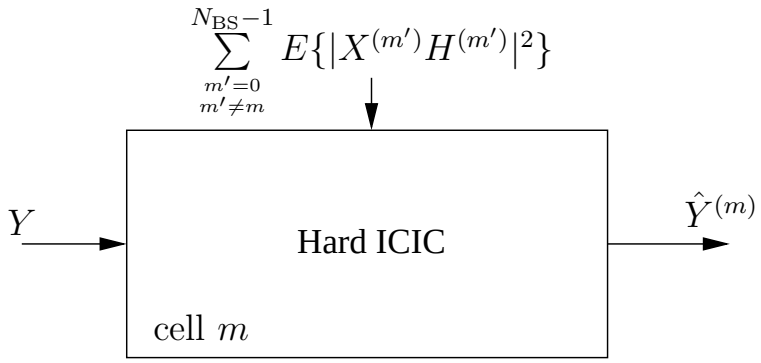

Figure 5.4: Use of signal power information in hard ICIC concept

hard decided output. Since the decoding and re-encoding process is not used in the hard ICIC concept, the performances of the D-ICIC and I-ICIC suffer from wrong recovered signals in the reconstruction process for high C/I values. This should be avoided by the soft ICIC concept.

5.1.2 Use of Signal Power in Hard ICIC

Due to the use of orthogonal signaling between the cells, pilot signals can be used to achieve the received signal power, for example, if the communication system is sufficient synchronized. Therefore, this information is used for the equalization process (cf. (3.14)) and MAP demodulator for all ICIC concepts (cf. Figure 5.4) which should influence and improve the overall performance of the hard ICICs.

Figure 5.5 shows the performance gains of the different combinations for hard ICIC with the proposed knowledge of the received signal powers. Since the D-ICIC tries to remove only the interfering signal,

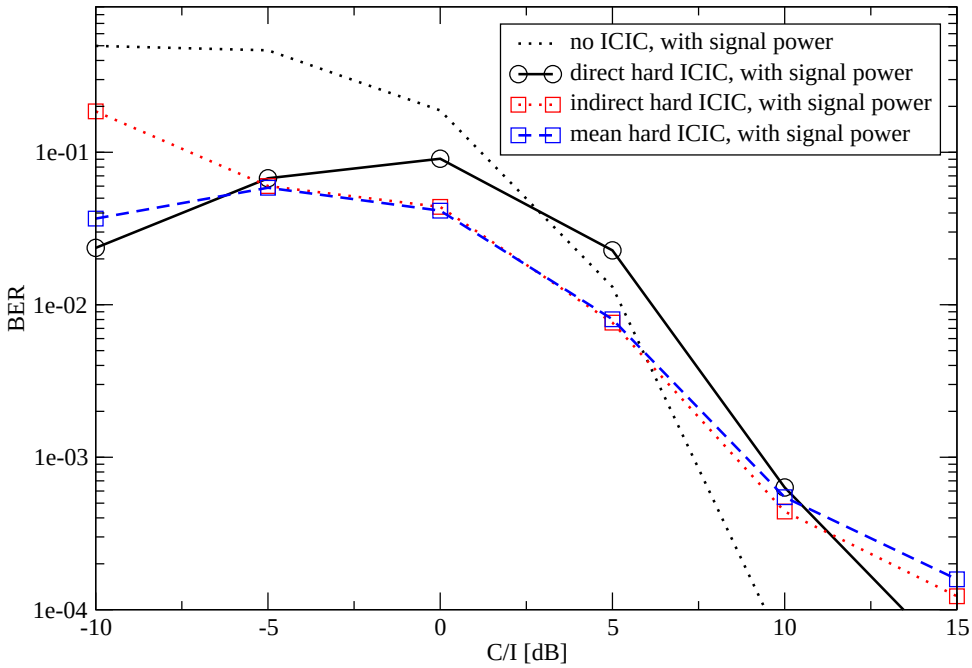

Figure 5.5: Performance of half-loaded system with different hard ICIC concepts in the cell border area, $\gamma_{\mathrm{C/I,dB}} = 10\ \mathrm{dB}$, with signal power knowledge

it cannot profit from both signal powers and does not outperform the I-ICIC in contrast to Figure 5.3 and [DL07]. Only for high inter-cell interference scenarios the D-ICIC reconstructs and removes the interfering signal better than I-ICIC. There is no performances difference between the I-ICIC and M-ICIC for $C/I \geq -5\ \mathrm{dB}$. Only for larger inter-cell interference the M-ICIC benefits from the parallel D-ICIC for interfering cell $m = 1$ (cf. Figure 5.2). But the inner I-ICIC still causes errors and the pure D-ICIC outperforms the M-ICIC.

By comparing Figure 5.3 and Figure 5.5 a performance difference exists of the reference curves without an applied hard ICIC concept due to the knowledge of the interfering signal power. There is also a large performance gain for the hard ICIC concepts with the additional information of this power. In terms of the C/I ratio, the M-ICIC or I-ICIC can gain at the cell border about $2.5\ \mathrm{dB}$ with the additional power information compared to the M-ICIC without power knowledge.

5.2 Soft Iterative Cancellation Techniques

A more sophisticated approach to cancel the inter-cell interference is based on the use of the more reliable soft-values. In the following, a *soft* ICIC technique for an arbitrary number of interfering cells is described. Figure 5.6 shows the block diagram of the proposed soft ICIC. The received signal Y is processed as described in Section 2.2.3 in respect to its specific cell parameters m for the desired and inter-cell interference signals in parallel. Furthermore, the received signal power as for the hard ICIC concept is assumed to be known. In contrast to the hard ICIC process, the demodulator computes from the received symbols soft-demodulated extrinsic log-likelihood ratios $L^{\mathrm{E}}_{\mathrm{Demod}}(c)$. Unlike the demodulator in (2.29), here the demodulator exploits the knowledge of *a priori* LLRs $L^{\mathrm{A}}_{\mathrm{Demod}}(c)$ with

$$L^{\mathrm{A}}_{\mathrm{Demod}}(c) = \log \frac{P(c=0)}{P(c=1)} \tag{5.4}$$

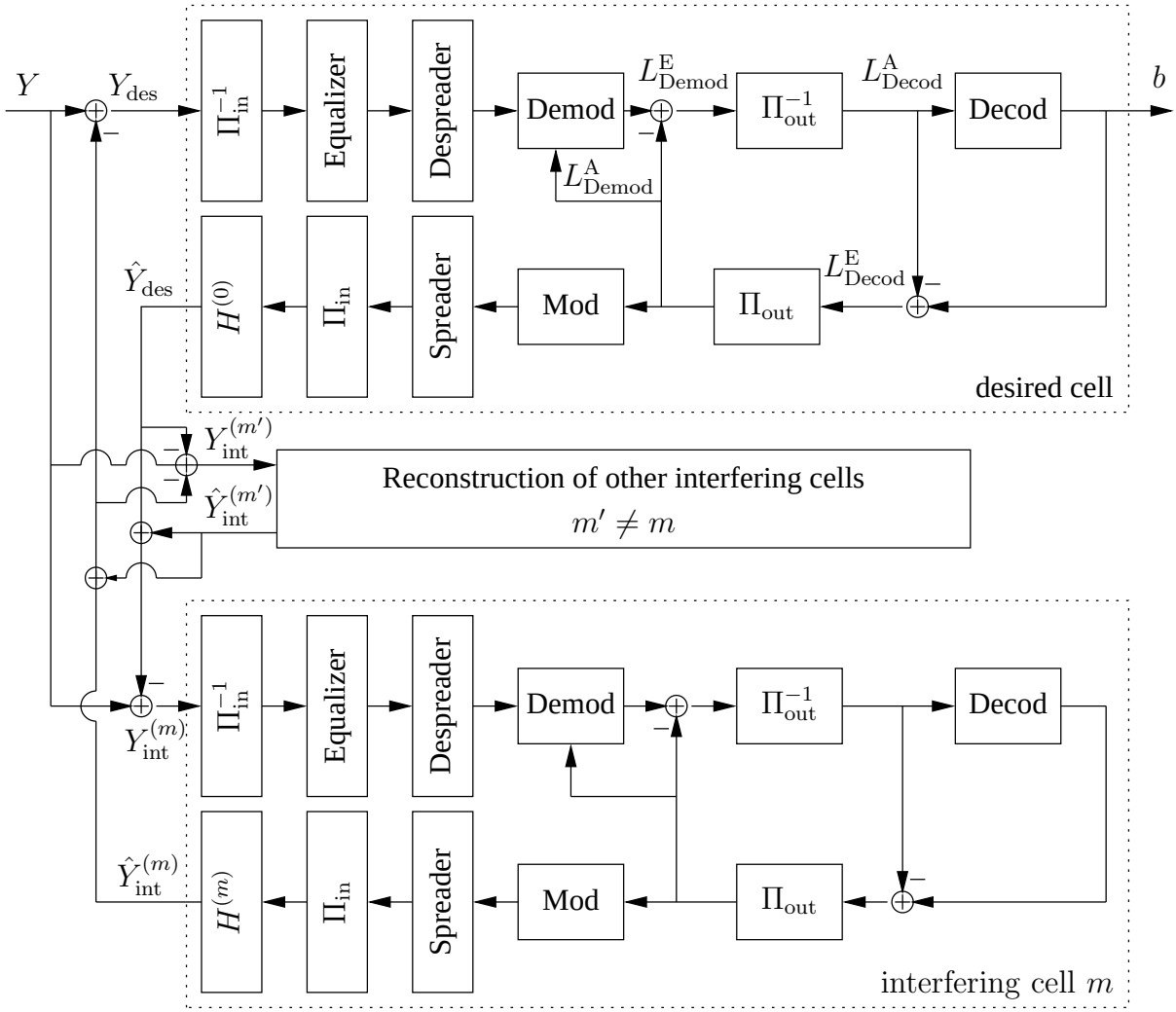

Figure 5.6: Concept of soft ICIC

coming from the decoder. $L^{\mathrm{E}}_{\mathrm{Demod}}(c)$ is given by

$$L^{\mathrm{E}}_{\mathrm{Demod}}(c) = \log \frac{P(c=0|\tilde{d}, L^{\mathrm{A}}_{\mathrm{Demod}}(\mathbf{c}))}{P(c=1|\tilde{d}, L^{\mathrm{A}}_{\mathrm{Demod}}(\mathbf{c}))} - L^{\mathrm{A}}_{\mathrm{Demod}}(c)\,. \tag{5.5}$$

In the initial iteration, the LLRs $L^{\mathrm{A}}_{\mathrm{Demod}}(c)$ for the demodulator are set to zero. After deinterleaving, the extrinsic LLRs $L^{\mathrm{E}}_{\mathrm{Demod}}(c)$ become the *a priori* LLRs $L^{\mathrm{A}}_{\mathrm{Decod}}(c)$ of the channel decoder. The channel decoder computes for all code bits the *a posteriori* LLRs $L(c|\mathbf{q})$ using the MAX-Log-MAP algorithm (cf. (2.30)) and the extrinsic information $L^{\mathrm{E}}_{\mathrm{Decod}}(c)$ is given by

$$L^{\mathrm{E}}_{\mathrm{Decod}}(c) = L(c|\mathbf{q}) - L^{\mathrm{A}}_{\mathrm{Decod}}(c)\,. \tag{5.6}$$

The extrinsic LLRs $L^{\mathrm{E}}_{\mathrm{Decod}}(c)$ are then interleaved to become the *a priori* LLRs $L^{\mathrm{A}}_{\mathrm{Demod}}(c)$ used in the next iteration in the demodulator. The signals of the desired cell $\hat{Y}_{\mathrm{des}}$ and the interfering cells $\hat{Y}^{(m)}_{\mathrm{int}}$ are reconstructed and for the next iteration step the inputs of the processing blocks are

$$Y_{\mathrm{des}} = Y - \sum_{m=1}^{N_{\mathrm{BS}}-1} \hat{Y}^{(m)}_{\mathrm{int}}\,, \tag{5.7}$$

$$Y^{(m)}_{\mathrm{int}} = Y - \left(\hat{Y}_{\mathrm{des}} + \sum_{\substack{m'=1 \\ m' \neq m}}^{N_{\mathrm{BS}}-1} \hat{Y}^{(m')}_{\mathrm{int}} \right)\,. \tag{5.8}$$

The iterative cancellation process requires high computational complexity and storage capacities at the receiver. Each canceled interfering signal needs the same processing as the desired signal. Furthermore, this complexity is multiplied by the number of processed iterations.

In contrast to the hard ICIC concepts, the soft ICIC is not limited to one processing iteration. With this iterative approach the inter-cell interference can be stepwise removed from the received signal.

Figure 5.7 illustrates the performance regarding the BER versus SNR. Due to the results of Section 3.1, a two-cell environment is chosen, and therefore, the strongest interfering cells are given and canceled. The MS is located directly at the cell border ($d_0 = 1.0, \alpha = 30°$) and a single-user scenario is given. As an upper bound of the system the performance with no ICIC is illustrated. The lower bound is represented by the single-user performance without any inter-cell interference. Already the first iteration increases the performance for $\gamma_{i,\mathrm{dB}} > 2\,\mathrm{dB}$. The second iteration can increase the performance significantly. Even the single-user bound can be almost reached within 2 iterations for higher SNRs. With 4 iterations it is possible to reach the single-user bound, and therefore, the inter-cell interference is removed.

For comparison the performance curves of the hard ICIC concepts are included in Figure 5.7. Since no decoding is taken into account in this cancellation technique, the performance does not reach the first iteration performance of the soft ICIC. Still the M-ICIC and D-ICIC can improve the performance significantly compared to no applied ICIC. In contrast to a two cell scenario (cf. Figure 5.5), the I-ICIC cannot handle the inter-cell interference of several interfering cells appropriately, and therefore, there exists a large performance loss.

The performance in the cell border area for the soft ICIC is presented in Figure 5.8. The SNR is set to $10\,\mathrm{dB}$ and the system is half loaded in all seven cells. The desired and the two closest interfering cells are chosen to be processed in the soft ICIC. The mobile station moves along a straight line from $d_0 = 0.6$ to $d_0 = 1.6$ with $\alpha = 30°$. The performance without any applied ICIC technique

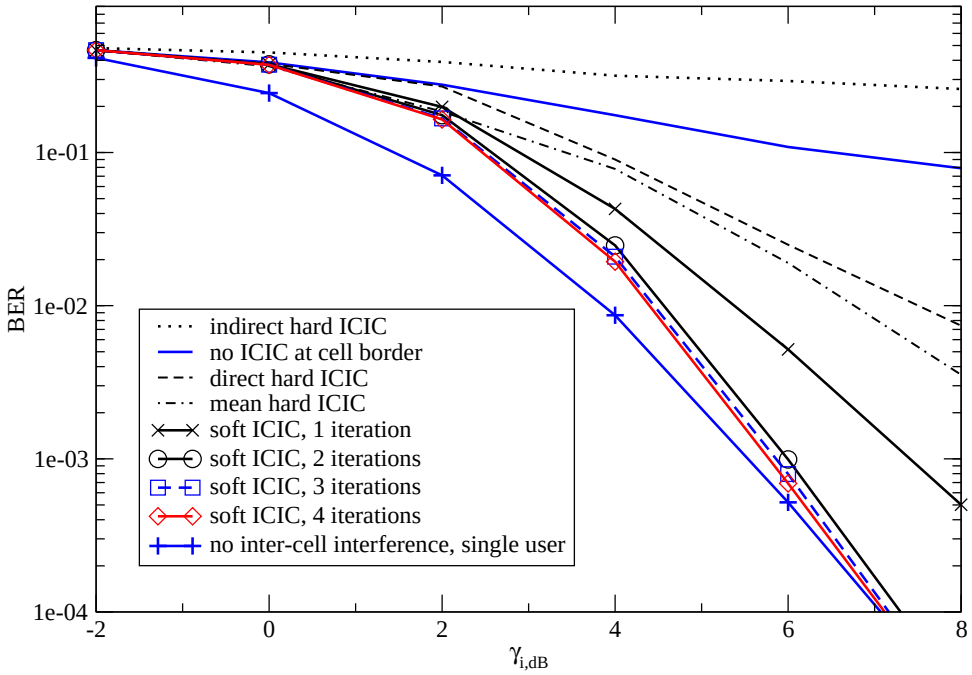

Figure 5.7: Performance of the soft ICIC for the single-user case at the cell border for different SNR values

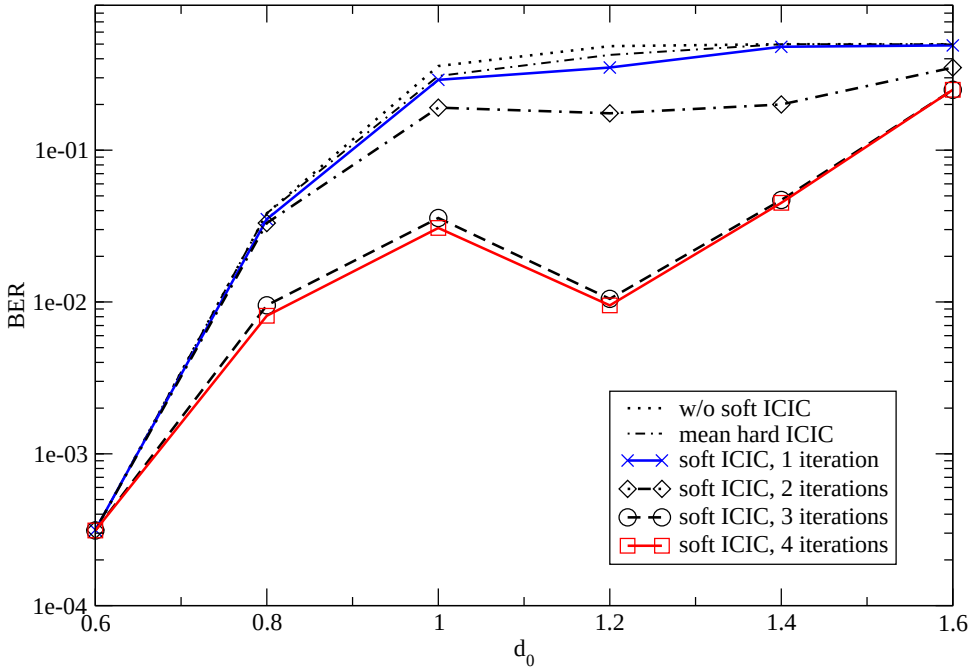

Figure 5.8: Performance of a half loaded system with soft ICIC in the cell border area; $\gamma_{i,\mathrm{dB}} = 10\ \mathrm{dB}$

Table 5.1: Mean received signal power

	$\mathrm{BS}^{(\mathrm{I},1)}$		$\mathrm{BS}^{(\mathrm{I},2)}$		$\mathrm{BS}^{(\mathrm{I},3)}$	
α	theor.	sim	theor.	sim	theor.	sim
$60°$	0.19	0.20	3.48	3.74	0.19	0.20
$70°$	0.13	0.13	2.89	3.03	0.32	0.32
$80°$	0.086	0.097	1.80	2.0	0.55	0.58
$90°$	0.062	0.066	1.0	1.04	1.0	1.06

is represented by the dotted line. For this scenario the first iteration cannot cancel out the inter-cell interference. Therefore, the hard ICIC concepts also fail for this scenario, represented by the M-ICIC performance. The second iteration of soft ICIC can achieve a small performance improvement. The so-called turbo cliff is reached with the third iteration and large performance gains can be achieved. A fourth iteration yields no appreciable improvement. All performance curves merge to the non-ICIC curve if they reach the inter-cell interference free case ($d_0 < 0.8$). Directly at the cell border ($d_0 = 1.0$) all processed signals are received with the same power, and therefore, the signals are at most difficult to separate and the soft ICIC performance is worst at this point. Due to the different received signal powers, the soft ICIC can maximize the performance at $d_0 = 1.2$. This performance is similar to the almost inter-cell interference free case at $d_0 = 0.8$. For larger distances to the desired BS ($d_0 > 1.2$), the performance degrades because the desired signal becomes weak and the final decoding step for the desired signal can fail.

Due to the half-loaded system, the inter-cell interference free performance cannot be approached because the existing MAI degrades the ICIC process. The MAI could be removed by the additional use of the interference cancellation principles introduced in [KH97].

5.2.1 Choice of Interfering Signals

The iterative cancellation process requires very high computational complexity at the receiver and additionally introduces a delay to the signal processing for each iteration. Each canceled interfering signal needs the same processing as the desired signal. Furthermore, this large complexity is multiplied by the number of processed iterations.

The main interferers are the two closest interfering BSs to the desired MS (cf. Section 3.1). Therefore, it is sufficient to cancel only the two strongest interfering cells or even the strongest interferer at the receiver. This reduces essentially the complexity. The signal power of the interfering signals can be compared and the most powerful can be chosen for the further iterative processing in the soft ICIC. This selection process can be done frame-by-frame.

Taking into account the propagation and cellular setup as given in Figure 2.1 and Section 2.1 the mean power of the received signals from the three closest neighboring cells follow Table 5.1. The received signal power from each BS is assumed to be normalized to one at $d_m = 1.0$. The simulated received mean power is also given on Table 5.1 for comparison which confirms the simulations.

Table 5.1 shows the varying influence of the neighboring BSs regarding the MS position. $\mathrm{BS}^{(\mathrm{I},2)}$ is the most dominant interfering BS which has to be always canceled. The influence of $\mathrm{BS}^{(\mathrm{I},1)}$ vanishes for larger α. Still for $\alpha = (60°, 70°)$, the receiver has to decide which BS should be canceled out of

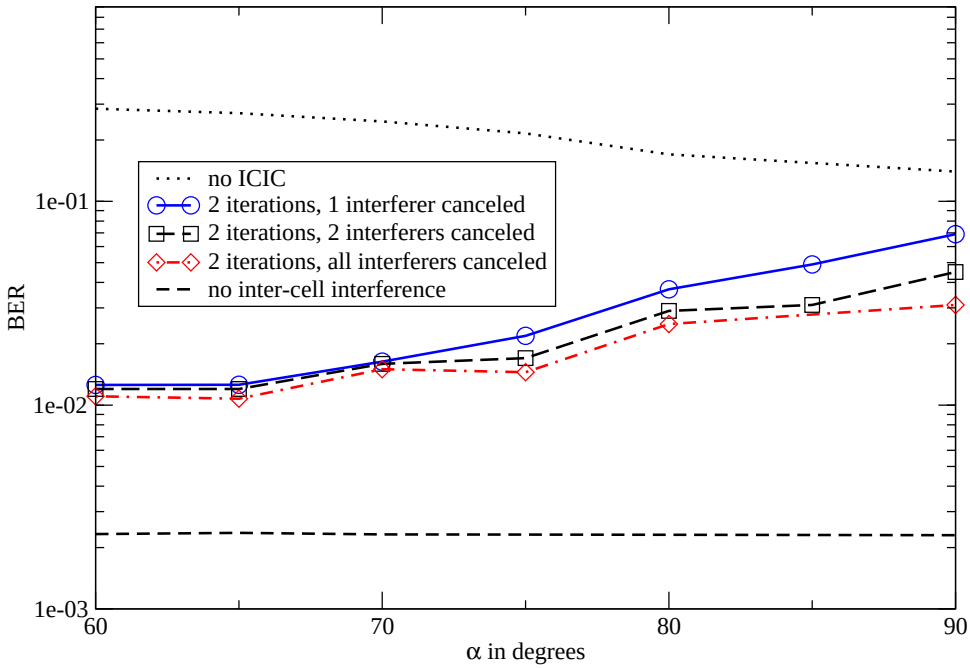

Figure 5.9: Performance for the single-user case and varying α at $d_0 = 1.0$ for different number of subtracted interfering signals; $\gamma_{i,\mathrm{dB}} = 5$ dB

$\mathrm{BS}^{(\mathrm{I},1)}$ and $\mathrm{BS}^{(\mathrm{I},3)}$. The same situation occurs for $\alpha = 90°$ between $\mathrm{BS}^{(\mathrm{I},2)}$ and $\mathrm{BS}^{(\mathrm{I},3)}$ if only one signal is going to be canceled.

In Figure 5.9 the performance results of two cancellation strategies are shown in a cellular setup with 4 cells. The first strategy cancels only the strongest interfering signal. The second strategy takes into account the two strongest interfering signals for the iterative ICIC process. 2 iterations are chosen as a good trade-off between complexity and performance gain for these simulations. A lower bound for the two strategies can be given by the performance with all canceled interfering signal within 2 iterations. Furthermore, the performance are limited by an upper bound without any ICIC technique and an absolute lower bound without any inter-cell interference. Since $\gamma_{i,\mathrm{dB}} = 5$ dB, the second iteration cannot reach the interference-free single-user bound (cf. Figure 5.7). Due to the higher number of simulated cells and the additional inter-cell interference, the performances do not match the performances of Figure 5.7 with 2 interfering cells.

The performance without any ICIC strategy gains the closer the MS is to the cell border of $\mathrm{BS}^{(\mathrm{I},2)}$ and $\mathrm{BS}^{(\mathrm{I},3)}$, i.e., $\alpha = 90°$. At $\alpha = 90°$ the least interference is received. In contrast, at $\alpha = 60°$ from the closest and the two nearby cells the largest interference is received. In the case of the applied ICIC schemes, the performances act contrary. The ICIC fails to distinguish the interfering signal at $\alpha = 90°$ due to the same received signal powers (cf. Table 5.1). For $\alpha = 60°$ the most dominant interfering signal (from $\mathrm{BS}^{(\mathrm{I},2)}$) can be successfully canceled which results in the best performance. The same characteristics can be seen for the two different cancellation strategies. There is no large performance difference for $\alpha < 70°$ by canceling one or two interfering signals due to the one dominant interferer. And for $\alpha > 75°$ two interfering cells are dominant, and therefore, the strategy with two interfering cells canceling outperforms the first strategy.

5.2.2 Evaluation of Extrinsic Information

It is possible to use the extrinsic information (cf. (5.6)) as a degree of reliability for the iterative process of the signal reconstruction. For the soft ICIC the mean of the absolute extrinsic information $L^{\mathrm{E}}_{\mathrm{Decod}}(c)$ over all desired bits within one OFDM frame is taken to calculate a reliability information of the decoded signal in the jth iteration following the definition of soft bits (cf. (2.31)) by

$$\lambda_j = \tanh\left(\frac{1}{N_{\mathrm{b}}}\sum_{n=0}^{N_{\mathrm{b}}} |L^{\mathrm{E}}_{\mathrm{Decod}}(c)|/2\right) \tag{5.9}$$

where N_{b} represents the total number of desired bits. Since the absolute value of $L^{\mathrm{E}}_{\mathrm{Decod}}(c)$ is taken, the range of λ_j is now

$$0 \leq \lambda_j \leq +1\,. \tag{5.10}$$

The lower λ_j the lower is the reliability of a correct reconstruction of the signal and vice versa. The difference

$$\Delta\lambda_{j+1,j} = \lambda_{j+1} - \lambda_j \tag{5.11}$$

represents the reliability change between the iterations.

A whole tier of cells, i.e., 6 interfering cells, around the desired cell are assumed for the following investigations. The reliability information λ_j of the desired signal is simulated for positions of the mobile station in the range of $d_0 = [0.4, 1.4]$ around the desired BS. The SNR is set to 5 dB and the system is half loaded. Figure 5.10(a) shows λ_1 depending on the position for the first iteration of the soft ICIC in a three dimensional illustration. It can be seen that in the inner part of the cell ($d_0 \leq 0.6$) λ_1 is mostly 1.0. Therefore, the desired signal should be detected appropriately in this region. For the outer parts ($d_0 > 0.6$) there is a large degradation of the reliability for the decoding process. Differences between the mobile station position are also visible, e.g., the mobile station experiences one strong interfering BS ($(x, y) = (-1.4, 0)$) or the mobile station is located between two weaker interfering BSs ($(x, y) = (-1.2, -0.7)$). The distribution of λ_2 for the second iteration is shown in Figure 5.10(c). Already the second iteration can increase λ_2 over the whole area for this scenario compared to λ_1. Even in the cell border area ($d_0 = [0.8, 1.2]$) λ_2 achieves values close to one. Therefore, this second iteration broadens the area for successful detection of the desired signal. Another representation of λ_j within the cellular environment is given in Figure 5.10(b) and Figure 5.10(d) for one and two iterations, respectively. The positions of the involved BSs are given by the rectangular marks. These plots show more precisely that in the first iteration the more reliable λ_1 values are limited to $d_0 < 1.0$. For the second iteration reliable λ_2 values stretch already to $d_0 \leq 1.2$.

Due to the large simulation complexity of the whole cellular environment and its reproduction, the difference $\Delta\lambda_{2,1}$ is provided in the three dimensional plot of Figure 5.11. It is clearly visible that the rim area gains in reliability for the decoding process for the second iteration. There are corridors without an increase of λ_2 due to the constellation of the cellular environment. Since the signal strength of the two closest interfering cells in these corridors (e.g., $\alpha = 30°$) do not differ significantly, the soft ICIC process cannot improve the already good λ_1 values in the second iteration. If only one BS is the major interferer (e.g., $\alpha = 0°$) and the signal strength between the desired and main interferer differ, the soft ICIC can detect both signals in the second iteration more precisely. This confirms the observations in Figure 5.9 of Section 5.2.1.

The distribution of λ_j depends directly on the chosen scenario. Figure 5.12 presents different SNR scenarios within an one-tier cellular environment. λ_j is investigated for the desired and the two closest interfering signals where the mobile station is located close to the cell border with almost the same

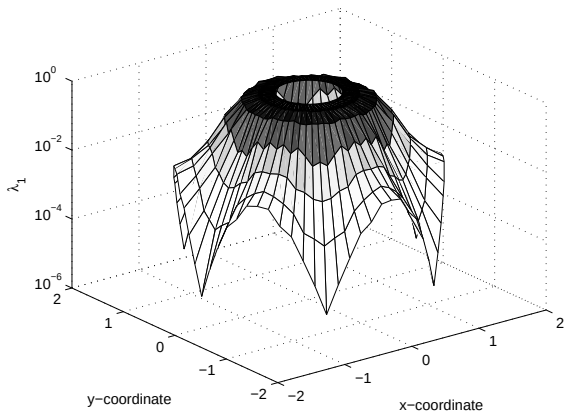

(a) 3D presentation of first iteration

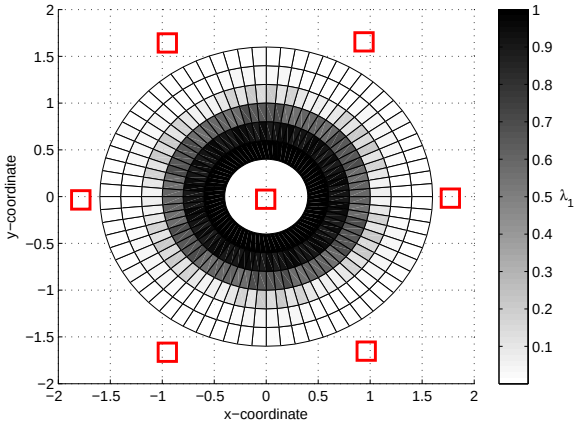

(b) 2D presentation of first iteration

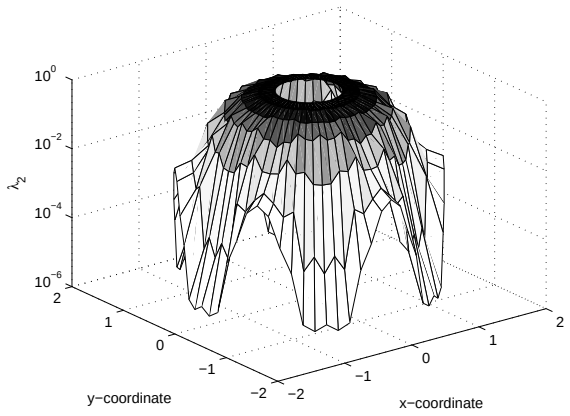

(c) 3D presentation of second iteration

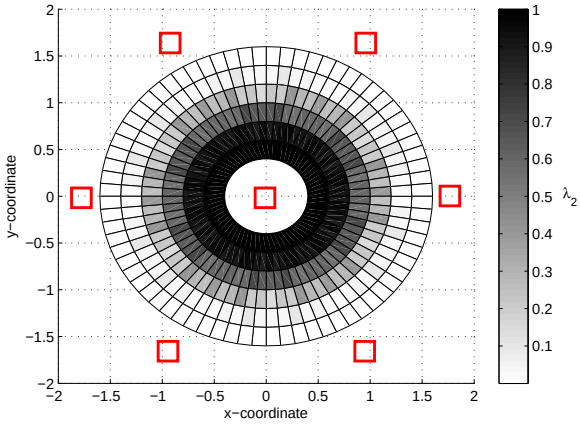

(d) 2D presentation of second iteration

Figure 5.10: Resulting values of λ_j for the desired signal within the coverage of the desired base station depending on the position of the mobile station (base stations have rectangular markers) in two and three dimensional representations

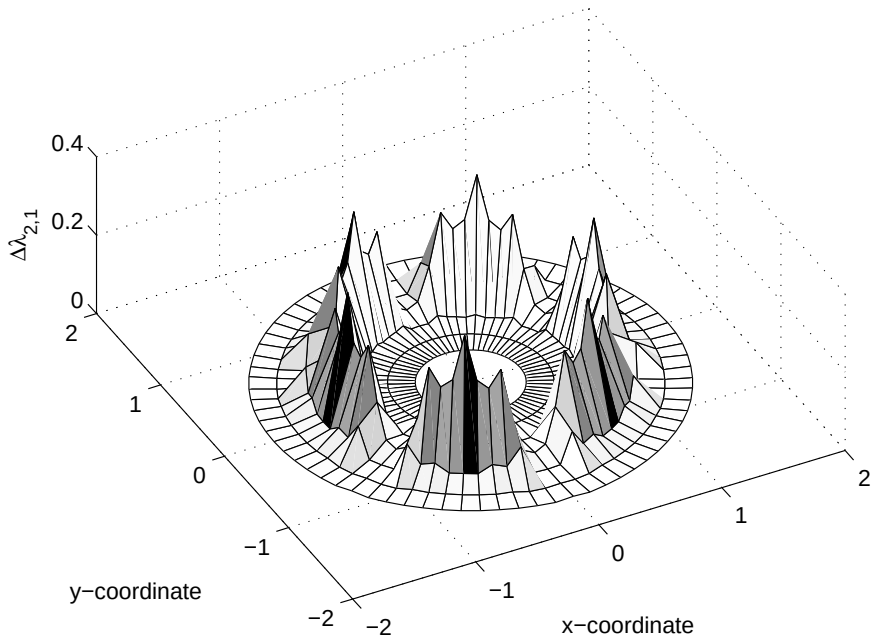

Figure 5.11: Difference $\Delta\lambda_{2,1} = \lambda_2 - \lambda_1$ of the reliability information between the first and second iteration of the soft ICIC process

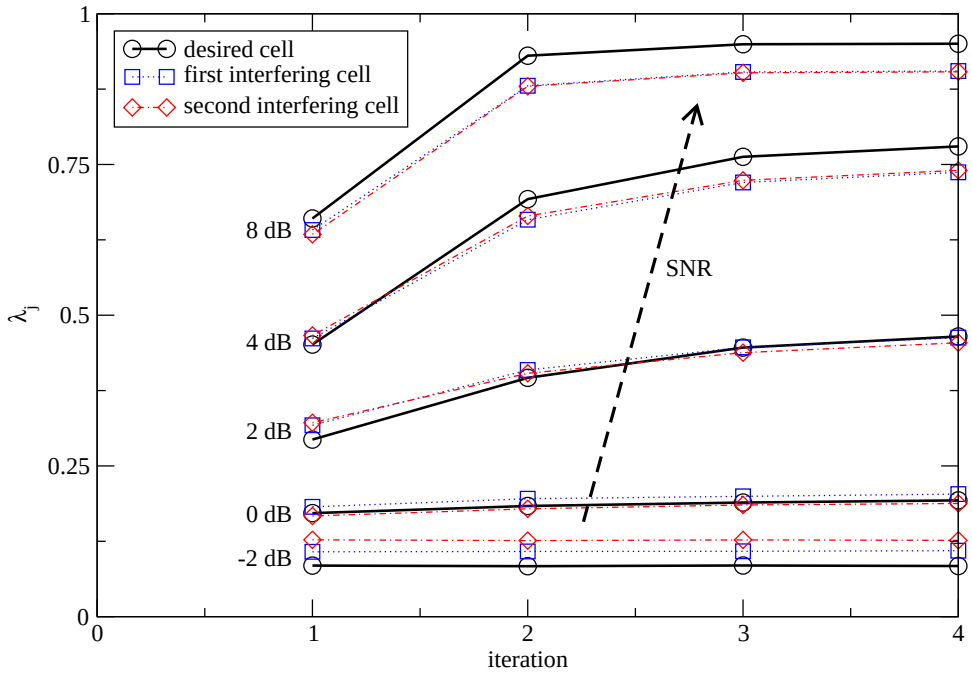

Figure 5.12: Reliability of decoding process of recovering the signals of different cells close to the cell border for several iterations at varying SNR scenarios

distance to all these three BSs, i.e., $d_0 = 0.9, \alpha = 30°$ or $(x, y) = (0.78, 0.45)$. The two closest interfering cells are taken into account for the soft ICIC process. Furthermore, a single-user case is assumed within all cells. For low SNR values ($\gamma_{i,\mathrm{dB}} \leq 0$ dB), low and constant values of λ_j are given over all iterations. If the SNR is larger than 2 dB λ_j increases for higher number of iterations. In the case of $\gamma_{i,\mathrm{dB}} = 8$ dB there exists a large step between the first and second iteration but the following iterations do not increase λ_j for $j > 2$ anymore. Due to the small power differences of the three received signals ($d_0 = 0.9$), the reliability information λ_j varies for the detected signals. It is obvious that a higher SNR provides better detection possibilities than low SNR scenarios for the desired signal. These investigations confirm the performance characteristics in Figure 5.7 and Figure 5.8 of Section 5.2.

5.2.3 EXIT Chart Analysis

A well established tool are extrinsic information transfer (EXIT) charts [tB00, DASR06] to predict and analyze the performance of iterative processes. The EXIT charts and its properties for the case of soft ICIC concepts in a cellular MC-CDMA environment are introduced in this section. It would be beneficial to know how many iterations are needed for reaching the turbo cliff for different inter-cell interference situations, modulation alphabets, mappings, code rates, or system loads.

The *a priori* LLRs $L^{\mathrm{A}}(c)$ for the EXIT chart analyzes has to be modeled as identically distributed Gaussian random variables [tB00], i.e.,

$$L^{\mathrm{A}}(c) = E\{L^{\mathrm{A}}(c)|c\} \cdot c + N_{L^{\mathrm{A}}(c)}. \tag{5.12}$$

Here $N_{L^{\mathrm{A}}(c)}$ is the AWGN with mean zero and variance σ_{A}^2. The mean of $L^{\mathrm{A}}(c)$ given c needs to fulfill $E\{L^{\mathrm{A}}(c)|c\} = \frac{\sigma_{\mathrm{A}}^2}{2}$.

To generate an EXIT characteristic for a component such as the decoder or demodulator in the EXIT chart, first the variance σ_{A}^2 from the mutual information I^{A} has to be computed. Then, the random variable $L^{\mathrm{A}}(c)$ according to (5.12) is generated and $L^{\mathrm{A}}(c)$ is used as *a priori* LLR in the component. At the output of the component, the extrinsic mutual information I^{E} from the extrinsic LLRs $L^{\mathrm{E}}(c)$ is estimated according to [Hag04]

$$I^{\mathrm{E}} \approx 1 - \frac{1}{N} \sum_{\mu=1}^{N_{\mathrm{samp}}} H_{\mathrm{b}} \left(\frac{1}{1 + e^{-|L^{\mathrm{E}}(c_\mu)|}} \right). \tag{5.13}$$

The underlying assumptions in (5.13) are that the random processes such as the noise and channel variations are ergodic and a large number of samples N_{samp} have been observed. In this case, the super channel for a received bit can be seen as a binary symmetric channel (BSC) with transition probability $p_{\mathrm{e}} = \frac{1}{1+e^{-|L^{\mathrm{E}}(c)|}}$. The mutual information of a BSC can be computed with the entropy $H_{\mathrm{b}}(p_{\mathrm{e}})$ as $1 - H_{\mathrm{b}}(p_{\mathrm{e}})$, which is averaged over N observations.

In the following, the BS index m is skipped for simplicity and without loss of generality. The MAP demodulator in MC-CDMA computes the extrinsic LLRs $L^{\mathrm{E}}_{\mathrm{Demod}}(c)$ by [DASR06]

$$L^{\mathrm{E}}_{\mathrm{Demod}}(c) = \ln \frac{\sum_{X_n(c_n):c=1} p(Y_n|X_n)p(X_n)}{\sum_{X_n(c_n):c=0} p(Y_n|X_n)p(X_n)} - L^{\mathrm{A}}_{\mathrm{Demod}}(c)\,, \tag{5.14}$$

where the index n represent the n-th transmitted or received symbol. The index n is related to the sub-carrier index i and MC-CDMA symbol index l by $n = i + l \cdot N_{\mathrm{c}}$. Finally, the resulting conditional

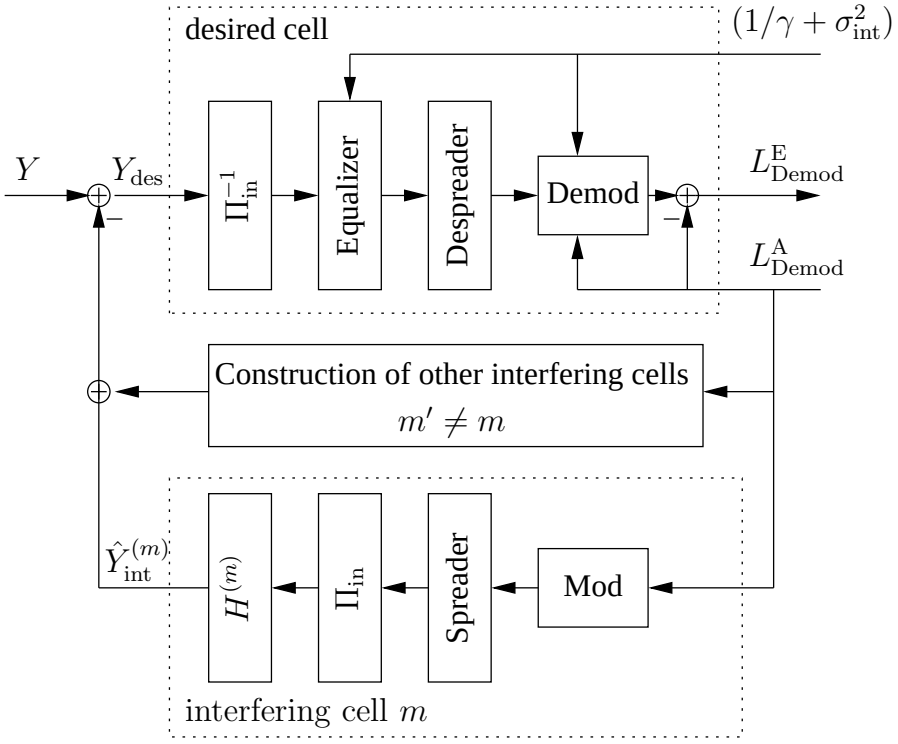

Figure 5.13: Block diagram of EXIT chart analysis for the desired cell signal in the soft ICIC

channel probability $p(Y_n|X_n)$ for the soft ICIC depends directly on the total power of the received signal, and therefore, it depends also on the inter-cell interference power (cf. (3.17)):

$$p(Y_n|X_n) = \frac{1}{\sqrt{2\pi(1/\gamma_l + \sigma^2_{\text{int}})}} e^{-\frac{|Y_l - H_l S_l|^2}{2(1/\gamma_l + \sigma^2_{\text{int}})}}. \tag{5.15}$$

The block diagram in Figure 5.13 shows the realization of the EXIT chart analysis for a cellular MC-CDMA system. For the analyzes, the same *a priori* values are assumed in each cell to facilitate the interpretability. Furthermore, the total received signal Y is ordinarily generated regarding (2.27). For the construction of the interfering signals, the modulator has to be considered as a soft modulator, i.e., it takes into account the LLRs $L^{\text{A}}_{\text{Demod}}(c)$.

For the investigations of the appropriate use of EXIT charts for soft ICIC concepts the influence of the choice of σ^2_{int} is studied. Three different approaches are chosen: First, the defined σ^2_{int} (cf. (2.38)) is taken for all iterations in the soft ICIC process. Since the inter-cell interference reduces after each iteration, this represents a *pessimistic* approach (marked by σ^2_{pess}). The second approach is based on *genie* knowledge about the inter-cell interference power on each iteration and this is expressed by σ^2_{genie}. The last choice is the opposite of the pessimistic approach. Due to the *optimistic* assumption, there is no inter-cell interference, and therefore, $\sigma^2_{\text{opt}} = \sigma^2_{\text{int}} = 0$. Figure 5.14 shows the influence of the mutual information on the normalized inter-cell interference power. For the EXIT chart analyzes, σ^2_{int} can be linearly approximated.

Figure 5.15 shows the EXIT chart of the soft ICIC concept within the same simulation environment as in Figure 5.7. An SNR of 8 dB is chosen. The extrinsic decoder curve is given for the used MAX-Log-MAP decoder. For the demodulator, three different extrinsic information performances are shown depending on the used $\sigma^2_{\text{int}} = [\sigma^2_{\text{pess}}, \sigma^2_{\text{genie}}, \sigma^2_{\text{opt}}]$.

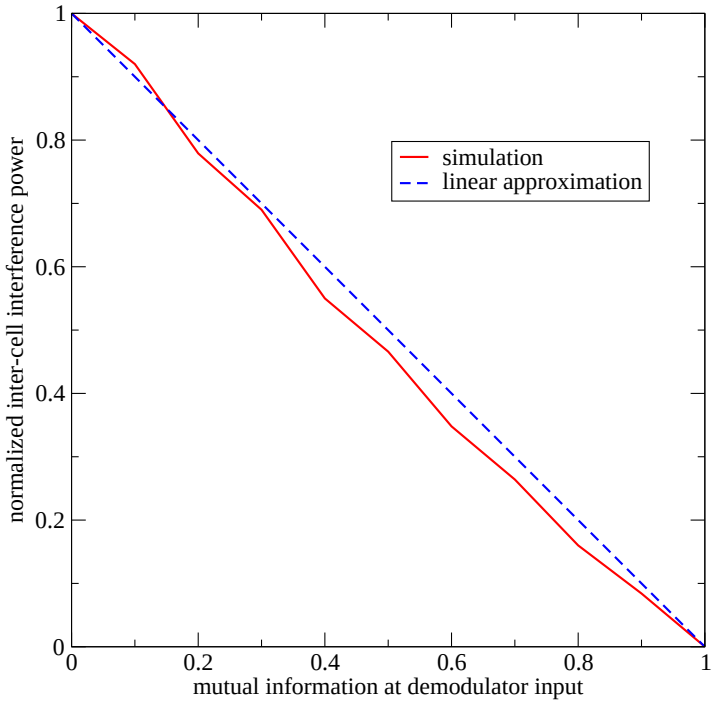

Figure 5.14: Influence of mutual information on inter-cell interference

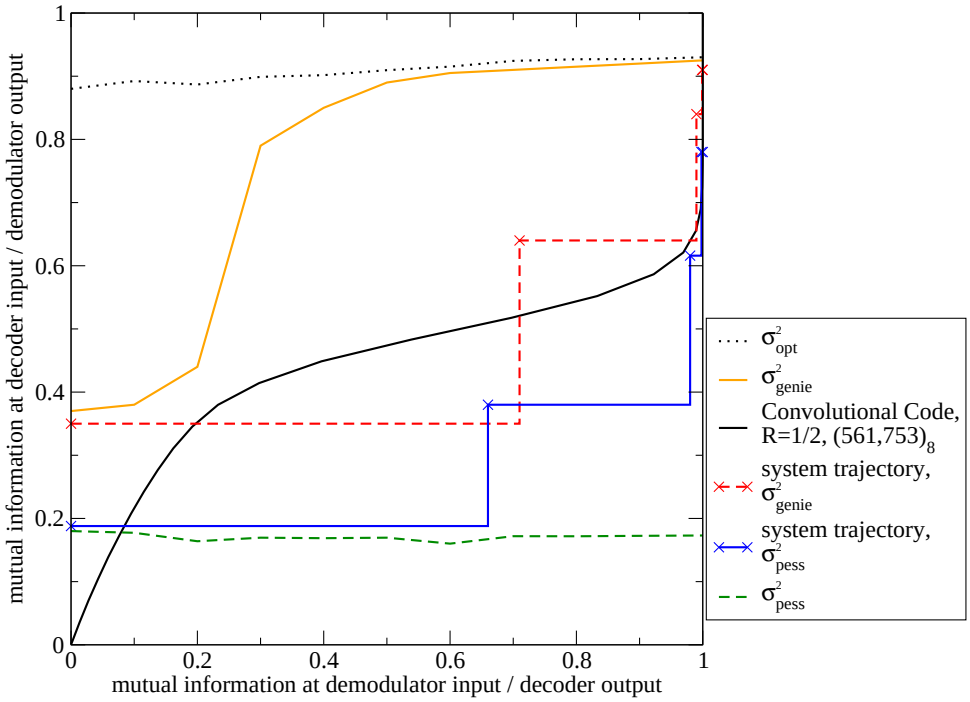

Figure 5.15: EXIT chart for single-user scenario at the cell border; $\gamma_{\mathrm{C/I,dB}} = 8\ \mathrm{dB}$

For σ^2_{pess} no convergence to low BERs would be expected as the demodulator characteristic and decoder characteristic intersect at the point $(I^{\text{E}}_{\text{Decod}}, I^{\text{E}}_{\text{Demod}}) = (0.1, 0.2)$ in the EXIT chart. On the other hand for σ^2_{genie}, the *tunnel* is open, and therefore, low BERs can be expected. Similar if no inter-cell interference power is assumed, i.e., $\sigma^2_{\text{int}} = \sigma^2_{\text{opt}} = 0$, the receiver can also achieve low BERs.

Considering the simulated system trajectories, a good fit is observed at no *a priori* information. Using σ^2_{genie} in the demodulator, the trajectory matches fairly well for high *a priori* information and shows a mismatch for medium *a priori* information. Still, the system converges as expected from the demodulator characteristics to low BERs. In contrast to the prediction of the EXIT chart, the ICIC system for σ^2_{pess} converges to low BERs. In this case, it seems that the demodulator output yields a to small $I^{\text{E}}_{\text{Demod}}$.

Figure 3.10 in Section 3.2 illustrates that the lower the number of interfering cells and users within a cellular system, the less Gaussian is the resulting overall interfering signal. Due to non-Gaussian interference, the actual interference contribution in (5.15) is over estimated. Thus, the demodulator estimates the LLRs in (5.14) too small. This in turn results into too small extrinsic information estimates in (5.13) and in the EXIT chart. Consequently, the demodulator output is too small for the system trajectory σ^2_{pess} in Figure 5.15.

At the same time, the decoder can better decode the code bits than expected. As there is less inter-cell interference in the actual signal than modeled by σ^2_{pess}, the decoder can correct more errors, and thus, the ICIC can compensate in the 2nd iteration more interference. Finally, it converges to the single-user bound. Note that in the current simulation setup, correlated channels and relatively short outer interleaver lengths of 1536 are considered. Therefore, both assumption for the LLRs in the EXIT charts, i.e., they are independent and Gaussian-distributed, are violated. Consequently, the demodulator and decoder characteristics in the EXIT chart are not tight bounds for the system trajectories.

5.3 Summary

The goal of inter-cell interference mitigation at the mobile station is to achieve high system capacity with an optimum frequency reuse factor. Therefore, the concept of inter-cell interference cancellation at the mobile station is introduced for cellular MC-CDMA systems in this chapter which combines frequency reuse of one and high system performance at the cell border.

The complexity of ICIC techniques is directly proportional to the number of included interfering BS signals in the cancellation process. Investigations in Chapter 3 concluded that the main inter-cell interference is contributed by the two closest interfering BSs. Therefore, practical implementations of inter-cell interference cancellation schemes may be limited to detecting the contributions of only two interfering BSs. The processing complexity can be split in two main different tasks: the inter-cell interference estimation and the subtraction of the inter-cell interference estimates from the received signal.

Both ICIC concepts (*hard* and *soft* ICIC) take into account these two processing steps. The first concept, namely hard ICIC, is based on the reconstruction of the received signal by using the hard decided outputs of the demodulator. Different combinations of the hard ICIC are investigated and with the additional use of the signal power information the overall performance benefits at the cell border.

The second concept, namely soft ICIC, is based on a more sophisticated approach which uses the soft outputs of the decoder to reconstruct iteratively the signals for cancellation. Performance results show that the soft ICIC approaches the single-user bounds without inter-cell interference, and therefore, the interference of the cellular environment can be almost eliminated. Furthermore, the profit of the soft ICIC depends directly on the given scenarios and the used number of iterations. The performance degradation due to a reduced number of canceled interfering signals is reasonable compared to the significant complexity reduction of the iterative process.

The extrinsic information of the decoding process can give a reliability information about the successful decoding process, and therefore, the behavior of the soft ICIC for different scenarios can be described and analyzed. Consequently, extrinsic transfer information charts are introduced for the ICIC concept. The additional inter-cell interference energy has to be taken into account in the log-likelihood ratio estimation of the demodulators. The EXIT chart analysis is only partially correct for such a complex cellular system, as the assumption of independent and Gaussian-distributed LLRs is violated. Therefore, the convergence characteristics have to be carefully interpreted in the EXIT chart.

Complexity of the interference estimation task depends strongly on the used technique. In the case of hard ICIC, the complexity is roughly equal to the demodulation complexity times the number of interferers. However, in the case of soft ICIC, the complexity for one interferer can be roughly evaluated as the demodulation complexity plus the channel decoding complexity times the number of processed iterations, which represents a high processing burden. Moreover, additional memory is required to store at the same time the received signal and the reconstructed interference signals, as well as the incoming signal received during the detection process. At last, interference cancellation schemes, especially when performed in an iterative manner, introduce additional processing delays due to the need to detect the interferers' signal before detecting the useful one.

On the other side, the different ICIC techniques allow significant gains in the cell border area due to the large influence of the inter-cell interference in this region. This gain can be expressed in terms of: lower transmit power, increase of cell coverage when defining the network planning, better quality-of-service, and especially higher data throughput because higher modulation orders or channel coding rate can be used. Due to the high complexity of iterative soft ICIC procedures these techniques can be considered if the MS has the needed processing capabilities. If the MS cannot support these large complex iterative decoding strategies, the less complex hard ICIC can still provide significant gains for dominant inter-cell interference influence on the desired signal.

Chapter 6

Use of Inter-Cell Interference

Multiple antenna transmission schemes have gained high attraction since they offer a capacity which rises proportional to the minimum of the number of transmit (TX) and receive antennas from information theory point of view [FG98]. In the recent years, several approaches have been proposed, which take advantage of multiple transmit or receive antennas. One representative of multiple antenna schemes is cyclic delay diversity (CDD) [DK01a]. CDD is a variant of delay diversity (DD) [Wit93] and adapted to communications systems with cyclic extensions as guard intervals such as MC-CDMA for instance. Signal delays in DD may cause inter-symbol interference. In contrast, CDD prevents such additional inter-symbol interference by using cyclic signal shifts. Typically, multi transmit/receive-antenna techniques like space-time block coding (STBC) [TSC98, Ala98] require signal processing in both the transmitter and the receiver but can achieve the maximum diversity gain. However, CDD as well as DD can be implemented solely at the transmitter, the receiver, or both sides. The fact that the counterpart — e.g., the receiver in case of a transmit sided implementation — need not be aware of the implementation makes these techniques transparent at the counterpart, i.e., standard compatible. They can be implemented as an extension for already existing systems without changing the standard.

In a centralized cellular network the MS switches the corresponding BS when it is requested by the resource management. The switch is defined as the handover procedure from one BS to another. The handover is seamless and soft when the MS is connected to both BSs at the same time. A softer handover exists when the MS moves between two sectors and is connected simultaneously to the two sectors. The sub-carrier resources in an MC-CDMA system within a spreading block are allocated to different users. Some users might not need a handover as they are either in a stable position or away from the cell border. In both cases these users can be effected by inter-cell interference as their resources are also allocated in neighboring cells. To separate the different demands of the users, users with similar demands can be combined within time-frequency units, e.g., chunks, in an OFDM frame. The requested parameters of the users combined in these chunks are similar, like a common pilot grid. The spectrum for the users could then be shared between two cells within a chunk by defining a broadcast region. By this the affected users of the two cells would reduce their effective spectrum in half. This is the price to pay for avoiding inter-cell interference (cf. Chapter 4). Inter-cell interference could be tackled by inter-cell interference cancellation techniques (cf. Chapter 5). Smart BSs could in addition try to balance the needed transmit power by risking an increase of inter-cell interference in neighboring cells.

The approaches presented in this chapter use inter-cell interference by defining the effected area as a broadcast region and applying transmit diversity schemes for a cellular system, like cyclic delay

diversity and STBCs. Therefore, transmit diversity is transformed to macro diversity. Part of the ineluctable loss of spectrum efficiency are compensated by exploiting additional diversity gains on the link layer, avoiding the need of complex inter-cell cancellation techniques and decreasing the overall inter-cell interference in the cellular network for the common good.

In this chapter, the term C/I (cf. (2.40)) can be seen as misleading, as the described schemes make beneficial use of transmitted signals from the neighboring BSs. Therefore, I is not interference anymore. On the other hand the term C/I describes the ratio of the power from the desired base station to the other involved base stations. This ratio also indicates where the mobile user is in respect to the base stations. For example in the case of two involved base stations, the MS is directly between the two BSs for $C/I = 0$ dB, see also Figure 2.10. In the case of $C/I > 0$ dB the MS is closer to the desired BS, and for $C/I < 0$ dB the MS is closer to the adjacent BS. Hence, the ratio C/I is retained in this chapter.

In the following, two cellular transmit/macro diversity techniques are in focus. The first is based on the cellular cyclic delay diversity (C-CDD) technique [14, 13] which increases the frequency diversity of the received signal and requires no change at the receiver to exploit the diversity. The resulting channel correlation characteristics are investigated [2]. Furthermore, an adaptive variation of C-CDD for the transmit power and cyclic delay choice is given which can also be seen as soft C-CDD [6]. The other technique applies the Alamouti scheme which flattens the frequency selectivity of the received signal, gains a higher diversity than CDD but requires an additional decoding process at the mobile. This technique is called cellular Alamouti technique (CAT) [11, 10]. As for C-CDD, an adaptive flavor of CAT is also presented. Finally, both schemes are compared and discussed [2]. Unless otherwise stated, all simulations are based on the simulation setup of *System B* (cf. Appendix C.2).

6.1 Cellular Cyclic Delay Diversity (C-CDD)

Transmit diversity techniques offer the possibility of more reliable link performances [Dam06]. Modified replicas of the original signal are sent from additional implemented transmit antennas. For OFDM based systems, shifts in time domain are possible signal modifications. Since the additional time domain shift influences the signal spectrum, these schemes are referred to as frequency domain diversity techniques. The goal of these techniques is to increase the frequency selectivity of the channel, and therefore, to decrease the coherence bandwidth. To exploit the additional diversity in an OFDM system, forward error correction (FEC) is needed. The elementary method, namely delay diversity [Wit93], transmits delayed replicas of a signal from several transmit antennas N_{T} with delays $\delta_n, n = 0, \ldots, N_{\mathrm{T}} - 1$, where δ_n is given in samples. In DD inter-symbol interference can occur if the maximum possible delay of the resulting received signal exceeds the guard interval length N_{GI} of the OFDM system:

$$N_{\mathrm{GI}} \geq \tau_{\max} + \max_n \delta_n \,. \tag{6.1}$$

Cyclic Delay Diversity (CDD)

A neat solution to provide delay diversity without exceeding the guard interval and the occurrence of ISI, and therefore, without reducing the bandwidth efficiency, is the cyclic delay diversity technique [DK01a, DK01b]. By applying CDD no changes at the receiver are needed, there exists no rate loss for higher number of transmit antennas, and there are no requirements regarding constant channel properties over several sub-carriers or symbols and transmit antenna numbers. This

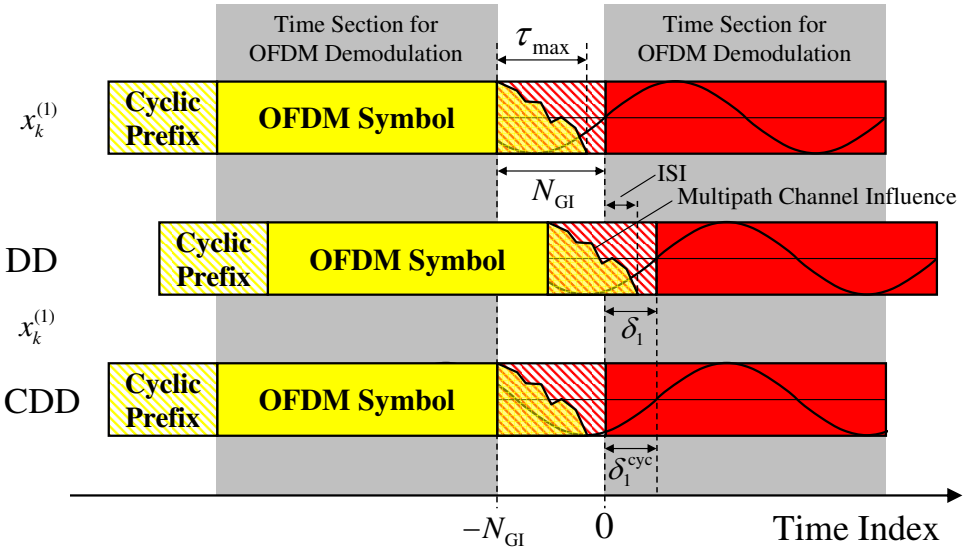

Figure 6.1: Principle of cyclic delay diversity

is an advantage compared to already established diversity techniques, e.g., orthogonal space time block codes [TSC98]. For simplicity of the notation, the transmission of one OFDM symbol is considered, and therefore, the time index l is omitted in the following. N_{FFT} data symbols $X_i, i = 0, \ldots, N_{\mathrm{FFT}} - 1$ are obtained from a precedent coding, modulation, and framing part (cf. Section 2.2.2). These complex valued symbols are transformed into the time domain by the OFDM entity using the IFFT (cf. (2.16)). This results in N_{FFT} normalized (balanced) time domain OFDM symbols, represented by the samples

$$x_k = \frac{1}{\sqrt{N_{\mathrm{FFT}}}} \sum_{i=0}^{N_{\mathrm{FFT}}-1} X_i \cdot e^{\mathrm{j}\frac{2\pi}{N_{\mathrm{FFT}}} ik} \,. \tag{6.2}$$

Before inserting a cyclic prefix as guard interval, the time domain OFDM symbol is shifted cyclically by δ_n^{cyc} (delays given in samples), which results in the signal

$$x_{k-\delta_n^{\mathrm{cyc}} \bmod N_{\mathrm{FFT}}} = \frac{1}{\sqrt{N_{\mathrm{FFT}}}} \sum_{i=0}^{N_{\mathrm{FFT}}-1} e^{-\mathrm{j}\frac{2\pi}{N_{\mathrm{FFT}}} i\delta_n^{\mathrm{cyc}}} \cdot X_i \cdot e^{\mathrm{j}\frac{2\pi}{N_{\mathrm{FFT}}} ik} \,. \tag{6.3}$$

The n-th antenna specific transmit signal is given by

$$x_k^{(n)} = \frac{1}{\sqrt{N_{\mathrm{T}}}} \cdot x_{k-\delta_n^{\mathrm{cyc}} \bmod N_{\mathrm{FFT}}} \,, \tag{6.4}$$

where the signal is normalized by $1/\sqrt{N_{\mathrm{T}}}$ to keep the average transmission power independent of the number of transmit antennas N_{T}. To avoid ISI within CDD, the guard interval length N_{GI} has to fulfill

$$N_{\mathrm{GI}} \geq \tau_{\max} \,, \tag{6.5}$$

which is independent of the cyclic delays δ_n^{cyc}. As long as the effective maximum delay $\tau'_{\max}$ of the resulting channel

$$\tau'_{\max} = \tau_{\max} + \max_n \delta_n^{\mathrm{cyc}} \tag{6.6}$$

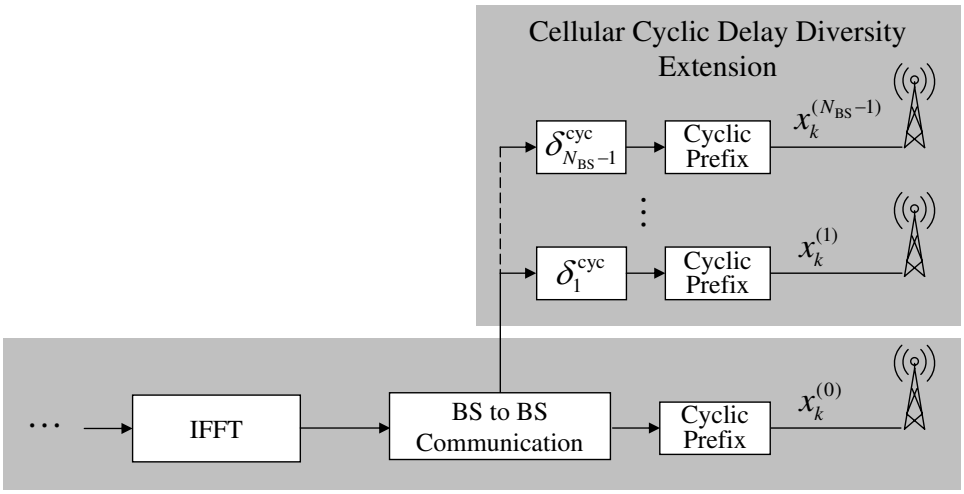

Figure 6.2: Block diagram of the C-CDD principle

does not intensively exceed N_{GI}, there is no configuration and additional knowledge at the receiver needed. If $\tau'_{\max} \gg N_{\text{GI}}$, the pilot grid and also the channel estimation process has to be modified [Aue04]. This can be circumvented by using differential modulation [Bau06].

Furthermore, the cyclic delays avoid delayed transmitted replica signals compared to DD which is beneficial for synchronization processes at the receiver. The principles of DD and CDD are shown in Figure 6.1 for the transmission of two successive OFDM symbols via 2 transmit antennas. Due to the introduced time delay in DD, ISI can occur which is not given by cyclic delays in CDD.

On the receiver side, the cyclic shift can be assigned formally to the channel transfer function, and therefore, the overall frequency domain channel transfer function

$$H_i = \frac{1}{\sqrt{N_{\text{T}}}} \sum_{n=0}^{N_{\text{T}}-1} e^{-\text{j}\frac{2\pi}{N_{\text{FFT}}}\delta_n^{\text{cyc}} \cdot i} \cdot H_i^{(n)} \tag{6.7}$$

is observed. $H_i^{(n)}$ represents the CTF from the nth antenna. The channel seen by the receiver for the CDD concept is transformed from a multiple-input single-output (MISO) channel to a single-input single-output (SISO) channel. Without loss of generality, $\delta_0^{\text{cyc}} = 0$. Since the receiver sees the overall CTF, the decoding process gains by the higher amount of frequency diversity for the new generated channel.

6.1.1 C-CDD Principle

For the defined broadcast region for users with similar demands or users within soft/softer handover procedures (cf. introduction of this chapter), the CDD principle can be applied within this cellular setup by using adjacent BSs. This leads to the cellular cyclic delay diversity (C-CDD) scheme. The main goal is to increase performance by avoiding interference, using the same sub-carrier resources, and increasing diversity at the most critical areas.

For C-CDD the neighboring BSs also transmit a copy of the users' signal as the desired BS to the designated MS located in the broadcast area. Additionally, a cyclic shift is inserted to these signals. A block diagram describes the principle of C-CDD in Figure 6.2. Therefore, the overall delay of the

signal from BS m in the cellular system can be expressed by

$$\delta_m = \delta(d_m) + \delta_m^{\mathrm{cyc}}\,, \tag{6.8}$$

where $\delta(d_m)$ represents the natural delay of the signal depending on distance d_m. The delays can be also represented in meters. The general relation can be expressed by

$$\delta\,[\text{meter}] = \mathrm{c} \cdot \delta\,[\text{sample}]\,, \tag{6.9}$$

where c is the speed of light. At the MS the received signal can be described by

$$Y_{l,i} = X_{l,i}^{(0)} \sum_{m=0}^{N_{\mathrm{BS}}-1} \alpha_{\mathrm{att}}^{(m)} H_{l,i}^{(m)} e^{-\mathrm{j}\frac{2\pi}{N_{\mathrm{FFT}}}\delta_m \cdot i} + N_{l,i}\,. \tag{6.10}$$

The usage of cyclic shifts prevents the occurrence of additional ISI. Additionally, the broadcast scenario from the BSs should ensure that the reception of all signals are within the guard interval, i.e.,

$$\Delta\delta_{\nu,\mu} = |\delta(d_\nu) - \delta(d_\mu)| \leq N_{\mathrm{GI}}\,, \qquad \text{for all} \quad \nu \neq \mu\,. \tag{6.11}$$

At the MS the superimposed statistically independent Rayleigh distributed channel coefficients from the different BSs sum up again in a Rayleigh distributed channel coefficient. For C-CDD no additional configurations at the MS for exploiting the increased transmit diversity are necessary and an arbitrary number of involved BSs can be chosen without a rate loss. Transmitting the same signals to the desired MSs from neighboring BS without the CDD principle (i.e., all $\delta_m^{\mathrm{cyc}} = 0$) results in pure macro diversity within a broadcast region.

6.1.2 Channel Correlation Properties of C-CDD

Since the influence of C-CDD on the system can be observed at the receiver as a change of the channel conditions, in the following this modified channel is investigated in terms of its channel transfer functions and fading correlation in time and frequency direction for two-cell environment. These correlation characteristics also describe the corresponding single transmit antenna channel seen at the MS for C-CDD. Due to $\delta_0^{\mathrm{cyc}} \neq \delta_1^{\mathrm{cyc}}$ and the relation in (6.8), the resulting performance regarding the MS position of C-CDD should have an asymmetric characteristic and can be investigated by the resulting channel correlation properties.

The frequency domain fading processes for different propagation paths are uncorrelated in the assumed quasi-static channel. Since the number of sub-carriers is larger than the number of propagation paths, there exists correlation between the sub-carriers in the frequency domain. The corresponding channel which influences the received signal $X_{l,i}^{(0)}$ (cf. (6.10)) at the receiver is represented by

$$H'_{l,i} = \sum_{m=0}^{N_{\mathrm{BS}}-1} \alpha_{\mathrm{att}}^{(m)} H_{l,i}^{(m)} e^{-\mathrm{j}\frac{2\pi}{N_{\mathrm{FFT}}}\delta_m \cdot i}\,. \tag{6.12}$$

Since the interest is based on the fading and signal characteristics observed at the receiver, the AWGN term $N_{l,i}$ of (6.10) is skipped for the following investigations. The expectation

$$\mathbf{R}(l_1, l_2, i_1, i_2) = E\{H'_{l_1,i_1} \cdot H'^{*}_{l_2,i_2}\} \tag{6.13}$$

yields the correlation properties of the frequency domain channel fading. Due to the path propagations $\alpha_{\text{att}}^{(m)}$ and the resulting power variations, the channel transfer functions $H_{l,i}^{(m)}$ is normalized by the multiplication factor $\frac{1}{\sqrt{\sum_{m=0}^{N_{\text{BS}}-1} {\alpha_{\text{att}}^{(m)}}^2}}$ which is included for $\mathbf{R}_{\text{n}}(l,i)$.

The fading correlation properties can be divided in three cases. The first represents the power, the second investigates the correlation properties between the OFDM symbols (time direction), and the third examines the correlation properties between the sub-carriers (frequency direction).

Case 1: Since uncorrelated sub-carriers are assumed the autocorrelation of the CTF ($l_1 = l_2 = l, i_1 = i_2 = i$) is

$$\mathbf{R}(l,i) = \sum_{m=0}^{N_{\text{BS}}-1} \underbrace{e^{-\text{j}\frac{2\pi}{N_{\text{FFT}}}\delta_m \cdot i} \cdot e^{+\text{j}\frac{2\pi}{N_{\text{FFT}}}\delta_m \cdot i}}_{=1} {\alpha_{\text{att}}^{(m)}}^2 \cdot \underbrace{E\{H_{l,i}^{(m)} \cdot H_{l,i}^{(m)*}\}}_{E\{|H_{l,i}^{(m)}|^2\}=1} = \sum_{m=0}^{N_{\text{BS}}-1} {\alpha_{\text{att}}^{(m)}}^2 , \tag{6.14}$$

and the normalized power is

$$\mathbf{R}_{\text{n}}(l,i) = \sum_{m=0}^{N_{\text{BS}}-1} {\alpha_{\text{att}}^{(m)}}^2 E\{|\frac{H_{l,i}^{(m)}}{\sqrt{\sum_{m=0}^{N_{\text{BS}}-1} {\alpha_{\text{att}}^{(m)}}^2}}|^2\} = 1 . \tag{6.15}$$

Case 2: The correlation in time direction is given by $l_1 \neq l_2, i_1 = i_2 = i$. Since the channels from the BSs are i.i.d. stochastic processes, $E\{H_{l_1,i}^{(m)} \cdot H_{l_2,i}^{(m)*}\} = E\{H_{l_1,i} \cdot H_{l_2,i}^*\}$ and

$$\mathbf{R}(l_1 \neq l_2, i) = E\{H_{l_1,i} H_{l_2,i}^*\} \sum_{m=0}^{N_{\text{BS}}-1} {\alpha_{\text{att}}^{(m)}}^2 , \tag{6.16}$$

$$\mathbf{R}_{\text{n}}(l_1 \neq l_2, i) = E\{\frac{H_{l_1,i} H_{l_2,i}^*}{\sum_{m=0}^{N_{\text{BS}}-1} {\alpha_{\text{att}}^{(m)}}^2}\} \sum_{m=0}^{N_{\text{BS}}-1} {\alpha_{\text{att}}^{(m)}}^2 = E\{H_{l_1,i} H_{l_2,i}^*\} . \tag{6.17}$$

In time direction, the correlation properties of the resulting channel are independent of the MS position.

Case 3: In frequency direction ($l_1 = l_2 = l, i_1 \neq i_2$) the correlation properties are given by

$$\mathbf{R}(l, i_1 \neq i_2) = E\{H_{l,i_1} H_{l,i_2}^*\} \cdot \sum_{m=0}^{N_{\text{BS}}-1} {\alpha_{\text{att}}^{(m)}}^2 \underbrace{e^{-\text{j}\frac{2\pi}{N_{\text{FFT}}}\delta_m \cdot (i_1 - i_2)}}_{\text{C-CDD component}} . \tag{6.18}$$

For large d_m ($\alpha_{\text{att}}^{(m)}$ gets small) the influence of the C-CDD component vanishes. And there is no beneficial increase of the frequency diversity close to a BS anymore. The normalized correlation properties yield

$$\mathbf{R}_{\text{n}}(l, i_1 \neq i_2) = E\{H_{l,i_1} H_{l,i_2}^*\} \cdot \underbrace{\frac{1}{\sum_{m=0}^{N_{\text{BS}}-1} {\alpha_{\text{att}}^{(m)}}^2} \cdot \sum_{m=0}^{N_{\text{BS}}-1} {\alpha_{\text{att}}^{(m)}}^2 e^{-\text{j}\frac{2\pi}{N_{\text{FFT}}}\delta_m \cdot (i_1 - i_2)}}_{\text{correlation factor } \rho_{\text{freq}}} . \tag{6.19}$$

The correlation factor ρ_{freq} is directly influenced by the C-CDD component and determines the overall channel correlation properties in frequency direction. Figure 6.3 shows the characteristics of ρ_{freq} for

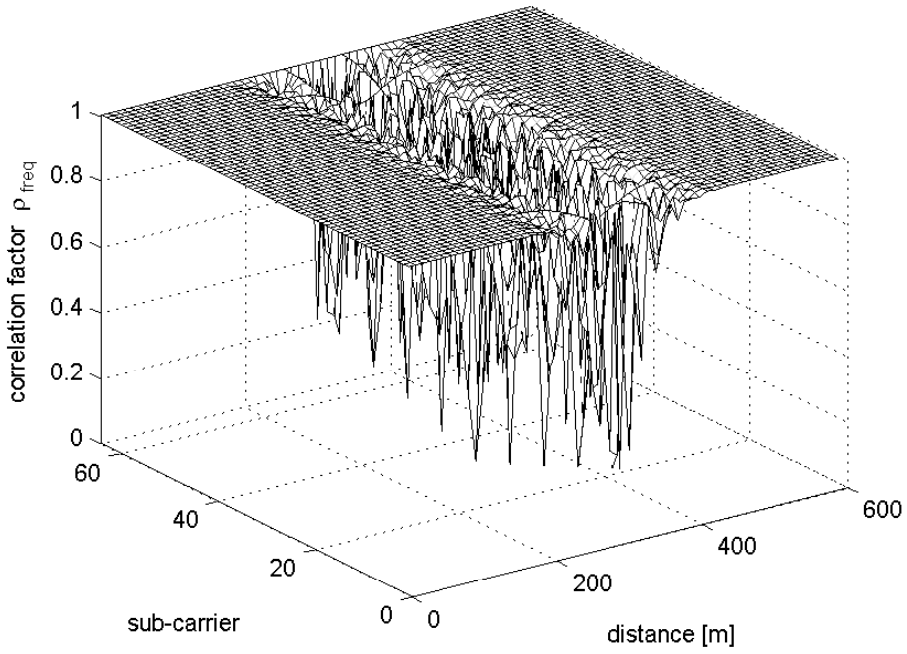

Figure 6.3: Characteristic of correlation factor ρ_{freq} over the sub-carriers depending on d_0

an exemplary system with $F_{\mathrm{s}} = 488.28$ Hz, $N_{\mathrm{FFT}} = 64, \gamma = 3.5, N_{\mathrm{BS}} = 2, r = 300m, \delta_0^{\mathrm{cyc}} = 0$, and $\delta_1^{\mathrm{cyc}} = 7$. One sample of the delay represents 32 μs or approximately 10 m. In the cell border area ($200m < d_0 < 400m$), C-CDD increases the frequency diversity by decorrelating the sub-carriers. As mentioned before, there is less decorrelation the closer the MS is to a BS.

A closer look on the area is given in Figure 6.4 where the inherent delay and the added cyclic delay are compensated, i.e., for $d_0 = 335m$ the delay difference is

$$\Delta\delta_{1,0} \overset{(6.11)}{=} \delta(265\ \mathrm{m}) + \delta_1^{\mathrm{cyc}} - \delta(335\ \mathrm{m}) - \delta_0^{\mathrm{cyc}} = 0\,. \tag{6.20}$$

The plot represents exemplarily three positions of the MS ($d_0 = [334\ \mathrm{m}, 335\ \mathrm{m}, 336\ \mathrm{m}]$) and shows explicitly the degradation of the correlation properties over all sub-carriers due to the non-existing delay in the system.

6.1.3 Impact of C-CDD

In the following, the impact of C-CDD on the performance within a two-cell environment is investigated for *System B*. The main outcome and conclusions can be also mapped onto higher number of interfering cells. For one interfering cell, the C/I ratio gives an appropriate interpretable measure.

The influence of the cyclic delay is given in Figure 6.5 for the BER and the SNR gain directly at the cell border for a fully-loaded C-CDD system. For $\delta_1^{\mathrm{cyc}} = 0$, pure macro diversity is existing and both signals are received simultaneously at the MS. By increasing the cyclic delay additional diversity is generated due to the higher frequency selectivity of the resulting channel. This affects directly the system performance and the BER reduces significantly. For higher cyclic delays there exists a saturation of the performance which reflects the results in [Bau05]. The SNR gain performance for a target BER of $P_{\mathrm{b}} = 10^{-3}$ depicts also the influence of the increased cyclic delay and the increase

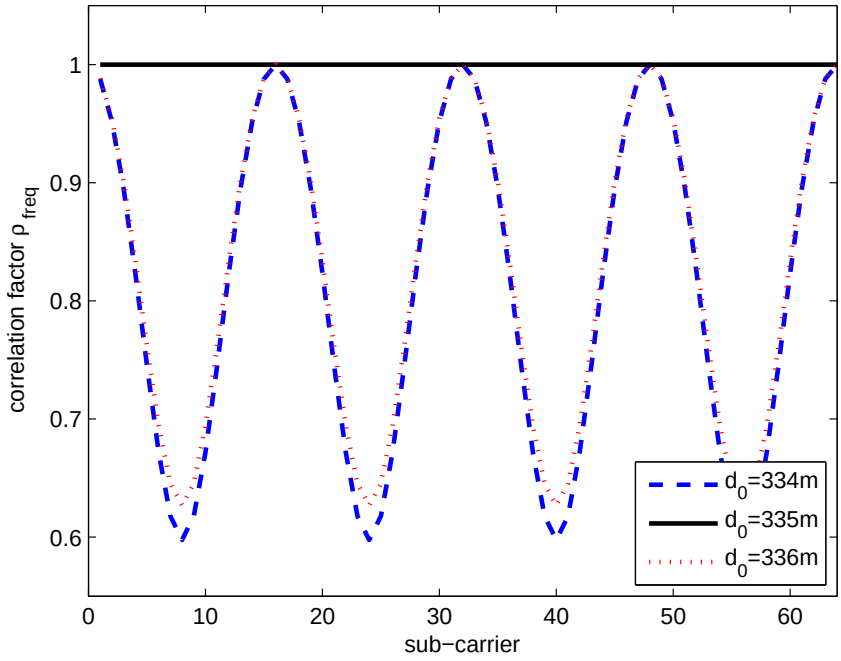

Figure 6.4: Correlation characteristics over the sub-carriers for $d_0 = [334\ \mathrm{m}, 335\ \mathrm{m}, 336\ \mathrm{m}]$

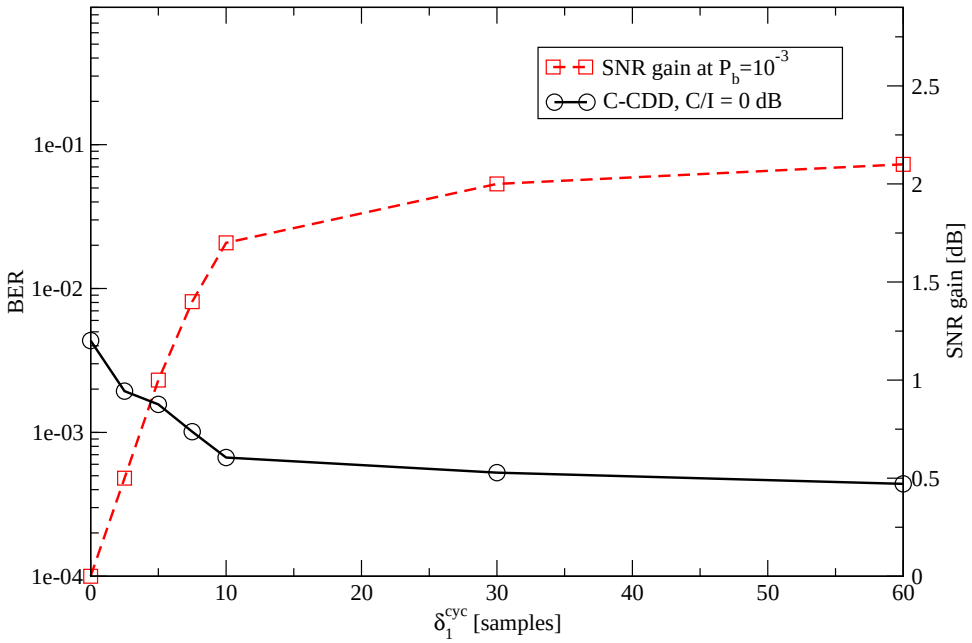

Figure 6.5: BER and SNR gain versus the cyclic delay at the cell border ($\mathrm{C/I} = 0$ dB)

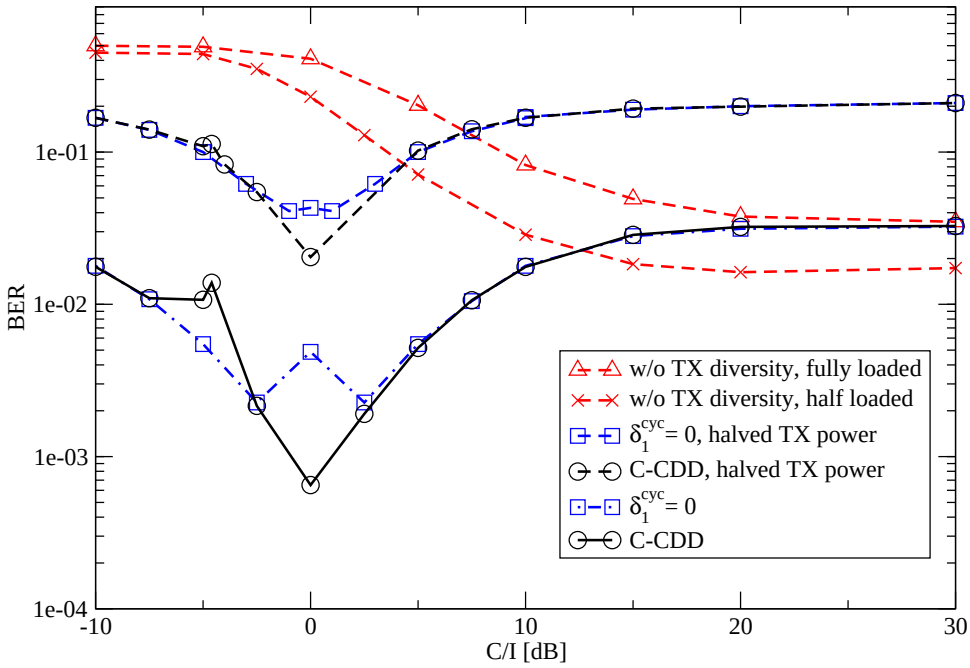

Figure 6.6: BER versus C/I using no transmit diversity technique and C-CDD for different scenarios; $\gamma_{i,\mathrm{dB}} = 5\ \mathrm{dB}$

frequency diversity, respectively. Similar to the BER performance the SNR gain saturates for higher delays with a gain of about $2\ \mathrm{dB}$. Therefore, a cyclic delay of 30 samples ($\hat{=}90\ \mathrm{m}$) is chosen in the following simulation setups unless otherwise stated.

The impact of C-CDD on the error performance for different MS locations is given in Figure 6.6. Since the C-CCD system is fully-loaded, the performance can be seen as an upper performance bound. For the reference system both BSs are transmitting independently their separate MC-CDMA signal. Therefore, this reference system does not use any transmit (TX) diversity technique. The reference system is half ($\mathrm{RL} = 0.5$) and fully loaded ($\mathrm{RL} = 1.0$). Due to the increased MAI for higher system loads, the fully-loaded MC-CDMA system performs worse than the lower loaded reference system. Clearly, the performance degrades the closer the MS is at the cell border ($C/I \leq 10\ \mathrm{dB}$). And in the inner part of the desired cell ($C/I > 10\ \mathrm{dB}$) the single cell BER performance is given for an SNR of $5\ \mathrm{dB}$ without inter-cell interference.

For this scenario with two BSs and the MS in direct line between the BSs ($\alpha = 0°$, cf. Figure 2.1), the distances of the BSs to the MS correspond directly to the delay $\delta(d_1) = 2r - d_0$. Since the transmitted powers at each BS are the same and equal shadowing factors are assumed, the following relations can be given

$$\gamma_{\mathrm{C/I}} \overset{(2.41)}{=} \left(\frac{d_0}{2r - d_0} \right)^{-\rho} \tag{6.21}$$

and

$$\Delta\delta_{1,0} = 2r - \left(\frac{4r}{\sqrt[\rho]{\gamma_{\mathrm{C/I}}} + 1} \right) + \delta_1^{\mathrm{cyc}} - \delta_0^{\mathrm{cyc}}\,. \tag{6.22}$$

A large performance gain in the close-by area of the cell border ($C/I = -10\ \mathrm{dB}, \ldots, 10\ \mathrm{dB}$) exists for the cellular diversity technique C-CDD. Furthermore, C-CDD enables an additional substantial performances gain at the cell border compared to pure macro diversity ($\delta_1^{\mathrm{cyc}} = 0$). The performance

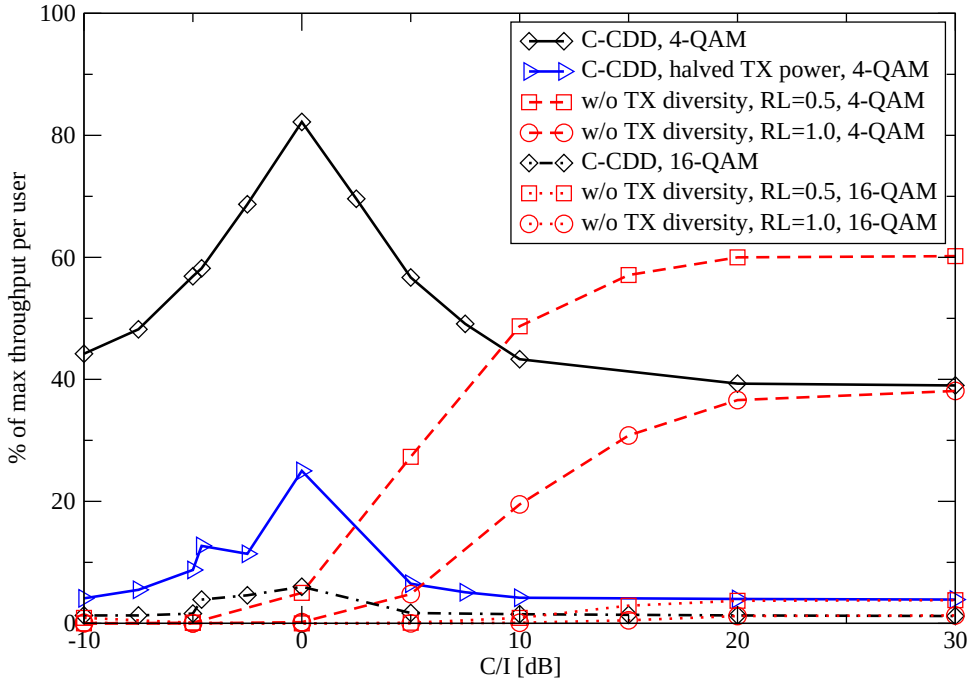

Figure 6.7: Throughput per user versus C/I using no transmit diversity or C-CDD with full and halved transmit power; $\gamma_{i,\mathrm{dB}} = 5$ dB

for pure macro diversity degrades at $C/I = 0$ dB because the delay difference is $\Delta\delta_{1,0} = 0$, and therefore, no transmit diversity is available. The same effect can be seen for C-CDD at approximately $C/I = -4.6$ dB where the delay difference (cf. (6.22)) for the chosen $\delta_1^{\mathrm{cyc}} = 30$ is also

$$\Delta\delta_{1,0} \overset{(6.9)}{=} 2 \cdot 300\ \mathrm{m} - \left(\frac{4 \cdot 300\ \mathrm{m}}{\sqrt[3.5]{10^{-4.6/10}} + 1} \right) + \mathrm{c} \cdot 30 \cdot 10\ \mathrm{ns} - 0 \approx 0\,. \tag{6.23}$$

Since both BSs in C-CDD transmit the signal with the same power as the single BS in the reference system, the received signal power at the MS is doubled. Therefore, the BER performances of C-CDD or pure macro diversity for $\Delta\delta_{1,0} = 0$ are still better than the best reference system performance. For higher C/I ratios, i.e., in the inner cell, the C-CDD transmit technique lacks the diversity from the other BS and additionally degrades due to the double load in each cell. Thus, the MS has to cope with the double MAI. The loss due to the MAI can be directly seen by comparing the transmit diversity performance with the half-loaded reference system. The fully-loaded reference system has the same MAI as the C-CDD system, and therefore, the performances merge for high C/I ratios.

To establish a more detailed understanding, C-CDD with halved transmit power is also analyzed in Figure 6.6. For this scenario, the total designated received power at the MS is equal to the conventional MC-CDMA system. There is still a performance gain due to the exploited transmit diversity for $C/I < 5$ dB. The performance characteristics are the same for halved and full transmit power. The benefit of the halved transmit power is a reduction of the inter-cellular interference for the neighboring cells. In the case of varying channel models or conditions in the adjacent cells, the basic performance characteristics will be the same but won't have this symmetric behavior anymore.

The maximal achievable throughput for the two-cell scenario for C-CDD and the reference system is shown in Figure 6.7. 4-QAM and 16-QAM are chosen for the modulation alphabets. The simulation results represent the rate of the maximum throughput per user (cf. 4.10) versus the C/I ratio. The conventional system is outperformed by C-CDD at the cell border for all scenarios. For 4-QAM and

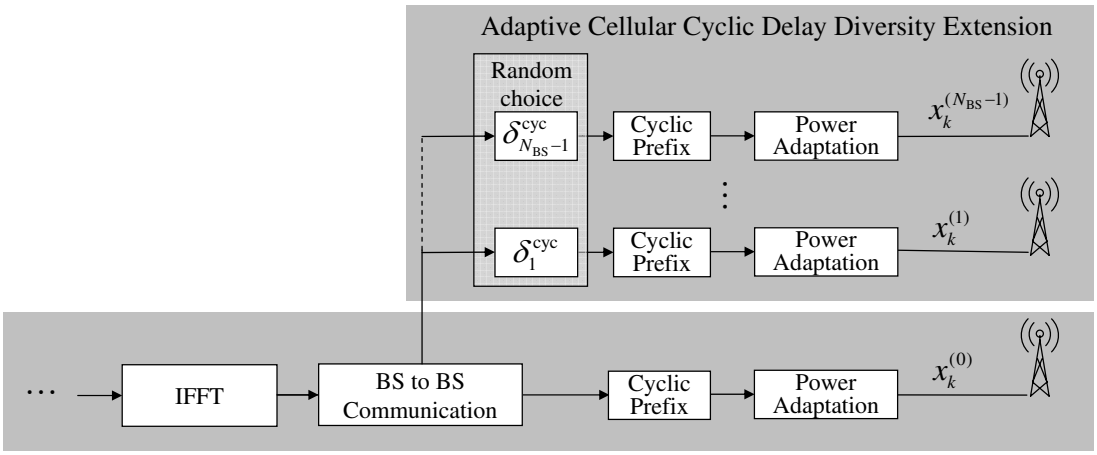

Figure 6.8: Block diagram of the adaptive soft C-CDD principle

C-CDD, a reliable throughput along the cell border is achieved. Since C-CDD with halved transmit power still outperforms the conventional system, it is possible to decrease the inter-cellular interference by reduced signal powers within the cells. Due to the almost vanishing performance for 16-QAM with halved transmit power for an SNR of $5\ \mathrm{dB}$, this performance curve is not depicted.

6.1.4 Adaptive C-CDD

The goal of the C-CDD technique is to improve the performance directly at the cell border. Since the impinging signals at the MS have already a geographical dependent delay, these signals include inherently pure macro diversity and there is no performance gain by applying C-CDD beyond the cell border. On the other side, the system has a performance degradation without the applied C-CDD if the MS is at a *neutral* position with the same delay properties from all BSs. Especially at this position the MS experiences the highest inter-cell interference. By using C-CDD, a large performance gain is given. Therefore, C-CDD can combat this degradation and can provide reliable performance. There is also a worst case for C-CDD (cf. Figure 6.6) if the cyclic delays and the inherent delay cancel out each other ($\Delta\delta_{\nu,\mu} = 0$, cf. (6.11)). With a proper choice of the cyclic delays, the drawbacks of both scenarios (neutral location and $\Delta\delta_{\nu,\mu} = 0$) can be circumvented without the need of additional information at the transmitter and the resulting benefits can be utilized.

A further step for an adaptive component in C-CDD is the variation of the transmit powers from the involved BSs in the case of an available feedback channel. This leads to the so-called soft C-CDD.

Choice of Cyclic Delay

The cyclic delay can be chosen in the following way. For each symbol transmission a cyclic delay is randomly chosen out of a set of cyclic delays $\mathbb{S}$. For systems with channel estimation based on scattered pilots, the maximum cyclic delay $\delta^{\text{cyc}}_{\max}$ of $\mathbb{S}$ is restricted by (6.6). Furthermore, the case of $\Delta\delta_{\nu,\mu} = 0$ can be avoided by excluding potential cyclic delays which causes $\Delta\delta_{\nu,\mu} = 0$ starting $\mathbb{S}$ with $\Delta\delta^{\text{cyc}}$. Therefore, the interval for the randomly chosen cyclic delays is given by

$$\mathbb{S} = [\Delta\delta^{\text{cyc}}, \delta^{\text{cyc}}_{\max}]\,. \tag{6.24}$$

Soft C-CDD — Transmit Power Adaption

Due to the influence of the propagation path loss, the maximum diversity received from all involved BSs for C-CDD is achieved directly at the cell border or by the same received signal strengths from all BSs, respectively. Therefore, the idea is to broaden the maximum diversity area by adapting the transmit powers regarding to the position of the MS. For this scenario, the location of the MS is expressed by the received C/I ratio. This information can be transmitted to the BS from the MS in the uplink.

Since the BSs are limited to a maximum transmit power $P_{\max}$, the adaption of the transmit power $P_{\mathrm{t},m}$ of each BS in C-CDD has to follow the constraint:

$$\sum_{m=0}^{N_{\mathrm{BS}}-1} P_{\mathrm{t},m} = P_{\max}\,. \tag{6.25}$$

We assume that the maximum transmit power is normalized to one and an adaptive power factor $a_m \in [0,1]$ regulates the transmit powers of each BS,

$$\sum_{m=0}^{N_{\mathrm{BS}}-1} E\{|a_m|^2\} \stackrel{!}{=} 1\,. \tag{6.26}$$

With these assumptions, the expectation values in (2.40) are equal except the adaptive power factors a_m. Thus, from (2.40) and (6.25) the adaptive power weighting factors are given by

$$a_0 = 1 - \sum_{m=1}^{N_{\mathrm{BS}}-1} a_m\,, \qquad a_m = \frac{1}{1+\gamma_{\mathrm{C/I}}} - \sum_{\substack{m'=1 \\ m'\neq m}}^{N_{\mathrm{BS}}-1} a_{m'}\,. \tag{6.27}$$

It is also possible to describe the power distribution by one parameter

$$\Delta P = 10 \cdot \log \frac{|a_0|^2}{1-|a_0|^2} \quad [\mathrm{dB}]\,. \tag{6.28}$$

The parameter ΔP allows to switch on/off C-CDD softly. Therefore, the adaptive power weighting within C-CDD can be called soft C-CDD. Note that $\Delta P = +\infty$ completely switches off C-CDD. If the transmission system does not offer a feedback channel, the principle of soft C-CDD can be also used by using ΔP to reduce or increase the influence of the cellular diversity scheme.

Combination of Delay Choice and Power Adaption

It is also possible to combine simultaneously the random choice of the cyclic delays and the adaptive transmit power within C-CDD. This should guarantee a widened maximum diversity region around the cell border and an avoidance of $\Delta\delta_{\nu,\mu} = 0$. The C-CDD principle with the extension of a combined random delay and an adaptive transmit power is shown in Figure 6.8.

Influence of Cyclic Delay Choice

Within the given simulation environment of *System B*, a sample duration is $10\ \mathrm{ns}$ corresponding to a sample length of $3\ \mathrm{m}$. The maximum channel delay is $\tau_{\max} = 200\ \mathrm{ns}$ and the length of the guard

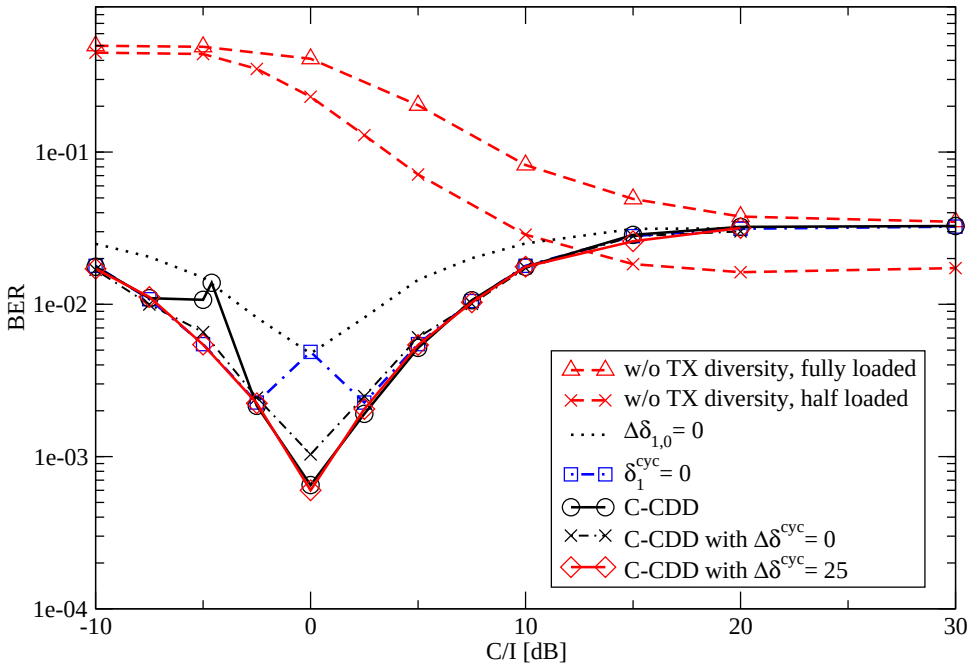

Figure 6.9: BER versus C/I using different methods of choosing the cyclic delays for C-CDD with MC-CDMA; $\gamma_{i,\mathrm{dB}} = 5\ \mathrm{dB}$

interval is 80 samples. According to (6.6), the maximum cyclic delay should be $\delta_{\max}^{\mathrm{cyc}} = 60$. If approximately $40\ \mathrm{m}$ around the cell border should be served by C-CDD in a two-cell environment and the assumed cell radius is $300\ \mathrm{m}$, delays smaller than 25 samples have to be excluded to guarantee $\Delta\delta_{1,0} \neq 0$. Therefore,

$$\mathbb{S} = [25, 60]\,. \tag{6.29}$$

The simulation results in Figure 6.9 show the BER performance characteristics by using different choices of $\Delta\delta^{\mathrm{cyc}}$. A lower performance bound is given by choosing the total delay of the system $\Delta\delta_{1,0} = 0$, represented with the dotted line. Two performance curves for different $\Delta\delta^{\mathrm{cyc}}$ of $\mathbb{S}$ for the random cyclic delay choice are given, i.e., $\Delta\delta^{\mathrm{cyc}} = 0$ and $\Delta\delta^{\mathrm{cyc}} = 25$. The performance loss in the area around $C/I = -4.7\ \mathrm{dB}$ can be compensated. For $\Delta\delta^{\mathrm{cyc}} = 0$ there are still cyclic delays possible which cause $\Delta\delta_{1,0} = 0$. Therefore, the performance is slightly worse compared to $\Delta\delta^{\mathrm{cyc}} = 25$.

Figure 6.10 shows the BER gain compared to the standard C-CDD system for the different possible choices of cyclic delays. The performance with $\Delta\delta^{\mathrm{cyc}} = 25$, i.e., a restricted random choice out of $\mathbb{S}$, achieves the best performance over the whole cell border area. Therefore, the drawbacks of the neutral position and $\Delta\delta_{1,0} = 0$ are compensated.

Influence of Adaptive Transmit Powers

For the simulation setup with two cells using the C-CDD technique, the power weighting factors a_0 and a_1 (cf. (6.27)) are

$$a_0 = 1 - a_1\,, \tag{6.30}$$

$$a_1 = \frac{1}{1+\gamma_{\mathrm{C/I}}} \overset{(6.21)}{=} \left(1 + \left(\frac{d_0}{2r - d_0}\right)^{-\rho}\right)^{-1}. \tag{6.31}$$

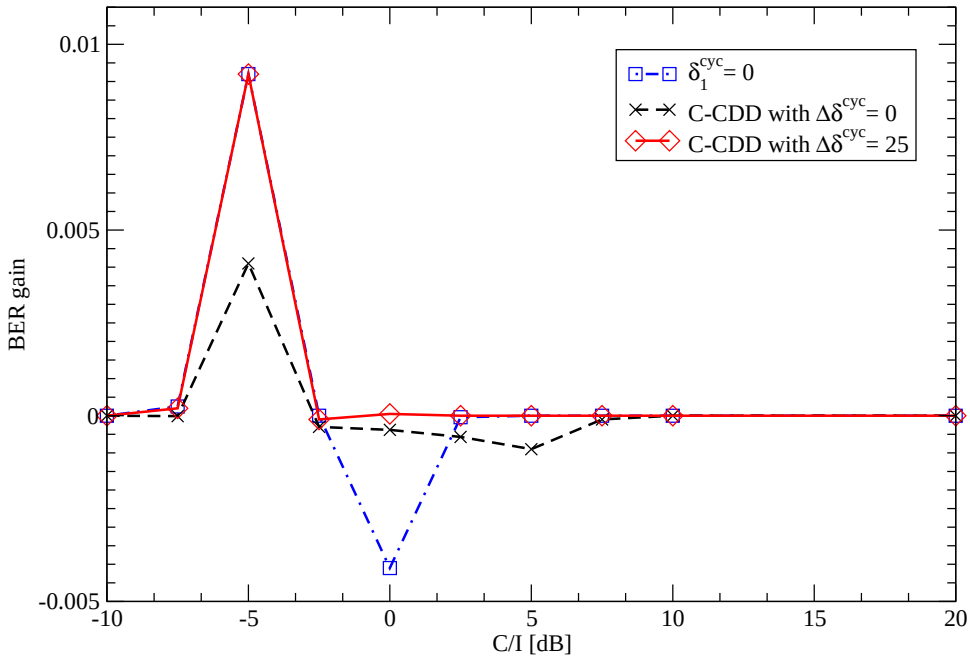

Figure 6.10: BER gain compared to the standard C-CDD system versus C/I using different methods of choosing the cyclic delays

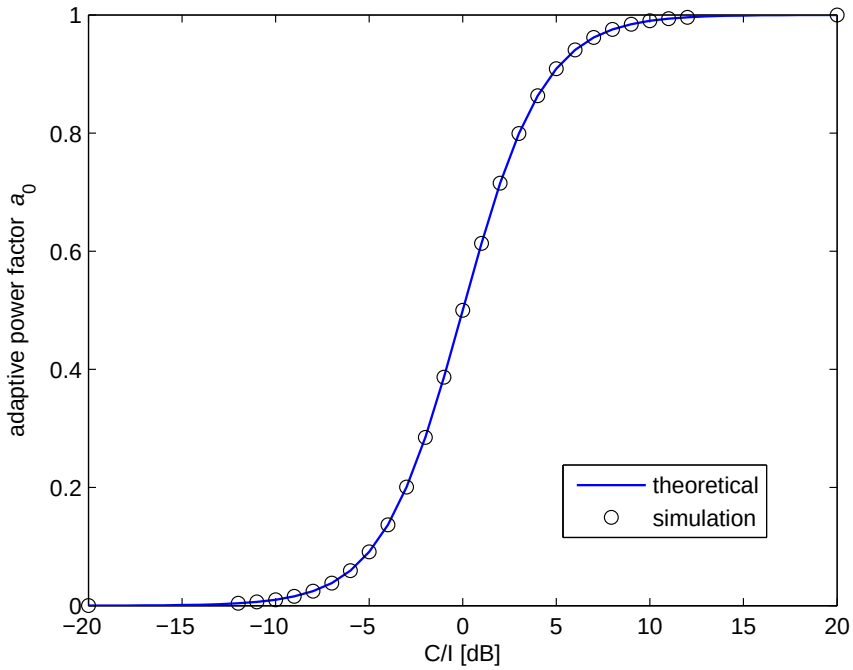

Figure 6.11: Adaptive power factor a_0 depending on the C/I ratio; theoretical and simulation results

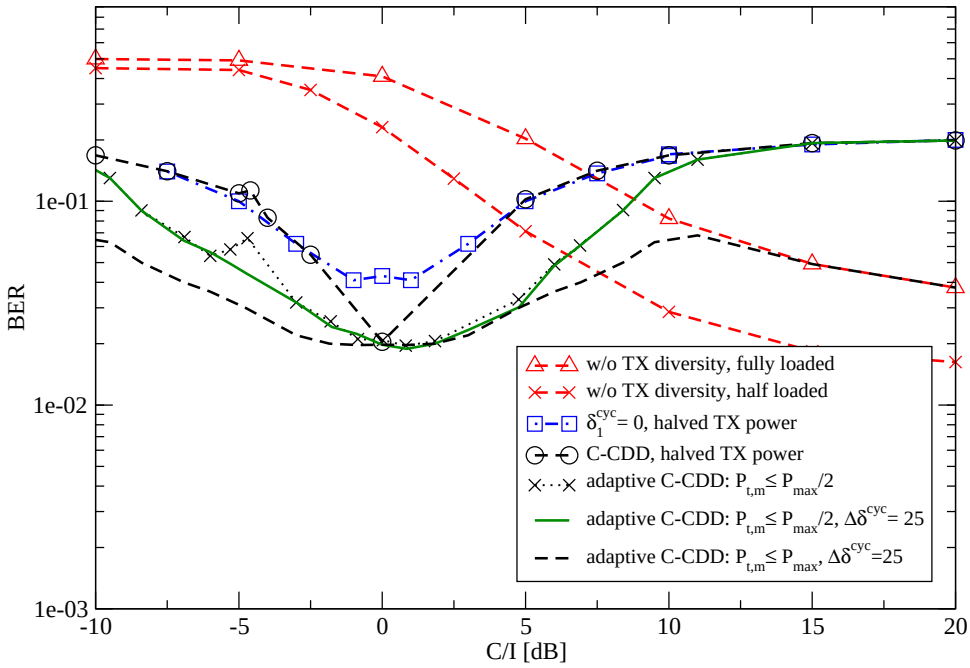

Figure 6.12: BER versus C/I using adaptive power factors and in combination with randomly chosen cyclic delays for C-CDD; $\gamma_{i,\mathrm{dB}} = 5\ \mathrm{dB}$

Figure 6.11 shows the dependence of the power weighting factor a_0 and the C/I ratio. The derived relationship is confirmed by simulation results. The results illustrate that only the cell border area $C/I = [-5\ \mathrm{dB}, \ldots, 5\ \mathrm{dB}]$ is influenced by both stations due to the propagation path loss. The other areas are only served by one BS, and therefore, C-CDD has no bearing on the MS.

For the following simulations, the relationship between a_0, a_1, and $\gamma_{\mathrm{C/I}}$ is used for the power adaption. Applying the power adaption results in the performance curves shown in Figure 6.12. Each BS is restricted to a maximum transmit power in a regulated cellular system (for these simulations a normalized power of $P_{\max} = 1$ is assumed). Two cases are investigated: first, both BSs will transmit at most $P_{\max}/2$ simultaneously; secondly, one BS can transmit at most $P_{\max}$ according to (6.25).

The C-CDD reference system is based on halved transmit powers at both BSs for comparison. Still, there is a performance gain in the cell border area compared to the reference system without transmit diversity. Furthermore, the fully-loaded C-CDD system achieves a better performance at the cell border than the half-loaded reference system without inter-cell interference ($C/I > 15\ \mathrm{dB}$).

For the first case ($P_{\mathrm{t},m} \leq P_{\max}/2$), the dotted line represents the performance by using the adaptive power factor throughout the cell border area. The received diversity and the resulting performance gain is increased in a wider area around the cell border. The influence of the second BS vanishes for larger absolute values of C/I due to the propagation path loss influence. The performance degradation due to $\Delta\delta_{1,0} = 0$ for $C/I = -4.7\ \mathrm{dB}$ is still existent. This can be compensated with the combination of adaptive power and an appropriate choice of the cyclic delays $\Delta\delta^{\mathrm{cyc}} = 25$ in C-CDD. A further performance gain can be achieved by the second case ($P_{\mathrm{t},m} \leq P_{\max}$). Obviously due to the higher transmit power, the performance is maximized over the whole cell border area.

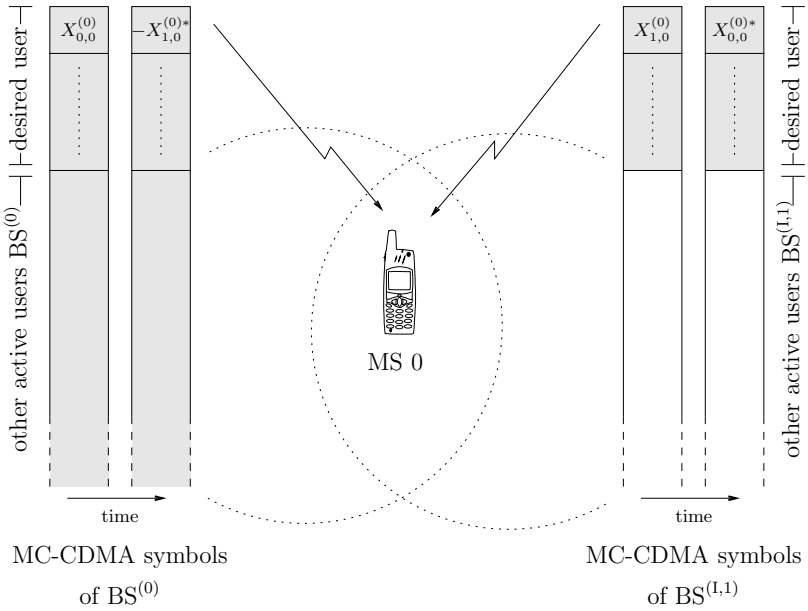

Figure 6.13: MC-CDMA symbol design for CAT

6.2 Cellular Alamouti Technique (CAT)

In this section, the concept of transmit diversity by using the space-time block codes from orthogonal designs [TJC99] is introduced, namely the Alamouti code. Since the space dimension in STBCs is given by multiple transmit antennas at the transmitter, the space dimension can be also shifted to simultaneously transmitting BSs in a cellular communications system. The use of the simple Alamouti code as a special case of STBCs leads to the cellular Alamouti technique (CAT).

The STBCs are based on the theory of (generalized) orthogonal designs for both real and complex valued signal constellations. The complex valued STBCs, can be described by a matrix

$$\mathbf{B} = \begin{array}{c} \leftarrow \text{ space } \rightarrow \\ \left(\begin{array}{ccc} b_{0,0} & \cdots & b_{0,N_\mathrm{T}-1} \\ \vdots & \ddots & \vdots \\ b_{l_\mathrm{c}-1,0} & \cdots & b_{l_\mathrm{c}-1,N_\mathrm{T}-1} \end{array} \right) \end{array} \begin{array}{c} \uparrow \\ \text{time or frequency} \\ \downarrow \end{array} , \tag{6.32}$$

where l_c is the STBC length. The simplest case is the Alamouti code [Ala98] with $N_\mathrm{T} = 2$ transmit antennas and $l_\mathrm{c} = 2$. The coding rate of this STBC is one. The transmitted symbols x_l are mapped to the transmit antennas by

$$\mathbf{B} = \begin{pmatrix} x_0 & x_1 \\ -x_1^* & x_0^* \end{pmatrix}. \tag{6.33}$$

Due to the orthogonal design of the Alamouti code, a simple linear combination can separate the symbols at the receiver by assuming quasi-static fading condition and uncorrelated transmit antennas.

The principles of the Alamouti code can be applied to a cellular setup which transforms the transmit diversity to macro diversity. Similar to the C-CDD technique, the transmitting antennas N_T for the Alamouti code are replaced by two neighboring BSs. This fulfills strictly the need of uncorrelated transmit antennas. The resulting mapping matrix in frequency domain for the cellular Alamouti

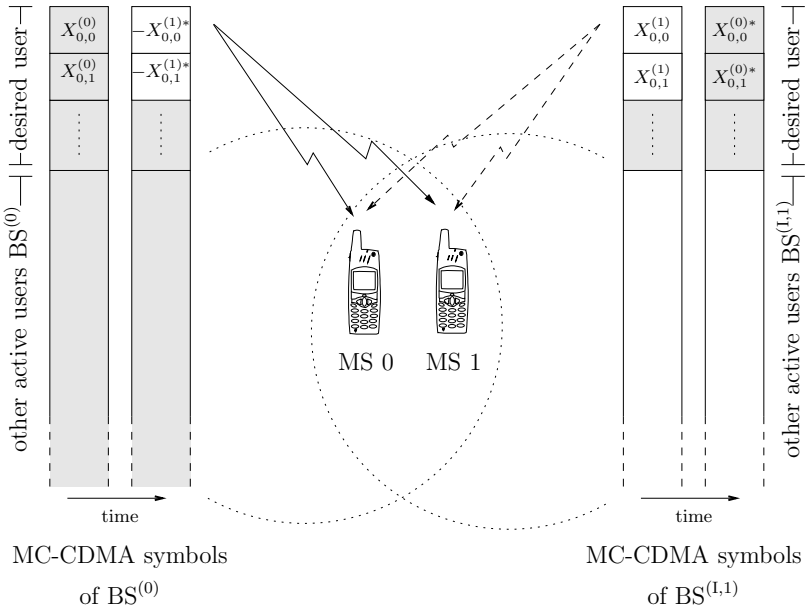

Figure 6.14: MC-CDMA symbol design for CAT serving 2 MSs simultaneously

technique is

$$\mathbf{B}_{\mathrm{CAT}} = \begin{array}{c} \begin{array}{cc} \mathrm{BS}^{(0)} & \mathrm{BS}^{(\mathrm{I},1)} \end{array} \\ \begin{pmatrix} X_{l,i}^{(0)} & X_{l+1,i}^{(0)} \\ -X_{l+1,i}^{(0)*} & X_{l,i}^{(0)*} \end{pmatrix} \end{array} . \tag{6.34}$$

Figure 6.13 illustrate the applied mapping of the CAT for one served MS. Since a mobile radio channel is more likely to be time non-selective, i.e., the fading is almost constant during two successive symbols, the mapping in $\mathbf{B}_{\mathrm{CAT}}$ follows the time dimension. For the used simulation environment *System B* the coherence time (cf. (2.6)) of the used channel is $(\Delta t)_{\mathrm{c}} \approx 0.034$ s and the coherence bandwidth (cf. (2.7)) is $(\Delta f)_{\mathrm{c}} \approx 5$ MHz. The channel is said to be time non-selective and frequency non-selective for

$$(\Delta t)_{\mathrm{c}}/T_{\mathrm{s}} > 1\,, \quad \text{and} \quad (\Delta f)_{\mathrm{c}}/B > 1\,. \tag{6.35}$$

For the simulation setup both coherence characteristics confirm the CAT in time direction, i.e.,

$$(\Delta t)_{\mathrm{c}}/T_{\mathrm{s}} = 0.034\,\mathrm{s}/16.64\,\mu\mathrm{s} > 1 \Rightarrow \text{time non-selective}\,, \tag{6.36}$$

$$(\Delta f)_{\mathrm{c}}/B = 5\,\mathrm{MHz}/100\,\mathrm{MHz} < 1 \Rightarrow \text{frequency selective}\,. \tag{6.37}$$

For STBCs from orthogonal designs, channel estimation for each transmit antenna at the receiver is mandatory. Disjoint pilot symbol sets for the transmit antenna branches can guarantee a separate channel estimation for each BS [IFN02].

Since the correlation of the sub-carrier fading coefficients in time direction is decreasing with increasing Doppler spread — i.e., the quasi-stationarity assumption of the fading is incrementally violated — the performance of this STBC class will suffer from higher Doppler frequencies. This is not necessarily true as the stationarity of the fading could also be detrimental in case of burst errors in fading channels which is shown in the subsequent section.

Figure 6.14 shows two mobile users being situated within the broadcast region. Both users' data is spread within one spreading block and transmitted by the cellular Alamouti technique using two base

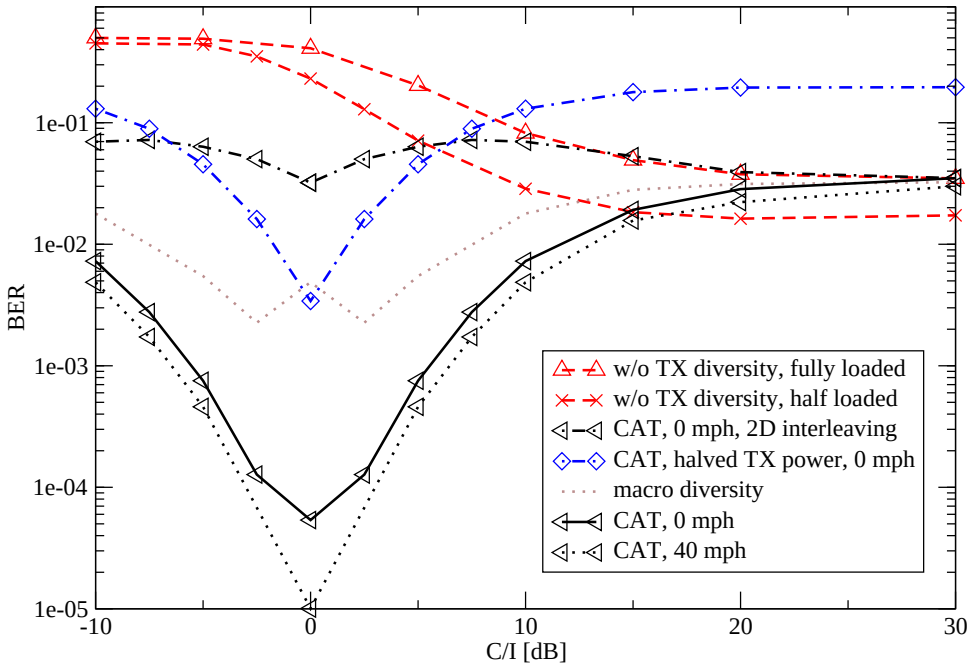

Figure 6.15: BER versus C/I using no transmit diversity technique and CAT for different scenarios; $\gamma_{i,\mathrm{dB}} = 5\ \mathrm{dB}$

stations. The base stations exploit information from a feedback link that the two MSs are in a similar location in the cellular network. By this, both MSs are served simultaneously avoiding any inter-cell interference between each other and exploiting the additional diversity gain. For this scenario the mapping matrix of the cellular Alamouti technique is

$$\mathbf{B}_{\mathrm{CAT},2} = \begin{array}{c} \begin{array}{cc} \mathrm{BS}^{(0)} & \mathrm{BS}^{(\mathrm{I},1)} \end{array} \\ \begin{pmatrix} X_{l,i}^{(0)} & X_{l,i}^{(1)} \\ -X_{l,i}^{(1)*} & X_{l,i}^{(0)*} \end{pmatrix} \end{array} . \tag{6.38}$$

Since in MC-CDMA the transmitted symbol $X_{l,i}^{(m)}$ represent a chip of several users, the described setup for two simultaneously served MSs can be extended to a setup of two sets of several MSs.

6.2.1 Impact of CAT

Figure 6.15 shows the performances of the applied CAT in the cellular system for different scenarios. Unless otherwise stated, the systems are using a 1D interleaving for the inner interleaver Π_{in}. In contrast to the conventional system, the BER can be dramatically improved at the cell border. By using the CAT, the MS exploits the additional transmit diversity where the maximum is given at the cell border. The CAT performances represent an upper bound due to a fully-loaded simulated system. If the MS moves with higher velocity ($40\ \mathrm{mph}$), the correlation of the sub-carrier fading coefficients in time direction decreases. This incremental violation of the quasi-stationarity assumption of the fading is profitable compensated by the channel code. The total violation of the aforementioned constraint of CAT is achieved by a fully-interleaved (2D) MC-CDMA frame. There is a large performance degradation compared to the CAT performance with a 1D-interleaved frame. Nevertheless, a residual transmit diversity exists, the MS benefits at the cell border, and the performance is improved. The

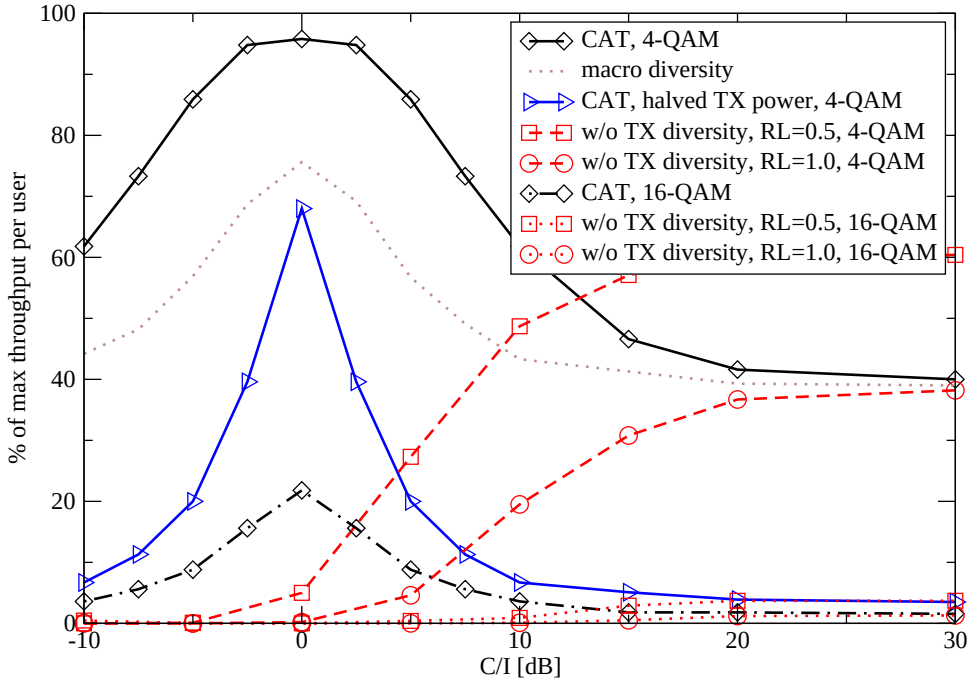

Figure 6.16: Throughput per user versus C/I using no transmit diversity or CAT with full and halved transmit power; $\gamma_{i,\mathrm{dB}} = 5$ dB

applied CAT is not only robust for varying MS velocities but also for non-quasi-static channel characteristics. Similar to C-CDD, there is still a performance gain due to the exploited transmit diversity for $C/I < 5$ dB in the case of halved transmit powers at both BSs.

The same performance characteristics as in C-CDD regarding the throughput can be seen in Figure 6.16 for applying the transmit diversity technique CAT. Due to the combination of two signals in the Alamouti scheme, CAT can provide a higher throughput than C-CDD in the cell border area. The CAT can almost achieve the maximum possible throughput in the cell border area.

Comparing the CAT BER or throughput performances with the pure macro diversity shows a significant performance gain over the whole cell border area.

6.2.2 Soft CAT

The same principles of adaptive transmit power in C-CDD (cf. Section 6.1.4) can be applied for CAT. This will also neglect the influence of the propagation path loss to a certain amount. By using the same setup of the adaptive power weighting factors a_m of (6.27) the CAT can be also switched on/off softly, leading to soft CAT. The adaptive transmit powers are limited, i.e., $P_{\max}/2$ or $P_{\max}$.

Figure 6.17 shows the BER performance for the soft CAT principle. Due to the power constraints of $P_{\max}$ the halved TX power performances are taken as reference performances. Within the broadcast area, the diversity area can be considerably broadened by applying the adaptive transmit power scheme. A wider area is given by choosing $P_{\mathrm{t},m} \leq P_{\max}$. Again, the soft CAT performance can improve significantly the performance compared to pure macro diversity.

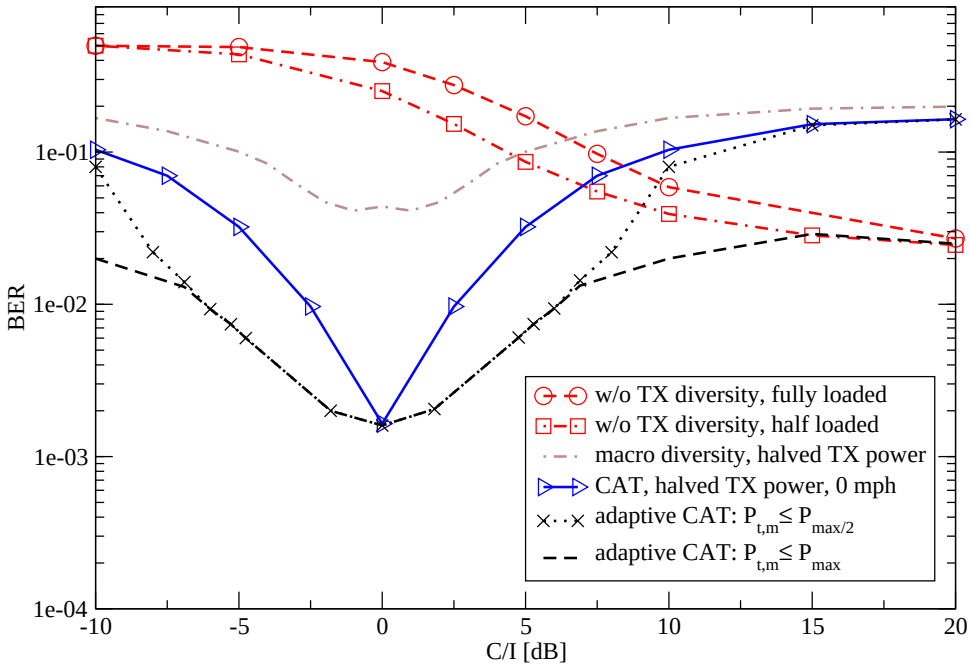

Figure 6.17: BER versus C/I using adaptive power factors for CAT; $\gamma_{i,\mathrm{dB}} = 5$ dB

6.3 Comparing C-CDD and CAT

Radio resource management works perfectly if all information about the mobile users, like the channel state information, is available at the transmitter [TV05]. This is especially true if the radio resource management could be intelligently managed by a single genie manager. As this will be very unlikely the described schemes C-CDD and CAT offer an improved performance especially at the critical cell border without the need of any information about the channel state information on the transmitter side. The main goal is to increase performance by avoiding interference and increasing diversity at the most critical environment.

Since the signal of the neighboring BSs for the desired users are not seen as interference, the MMSE equalizer coefficients of (3.17) need no modification as in the inter-cell interfering case. Therefore, the transmit diversity techniques require no knowledge about the inter-cell interference at the MS. By using C-CDD or CAT the critical cell border area can be also seen as a broadcast scenario with a multiple access channel [Cov72].

For the cellular transmit diversity concepts C-CDD and CAT each involved BS has to transmit additionally the signal of the adjacent cell, and therefore, a higher amount of resources are allocated at each BS. Furthermore, due to the higher RL in each cell the MAI for an MC-CDMA system is increased. There will be always a trade-off between the increasing MAI and the increasing diversity due to C-CDD or CAT.

Since the desired signal is broadcasted by more than one BS, both schemes can reduce the transmit signal power, and therefore, the overall inter-cell interference. Using MC-CDMA for the cellular diversity techniques the same spreading code set has to be applied at the involved BSs for the desired signal which allows simple receivers at the MS without multi-user detection processes.

Additionally, if a single MS or more MSs are aware that they are at the cell border, they could already ask for the C-CDD or CAT procedure on the first hand. This would ease the handover procedure and would guarantee a reliable soft or softer handover.

Table 6.1: Comparing C-CDD and CAT

	C-CDD	CAT
change at receiver	⇑ no	⇓ yes
new channel estimation & pilot grid	⇑ no	⇓ yes
number of involved BSs	⇑ unlimited	⇓ restricted to 2 BSs
performance gain	⇓ directly at the cell border	⇑ over whole broadcasted area

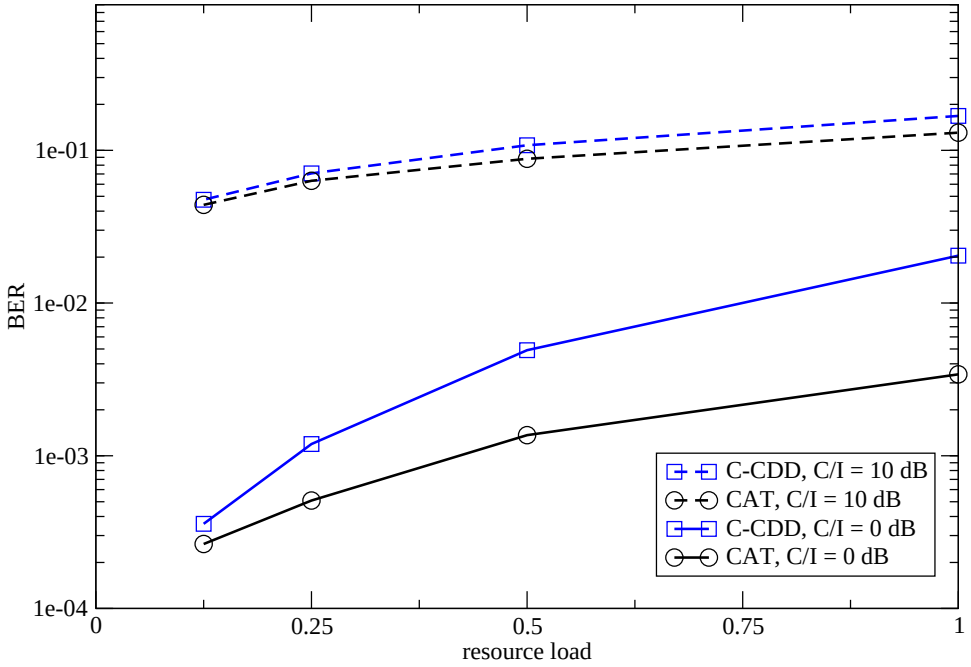

Figure 6.18: Influence of the MAI to the BER performance for varying resource loads at the cell border and the inner part of the cell

Two main differences between C-CDD and CAT should be pointed out. For C-CDD no changes at the receiver are needed, there exists no rate loss for higher number of transmit antennas, and there are no requirements regarding constant channel properties over several sub-carriers or symbols and transmit antenna numbers. This is an advantage over already established diversity techniques [TJC99] and CAT. On the other side, the Alamouti scheme based technique CAT provides a better performance due to the coherent combination of the two transmitted signals [Sch06].

The benefits and drawbacks of the two cellular transmit diversity scheme are summarized in Table 6.1. Furthermore, the two schemes are also compared in Figure 6.18 for a varying resource load within two scenario, namely directly at the cell border ($C/I = 0$ dB) and in the inner cell ($C/I = 10$ dB). These results show the direct influence of the MAI. Both transmit diversity schemes suffer from the increased MAI for higher resource loads which is in the nature of the used MC-CDMA system. More than 1 decade difference of the BERs exist. CAT is not influenced by the MAI as much as C-CDD for both scenarios. The performances merge for $C/I = 10$ dB because the influence of the transmit diversity techniques is highly reduced in the inner part of the cell. Furthermore, CAT outperforms always C-CDD due to the higher amount of diversity.

6.4 Summary

The cell border areas can be seen as a broadcast region due to the overlapping coverage areas of neighboring base stations. This geographical setting provides the possibility to introduce macro diversity schemes to benefit from this inter-cell interference arrangement. In this chapter two transmit diversity schemes are addressed by using different base stations for the desired signal to a mobile terminal within a cellular setup. This transforms the transmit diversity to macro diversity. The resulting additional diversity gains on the link layer can be exploited which compensate the inescapable spectrum efficiency losses using the diversity schemes.

The introduced cellular cyclic delay diversity and cellular Alamouti technique are capable to improve the performance at the severe cell borders. An upper bound of the cellular diversity schemes is given by the fully-loaded system performances. Lower loaded systems can additionally achieve a gain of BERs of 1 to 2 decades within the cell border areas. Furthermore, the techniques reduce the overall inter-cellular interference. Therefore, it is desirable to use C-CDD and CAT in the outer part of the cells, depending on available resources in adjacent cells. For example, these cellular diversity techniques can be utilized for more reliable soft and softer handover concepts.

The correlation properties of the resulting channel in C-CDD show the direct influence of the chosen cyclic delay on the location of the MS. The inducing degradation due to the loss of uncorrelated channel characteristics can be compensated by a randomized cyclic delay choice out of a set of cyclic delays. C-CDD offers no changes at the receiver, no rate loss for higher number of transmit antennas, and no requirements regarding constant channel properties over several sub-carriers or symbols and transmit antenna numbers.

In contrast to C-CDD, the introduced CAT offers diversity gains over the whole cell border area. On the other side, the underlying Alamouti code requires an additional signal processing and channel estimation at the MS. The reliable performance within the broadcast area can be simultaneously provided to two sets of mobile stations without any additional inter-cell interference. Furthermore, the investigations show a robust performance to different velocities and to non-stationary fading values.

For both cellular diversity techniques, a power adaptation from the BSs opens the possibility for the MS to request a higher throughput in the critical cell border area. The power adaption combats the propagation path loss degradations, and therefore, it broadens the diversity area. For the power adaption, an additional feedback of the received signal power at the MS has to be given within the system.

Concluding, the two cellular diversity schemes use the inter-cell interference setup (i.e., broadcast area) and exploit additional diversity compared to coordination schemes. Furthermore, C-CDD and CAT avoid the need of complex inter-cell cancellation techniques and decrease the overall inter-cell interference in the cellular network.

Chapter 7

Summary

The demand on high data rates for new applications in mobile communications, e.g., video streaming, requires a data packet flexible and spectral efficient transmission technique. Multi-carrier code division multiple access (MC-CDMA) satisfies both demands. Another major challenge to reach the envisaged data rates is the required efficient use of the available spectrum in all areas of the cellular system. Therefore, the system designs tend to apply a frequency reuse factor of one, i.e., the same spectrum is used in each cell. The challenges, new techniques, and requirements for handling emerging inter-cell interference in a next generation cellular MC-CDMA downlink on the link level are investigated in this thesis.

The importance of studying the characteristics of the inter-cell interference influence is endorsed by the shown performance degradations in the peripheral cell areas in Chapter 3. The major influence is caused by the two closest interfering base stations to the desired mobile user throughout the whole cell. Therefore, it is necessary to consider at least these two base stations for cellular investigations. Additionally, the higher the number of involved base stations and the higher the load of the system, the more the resulting inter-cell interfering signal is Gaussian like. This Gaussian approximation offers a simple modeling of a multi-cell environment by an appropriate additional Gaussian noise term on the desired signal. The influence of the overall cellular signal power has to be taken into account at the receiver by a modified MMSE equalizer. For interference mitigation techniques which are taking advantage of specific signal properties, the Gaussian approximation cannot be used but for background interferers.

Coordination of orthogonal resources can avoid and mitigate emerging inter-cell interference. Two resources are investigated for the cellular MC-CDMA system. First, frequency resources can separate the neighboring cells or interfering users. Due to the spreading nature of several users on chips in MC-CDMA, different frequency reuse factors can be applied. On the other side, this averaging effect excludes burst inter-cell interference to one user compared to the OFDM access scheme OFDMA. In Chapter 4 the MC-CDMA and OFDMA scheme are compared. OFDMA represents a challenging scheme for MC-CDMA because each user can be coordinated separately in each cell to avoid inter-cell interference. The beneficial properties of MC-CDMA by averaging inter-cell interference and exploiting more frequency diversity show supremacy compared to basic OFDMA within the investigations. Using an omniscient coordination scheme for OFDMA to avoid double allocations of sub-carrier resources between cells, OFDMA can obviously outperform MC-CDMA. A hybrid fractional frequency reuse of the cells achieves maximum performance. The inner part of each cell is served by an MC-CDMA system with frequency reuse of one and the outer parts by OFDMA or MC-CDMA with frequency reuse of three.

The second resource which can be coordinated is the used orthogonal set of spreading codes in MC-CDMA. The correlation properties of the present multi-path channel environment determine the degree of orthogonality between the spreading codes, and therefore, the potential of avoiding inter-cell interference. Furthermore, the investigations point out the trade-off between orthogonality and frequency diversity depending on the correlation characteristics. As in all coordination schemes, the absolute avoidance of inter-cell interference is limited by the number of available and addressed resources. After reaching this limit the coordination schemes try to mitigate the influence of the inter-cell interference.

In contrast to coordination concepts, the cancellation of inter-cell interference at the mobile station has no influence on the network side. In Chapter 5 two different concepts of ICIC are studied. The first ICIC scheme makes use of the hard decided outputs of the demodulator to reconstruct the interfering signals. Different combinations including the additional use of the signal power information are investigated. The performance in the severe cell border area profits from this concept.

Another iterative approach is investigated to cancel the inter-cell interference by using the more reliable soft output of the decoder for the reconstruction process. The studies show that already the second iteration can almost remove the inter-cell interference for a single-user system, and therefore, the single-user bound of the system is reached. This soft ICIC principle can achieve significant gains in performance over the whole cell border area. The performance degradation due to a reduced number of canceled interfering signals is reasonable compared to the significant complexity reduction of the iterative process. Since the iterative process is based on an exchange of mutual information, the investigation of the extrinsic information reveals the geographical influence of the performance characteristics. A further useful tool is the EXIT chart analysis whereas the additional inter-cell interference energy has to be taken into account in the log-likelihood ratio estimation of the demodulators. The EXIT chart analysis is only partially correct for such a complex cellular system, as the assumption of independent and Gaussian-distributed LLRs is violated.

The overlapping coverage areas of adjacent cells can be seen as a broadcast region. In Chapter 6 this setup is used to introduce cellular diversity techniques. Therefore, the additional diversity gains on the link layer can be exploited which compensate the unavoidable spectrum efficiency loss. Two transmit diversity techniques are applied to the cellular setup: cyclic delay diversity and Alamouti coding. The investigations show the beneficial transformation of the transmit diversity to macro diversity, namely cellular diversity. The applied cellular cyclic delay diversity and cellular Alamouti technique are capable to improve significantly the performance at the severe cell borders. The techniques reduce the overall inter-cellular interference. C-CDD offers no changes at the receiver side, no rate loss for higher number of transmit antennas, and no requirements regarding constant channel properties over several sub-carriers or symbols and transmit antenna numbers. At the adjacent base stations there has to be an inter BS-to-BS communication for the simultaneous time synchronized transmission of the signals. In contrast to C-CDD, the introduced CAT offers diversity gains over the whole cell border area. On the other side, the underlying Alamouti code requires an additional signal processing and channel estimation at the mobile station. A more sophisticated approach for C-CDD and CAT includes a power adaptation of the signal transmit powers which requires a feedback of the received signal power at the mobile station. The use of C-CDD and CAT is desirable in the outer part of the cells, depending on available resources in adjacent cells. For example, these cellular diversity techniques can be utilized for more reliable soft and softer handover concepts or broadcasting services for single-frequency network.

Finally, all main concepts within this thesis are based on no feedback links or *a priori* channel knowledge at the transmitter. The potential of the introduced techniques would further increase by including

Table 7.1: Impact on cellular communications system

Principle	Processing Location	Complexity			System Impact
		MT	BS	network	
Coordination	Network / BS-to-BS	none	low	high	network communication
Cancellation	MT	high	none	none	none
Use	BS-to-BS (/ MT)	low	medium	high	BS-to-BS communication
		(/ none)	(/ low?)	(/ medium?)	

this additional information. An example is given by power adaptive C-CDD or CAT which provides more reliable performances over larger areas.

The basic impact on the overall cellular communications system applying the different concepts is summarized in Table 7.1.

Appendix A

Cellular MMSE Equalizer

The MMSE criterion for a cellular environment is derived for two cases: first, the inter-cell interference is assumed to be Gaussian; secondly, the Gaussian assumption does not hold. In general, the channel state information at the receiver is assumed to be estimated, and therefore, it is no random variable anymore. For brevity, but without loss of generality, the OFDM symbol and sub-carrier indices l and i are omitted. Furthermore, the Gaussian processes are assumed to be white and they have a zero mean, i.e., $E\{N\} = 0$.

Gaussian Inter-Cell Interference

The inter-cell interference is supposed to be Gaussian like. Therefore, $E\{N_{\mathrm{GA}}\} = E\{N\} = 0$, $E\{|N_{\mathrm{GA}}|^2\} = \sigma^2_{\mathrm{GA}}$, and $E\{|N|^2\} = \sigma^2$.

$$
\begin{aligned}
E\{\varepsilon Y^*\} &\stackrel{!}{=} 0 \\
&= E\{(X^{(0)} - G \cdot Y) \cdot (H^{(0)*}X^{(0)*} + (N^* + N^*_{\mathrm{GA}}))\} \\
&= E\{H^{(0)*}|X^{(0)}|^2\} - E\{G(H^{(0)}X^{(0)} + (N + N_{\mathrm{GA}}))H^{(0)*}X^{(0)*}\} \\
&\quad + \underbrace{E\{X^{(0)}(N^* + N^*_{\mathrm{GA}})\}}_{=0} - E\{G(H^{(0)}X^{(0)} + N + N_{\mathrm{GA}})(N^* + N^*_{\mathrm{GA}})\} \\
&= H^{(0)*} \cdot E\{|X^{(0)}|^2\} - G|H^{(0)}|^2 E\{|X^{(0)}|^2\} + GH^{(0)*} \cdot \underbrace{E\{(N + N_{\mathrm{GA}})X^{(0)*}\}}_{=0} \\
&\quad - GH^{(0)} \cdot \underbrace{E\{X^{(0)}(N + N_{\mathrm{GA}})\}}_{=0} - G\sigma^2 - G\sigma^2_{\mathrm{GA}} - G \cdot \underbrace{E\{NN^*_{\mathrm{GA}} + N^*N_{\mathrm{GA}}\}}_{=0} \\
&= H^{(0)*} \cdot E\{|X^{(0)}|^2\} - G|H^{(0)}|^2 E\{|X^{(0)}|^2\} - G\sigma^2 - G\sigma^2_{\mathrm{GA}} \qquad \text{(A.1)}
\end{aligned}
$$

The resulting MMSE coefficient is

$$
G = \frac{H^{(0)*}}{|H^{(0)}|^2 + \frac{\sigma^2 + \sigma^2_{\mathrm{GA}}}{E\{|X^{(0)}|^2\}}} \,. \qquad \text{(A.2)}
$$

Non-Gaussian Inter-Cell Interference

For scenarios in which the inter-cell interference cannot be assumed to Gaussian like, e.g., large line-of-sight components, the resulting properties have to be taken into account for the MMSE coefficient. Therefore, $E\{N_{\text{int}}\} \neq E\{N\} = 0$, $E\{|N_{\text{int}}|^2\} = \sigma_{\text{int}}^2$, and $E\{|N|^2\} = \sigma^2$.

$$\begin{aligned}
E\{\varepsilon Y^*\} &\stackrel{!}{=} 0 \\
&= H^{(0)*} \cdot E\{|X^{(0)}|^2\} - G \cdot E\{|H^{(0)}|^2|X^{(0)}|^2\} + GH^{(0)*} \cdot \underbrace{E\{NX^{(0)*}\}}_{=0} \\
&\quad + GH^{(0)*} \cdot E\{N_{\text{int}}X^{(0)*}\} + \underbrace{E\{X^{(0)}N^*\}}_{=0} + E\{N_{\text{int}}^*\} - GH^{(0)} \cdot \underbrace{E\{X^{(0)}N^*\}}_{=0} \\
&\quad - GH^{(0)} \cdot E\{X^{(0)}N_{\text{int}}^*\} - GE\{|N|^2\} - GE\{|N_{\text{int}}|^2\} - G \cdot \underbrace{E\{NN_{\text{int}}^* + N^*N_{\text{int}}\}}_{=0} \\
&= H^{(0)*} \cdot E\{|X^{(0)}|^2\} - G|H^{(0)}|^2E\{|X^{(0)}|^2\} + GH^{(0)*}E\{N_{\text{int}}X^{(0)*}\} + E\{N_{\text{int}}^*\} \\
&\quad - GH^{(0)}E\{X^{(0)}N_{\text{int}}^*\} - G\sigma^2 - G\sigma_{\text{int}}^2
\end{aligned} \tag{A.3}$$

The resulting MMSE coefficient is

$$\begin{aligned}
G &= \frac{H^{(0)*}E\{|X^{(0)}|^2\} + E\{N_{\text{int}}^*\}}{|H^{(0)}|^2E\{|X^{(0)}|^2\} - H^{(0)*}E\{N_{\text{int}}X^{(0)*}\} + H^{(0)}E\{X^{(0)}N_{\text{int}}^*\} + \sigma^2 + \sigma_{\text{int}}^2} \\
&= \frac{H^{(0)*} + \frac{E\{N_{\text{int}}^*\}}{E\{|X^{(0)}|^2\}}}{|H^{(0)}|^2 - \frac{H^{(0)*}E\{N_{\text{int}}X^{(0)*}\} + H^{(0)}E\{X^{(0)}N_{\text{int}}^*\} + \sigma^2 + \sigma_{\text{int}}^2}{E\{|X^{(0)}|^2\}}},
\end{aligned} \tag{A.4}$$

and finally

$$G = \frac{H^{(0)*} + \frac{E\{N_{\text{int}}^*\}}{E\{|X^{(0)}|^2\}}}{|H^{(0)}|^2 - \frac{2\text{Re}\{H^{(0)*}E\{N_{\text{int}}X^{(0)*}\}\} + \sigma^2 + \sigma_{\text{int}}^2}{E\{|X^{(0)}|^2\}}}. \tag{A.5}$$

Appendix B

SS-MC-MA for C-CDD

The described cellular cyclic delay diversity (C-CDD) technique in Chapter 6 can be also applied to another flavor of a multi-carrier spread spectrum, namely spread spectrum multi-carrier multiple access (SS-MC-MA) [FK03]. For SS-MC-MA, the sub-carrier allocation and re-allocation follows the block diagrams ins Figure B.1. The users are separated with a frequency division multiplexing component. L user data symbols are spread over the same L sub-carriers. Each user applies the whole set of orthogonal spreading codes by itself. Therefore, the L sub-carriers are exclusively used for one user. The benefits of SS-MC-MA are similar to MC-CDMA regarding, e.g., exploitation of frequency diversity, avoidance of ISI and ICI. MC-CDMA has to cope with multiple-access interference (MAI) [Kai95] which correspond to self-interference (SI) in SS-MC-MA. The variance of SI can be expressed by [6]

$$\sigma^2_{\mathrm{SI}} = \frac{L-1}{L}\left(\sum_{j=0}^{L}|G_jH_j|^2 - |\sum_{j=0}^{L}G_jH_j|^2\right) , \tag{B.1}$$

where G_j represents the equalizer coefficients. By applying SS-MC-MA in the context of C-CDD it is possible to use the scarce sub-carrier resources more efficiently. In a realistic scenario only individual users will cross the cell border or remain in the broadcast area. Therefore, these several single users can exclusively allocate a set of sub-carriers and allocate L-times more data symbols. It is also practicable to apply smaller spreading lengths for these users which results in less allocated sub-carriers in the total system. E.g., MC-CDMA uses $L = 8$, and therefore, each user transmits 1 data symbol on 8 sub-carriers. For SS-MC-MA, if only one user applies C-CDD, one can transmit

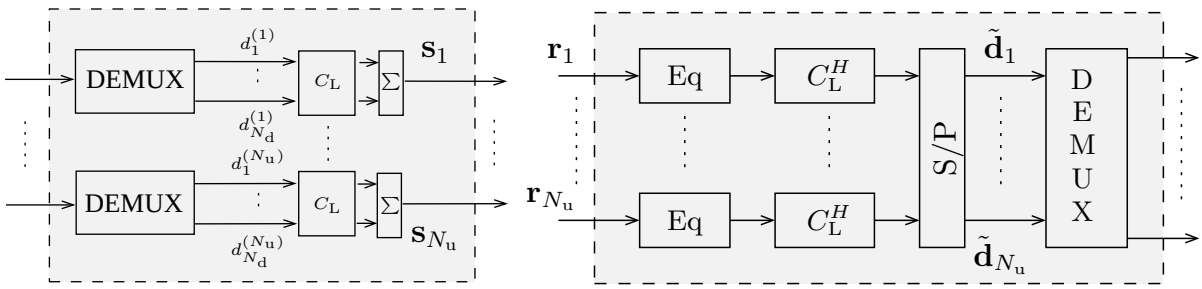

(a) allocation (b) re-allocation

Figure B.1: Principle of SS-MC-MA sub-carrier allocation and re-allocation

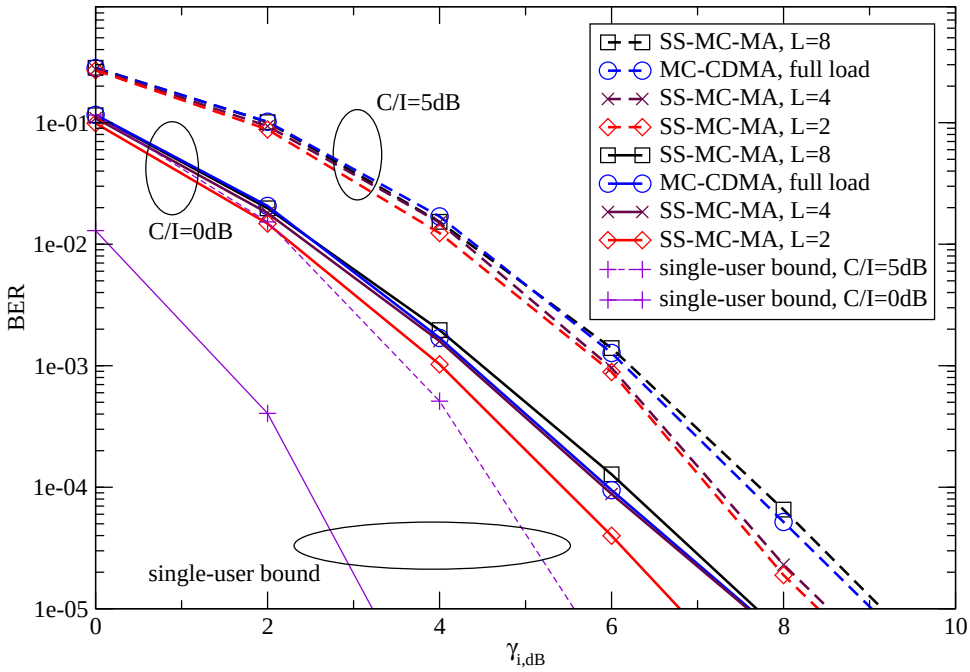

Figure B.2: BER versus SNR using MC-CDMA and SS-MC-MA for C-CDD

8 data symbols for $L = 8$. For $L = 4$ two users can transmit 4 data symbols each and for $L = 2$ four users have 2 data symbols by allocation the same sub-carrier resources. There also exists the contrariness of frequency diversity gain and self-interference loss for the choice of L.

Comparison of MC-CDMA and SS-MC-MA

The BER versus the SNR is shown in Figure B.2 where two C/I scenarios are chosen, $C/I = 0$ dB with solid lines and $C/I = 5$ dB with dashed lines. The simulation setup is based on *System B* as in Chapter 6. The single-user performances of MC-CDMA represent lower bounds for these scenarios. In the case of SS-MC-MA, the system is always fully loaded for the different spreading lengths. Due to the slightly higher frequency diversity, the fully loaded MC-CDMA system outperforms the SS-MC-MA performance with $L = 8$. For smaller spreading lengths ($L < 8$) the ratio of the first term in (B.1) becomes more influential and the SI distinctly reduces. This can be seen in a performance gain of 0.5 dB for $L \leq 4$ at $C/I = 0$ dB.

To conclude, the application of SS-MC-MA to C-CDD is favorable in terms of system resource exploitation and performance if less than L users are served in MC-CDMA.

Appendix C

System and Channel Parameters

Within this thesis two different system settings are used for the simulations, namely *System A* and *System B*. Tables and figures will give an overview of the system and channels parameters. Any variation of these parameters are explicitly mentioned in the simulation result. The interfering BSs have the identical parameters as the desired BS which also includes the number of active users. Perfect channel knowledge and signaling information of all cells is assumed. For each cellular link, the channels are independently simulated and are assumed to be constant over N_{s} OFDM symbols.

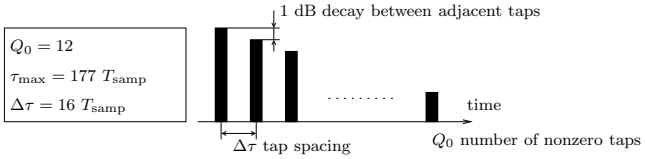

Figure C.1: Parameters of the used power delay profile of the channel model

C.1 System A

The basic parameters of *System A* are given in Table C.1. The channel model as shown in Figure C.1 is a tapped delay-line model with $\Delta\tau$ tap spacing, and an exponentially decaying power delay profile. The channel model has taps equidistant with a $1\ \mathrm{dB}$ decrease per tap and $\tau_{\max} = 1.31\ \mu s$.

Table C.1: Parameters of System A

Carrier Frequency	f_{c}	5 GHz	Spreading length	L	8
Signal Bandwidth	B	101.25 MHz	Channel coding		CC $(561, 753)_8$
Sub-carrier spacing	F_{s}	$131.85\ \mathrm{kHz}$	Channel coding rate	R	1/2
Number of sub-carriers	N_{c}	768	Modulation		QPSK?
FFT length	N_{FFT}	1024	inner interleaver	Π_{in}	2D
Guard interval length	N_{GI}	226	single-user equalizer		MMSE
Sampling time	T_{samp}	7.4 ns	normalized cell radius	r	1
OFDM symbol duration	T_{s}	$7.58\ \mu\mathrm{s}$	decay factor	ρ	3.5?
OFDM symbols per frame	N_{s}	16	MS velocity	v	$1.9\ \mathrm{mph}$

C.2 System B

For the *System B* environment the parameters are given in Table C.2. The used channel model is taken from the IEEE 802.11n standard [IEE04]. The chosen Model C represent a large open space (indoor and outdoor) with non-line-of-sight conditions of a short range scenario. Figure C.2 shows the power delay profile and the parameters of the the IEEE 802.11, Model C channel with $\tau_{\max} = 200$ ns.

Table C.2: Parameters of System B

Carrier Frequency	f_c	5 GHz	Spreading length	L	8
Signal bandwidth	B	81.25 MHz	Channel coding		CC $(561, 753)_8$
Sub-carrier spacing	F_s	48.828 kHz	Channel coding rate	R	1/2
Number of sub-carriers	N_c	1664	Modulation		4-QAM?
FFT length	N_{FFT}	2048	inner interleaver	Π_{in}	2D
Guard interval length	N_{GI}	128	single-user equalizer		MMSE
Sampling time	T_{samp}	10 ns	cell radius	r	300 m
OFDM symbol duration	T_s	20.48 μs	decay factor	ρ	3.5
OFDM symbols per frame	N_s	16	MS velocity	v	0 mph

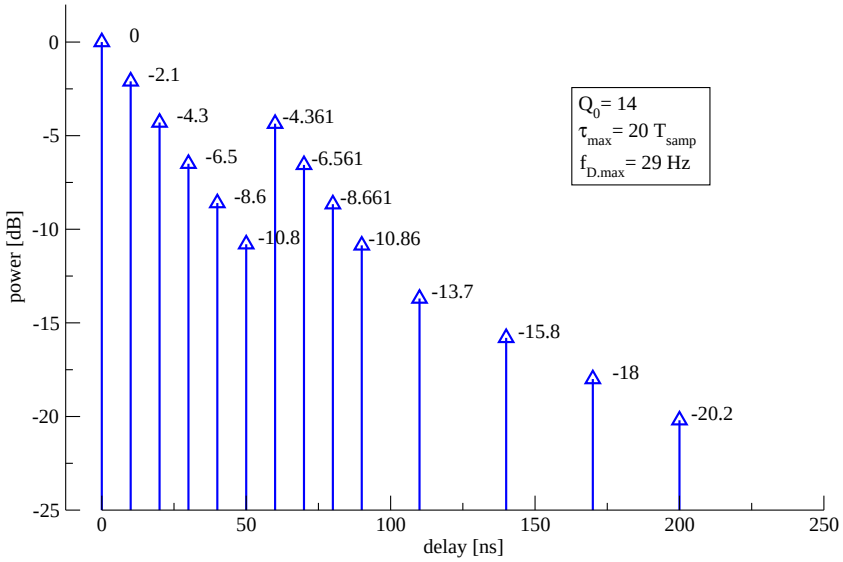

Figure C.2: Parameters of the power delay profile of the IEEE Channel 802.11n Model C

Appendix D

Abbreviations and Symbols

List of Abbreviations

1D	one-dimensional interleaving
2D	two-dimensional interleaving
AWGN	additive white Gaussian noise
ARQ	automatic-repeat-request
BER	bit error rate
BPSK	binary phase shift keying
BS	base station
BSC	binary symmetric channel
CAT	cellular Alamouti technique
CC	convolutional code
CDD	cyclic delay diversity
C-CDD	cellular CDD
CDMA	code division multiple access
C/I	carrier-to-interference ratio
CINR	carrier-to-interference-and-noise ratio
CIR	channel impulse response
CTF	channel transfer function
DAB	digital audio broadcasting
DD	delay diversity
DEMUX	demultiplexer
DFT	discrete Fourier transform
D-ICIC	direct ICIC
DVB-T	terrestrial digital video broadcasting
EXIT	extrinsic information transfer
FEC	forward error correction
FER	frame error rate
FFT	fast Fourier transform
GA	Gaussian approximation
GI	guard interval
GMC	generalized multi-carrier
GSM	global system for mobile communications
ICI	inter-carrier interference

ICIC	inter-cell interference cancellation
I-ICIC	indirect ICIC
IFFT	inverse FFT
ISI	inter-symbol interference
LLR	log-likelihood ratio
MAC	medium access control
MAI	multiple access interference
MAP	maximum *a posteriori* probability
M-ICIC	mean ICIC
MMSE	minimum mean square error
MUX	multiplexer
MC-CDMA	multi-carrier CDMA
MISO	multiple-input single-output
MS	mobile station
OFDM	orthogonal frequency division multiplex
OFDMA	orthogonal frequency division multiple access
PDF	probability density function
PIC	parallel interference cancellation
PSK	phase-shift keying
QAM	quadrature amplitude modulation
RL	resource load
SI	self-interference
SIC	successive interference cancellation
SISO	single-input single-output
SNR	signal-to-noise ratio
SS-MC-MA	spread spectrum multi-carrier multiple access
STBC	space-time block code
TX	transmit
UMTS	universal mobile telecommunications system
WLAN	wireless local area network

List of Symbols

α	angle between desired MS, $\mathrm{BS}^{(0)}$, and $\mathrm{BS}^{(I,1)}$
$\alpha_{\mathrm{att}}^{(m)}$	attenuation factor for BS m
α_i	fade amplitude variable on sub-carrier i
β	angle between direction of interest and boresight of antenna
$\beta_{3\mathrm{dB}}$	$3\ \mathrm{dB}$ beamwidth of antenna
δ_m	overall delay from BS m
δ_m^{cyc}	cyclic delay of BS m
$\delta_{\mathrm{max}}^{\mathrm{cyc}}$	maximum cyclic delay
$\delta(d_m)$	natural delay of the signal depending on distance d_m
δ_n	delay of antenna n
δ_n^{cyc}	cyclic delay of antenna n
$\Delta\delta^{\mathrm{cyc}}$	cyclic delay start for cyclic delay interval $\mathbb{S}$
$\Delta\delta_{\nu,\mu}$	delay difference between signals from BS ν and μ
ε	mean square value of error
$\varepsilon(n)$	error between real PDF and approximated PDF
$\varepsilon_{\mathrm{abs}}$	absolute error between real PDF and approximated PDF
$\varepsilon_{\mathrm{total}}$	total absolute error between real PDF and approximated PDF
η	throughput
η_m	shadowing factor for the mth BS
η_{max}	maximum throughput
γ_i	signal-to-noise ratio on sub-carrier i
$\gamma_{i,\mathrm{dB}}$	signal-to-noise ratio on sub-carrier i in decibel
γ_{CINR}	carrier-to-interference-and-noise ratio
$\gamma_{\mathrm{C/I}}$	carrier-to-interference ratio
$\gamma_{\mathrm{C/I,dB}}$	carrier-to-interference ratio in decibel
λ_j	reliability information of decoded signal of jth iteration
$\Delta\lambda_{j+1,j}$	reliability difference between iterations
$\lambda(c\|\mathbf{q})$	soft-bits of coded sequence $\mathbf{q}$
μ_{BPSK}	mean of p_{BPSK}
$\mu_{16-\mathrm{QAM}}$	mean of $p_{16-\mathrm{QAM}}$
ω	discrete values
ρ	path loss factor
ρ_{c}	overall correlation coefficient
ρ_{freq}	correlation factor in frequency direction
$\rho_{j,k}$	correlation coefficient between sub-carrier j and k
σ^2	variance of AWGN
σ_{A}^2	variance of I^{A}
σ_{BSPK}^2	variance of p_{BPSK}
$\sigma_{16-\mathrm{QAM}}^2$	variance of $p_{16-\mathrm{QAM}}$
σ_{GA}^2	variance of Gaussian approximation
$\sigma_{\mathrm{genie}}^2$	genie knowledge of total interfering signal variance or power
σ_{int}^2	variance or power of total interfering signal
σ_{opt}^2	optimistic total interfering signal variance or power
σ_{pess}^2	pessimistic total interfering signal variance or power
σ_{SI}^2	variance of SI
σ_η	standard deviation of η_m

$\Delta\tau$	tap spacing
$\tau_{\max}$	maximum delay spread
$\tau'_{\max}$	resulting maximum delay spread
$\tau_q^{(m)}$	delay of qth channel tap of BS m
ϑ_j	discrete uniform random variable
ζ	common near field component
ζ_m	BS m dependent near field component
Ω	random variable
Π_{in}	inner interleaver
Π_{out}	outer interleaver
$A(\beta)$	antenna gain
A_{m}	maximum antenna attenuation
B	signal bandwidth
$\mathbf{B}$	STBC matrix
$\mathbf{B}_{\text{CAT}}$	CAT mapping matrix
$\mathbf{B}_{\text{CAT},2}$	CAT mapping matrix serving 2 MSs
B_j	partial used signal bandwidth
$\text{BS}^{(0)}$	desired base station
$\text{BS}^{(\text{I},1)}$	interfering base station m
$\mathbf{C}_{\text{L}}$	spreading matrix
F_{s}	sub-carrier spacing
$\mathbf{G}$	diagonal equalization matrix
$G_{i,i}$	equalizer coefficient
H_{b}	entropy of received bit
$H_{l,i}^{(m)}$	channel transfer function
$H'_{l,i}$	resulting channel transfer function for C-CDD
I^{A}	*a priori* mutual information
I^{E}	extrinsic mutual information
J	mean square error
K	frequency reuse factor
L	spreading length
L_{free}	inter-cell interference free spreading factors
L^{A}	general *a priori* LLR value
L^{E}	general extrinsic LLR value
$L^{\text{A}}_{\text{Decod}}$	*a priori* decoding LLR values
$L^{\text{E}}_{\text{Decod}}$	decoded extrinsic LLR values
$L^{\text{A}}_{\text{Demod}}$	*a priori* demodulation LLR values
$L^{\text{E}}_{\text{Demod}}$	soft-demodulated extrinsic LLR values
$L(c)$	log-likelihood ratio of code bit c
$L(c\|\mathbf{q})$	LLR of coded sequence $\mathbf{q}$
M_{mod}	cardinality of modulation alphabet
$N_{l,i}$	noise term
N_{b}	number of desired bits
N_{BS}	number of base stations
N_{c}	number of sub-carriers
N_{d}	symbols per user

N_{DFT}	samples of DFT
N_{FFT}	samples of FFT
N_{GA}	Gaussian approximation noise term
N_{GI}	samples of guard interval
N_{int}	inter-cell interference noise term
$N_{L^{\mathrm{A}}(c)}$	noise of I^{A}
N_{s}	number of OFDM symbols
N_{samp}	number of samples
N_{T}	number of transmit antennas
N_{u}	number of active users
$N_{\mathrm{u,max}}$	number of maximum active users
$N_{\mathrm{u,M}}$	number of coordinated sub-carriers
$N_{\mathrm{u,R}}$	number of residual users in smart coordination scheme
ΔP	power distribution for soft C-CDD
P_{b}	target bit error rate
$P_{\mathrm{BSPK}}^{\mathrm{GA}}$	approximated PDF of BPSK modulation
$P_{16-\mathrm{QAM}}^{\mathrm{GA}}$	approximated PDF of 16-QAM modulation
P_m	received signal power from BS m
ΔP_m	interfering signal power weighting factor for BS m
$P_{\max}$	maximum transmit power
P_{s}	symbol power
$P_{\mathrm{t},m}$	transmitted signal power from BS m
Q_0	non-zero channel taps
R	code rate
$\mathbf{R}$	correlation function
$\mathbf{R}_{\mathrm{n}}$	normalized correlation function
RL	resource load
$\mathrm{RL}_{\mathrm{free}}$	inter-cell interference free RL factor
$\mathrm{RL}_{\mathrm{MC-CDMA}}$	resource load of MC-CDMA system
$\mathrm{RL}_{\mathrm{OFDMA}}$	resource load of OFDMA system
$\mathbb{S}$	set of cyclic delays
T_{GI}	guard interval duration
T_{s}	OFDM symbol duration
T_{s}'	overall OFDM symbol duration including the guard interval
T_{samp}	sampling time
$X_{l,i}^{(m)}$	frequency domain transmitted symbol
$Y_{l,i}$	frequency domain received signal
$\hat{Y}^{(m)}$	reconstructed signal of mth BS
$\hat{Y}^{(m)}_{\hat{Y}^{(0)}}$	estimated signal depending on the the first estimate
$\hat{Y}_{\mathrm{des}}$	reconstructed desired signal
$\hat{Y}_{\mathrm{int}}^{(m)}$	reconstructed interfering signal of mth BS
$\hat{Y}_{\mathrm{D}}$	output of direct ICIC
$\hat{Y}_{\mathrm{I}}$	output of indirect ICIC
$\hat{Y}_{\mathrm{M}}$	output of mean ICIC

a_m	adaptive power factor for BS m
$b_{l,n}$	entries of STBC matrix
c	speed of light $= 299792458\ \mathrm{m/s}$
$\mathbf{c}^{(n)}$	code bits of user n
d_m	distance of MS to mth BS
$\mathbf{d}_k$	modulated kth symbol of all users before spreading
$\tilde{\mathbf{d}}_k$	symbols for demodulator process
f_c	carrier frequency
$(\Delta f)_\mathrm{c}$	coherence frequency
$f_{\mathrm{D,max}}$	maximum Doppler frequency
f_i	center frequency of sub-carrier i
$h^{(m)}(\tau, t)$	channel impulse response
$h_q^{(m)}(t)$	amplitude of qth channel tap of BS m
i	sub-carrier index
i_m	sub-carrier index of BS m
$\mathbf{i}^{(n)}$	information bit stream of user n
k_cod	information length
l	time index
l_m	time index of BS m
l_c	STBC length
m	base station index
m_ccord	total number of coordinated base stations
m_int	number of coordinated interfering base stations
n_cod	code length
$p(Y_n\|X_n)$	conditional channel probability
p_e	transition probability
p_r	probability of randomized allocated sub-carrier in randomized coordination
p_rand	total probability of allocated sub-carrier for randomized coordination
p_s	probability of randomized allocated sub-carrier in smart coordination
p_smart	total probability of allocated sub-carrier for smart coordination
p_BPSK	PDF of BSPK modulation
$p_{16-\mathrm{QAM}}$	PDF of 16-QAM modulation
$p_{64-\mathrm{QAM}}$	PDF of 64-QAM modulation
q	soft-decision of demodulator
$\mathbf{q}$	coded sequence
r	cell radius
$\mathbf{r}_k$	block of symbols before equalization
$\mathbf{s}$	block of symbols
$(\Delta t)_\mathrm{c}$	coherence time
v	MS velocity
$x_{l,i}(t)$	time domain signal
$x^{(m)}(t)$	transmitted signal from BS m
$y(t)$	received signal

Bibliography

[3GP06] 3GPP TSG RAN WG4 document R4-060117. Analysis for simulation scenario definition to interference mitigation studies, February 2006.

[Ala98] Siavash M. Alamouti. A simple transmit diversity technique for wireless communications. *IEEE Journal on Selected Areas in Communications*, 16(8):1451–1458, October 1998.

[ASDK04] Gunther Auer, Stephan Sand, Armin Dammann, and Stefan Kaiser. Analysis of cellular interference for MC-CDMA and its impact on channel estimation. *European Transactions on Telecommunications*, 15(3):173–184, May–June 2004.

[Aue04] Gunther Auer. Channel estimation for OFDM with cyclic delay diversity. In *Proceedings IEEE International Symposium on Personal, Indoor and Mobile Radio Communications (PIMRC 2004), Barcelona, Spain*, volume 3, pages 1792–1796, September 2004.

[Bau05] Gerhard Bauch. Design of cyclic delay diversity with adaptive coding based on mutual information. In *Proceedings International OFDM Workshop (InOWo 2005), Hamburg, Germany*, September 2005.

[Bau06] Gerhard Bauch. Differential modulation and cyclic delay diversity in orthogonal frequency-division multiplex. *IEEE Transactions on Communications*, 54(5):798–801, May 2006.

[BHWD05] Franziskus Bauer, Erwin Hemming, Wolfgang Wilhelm, and Mohsen Darianian. Intercell interference investigation of MC-CDMA. In *Proceedings IEEE Vehicular Technology Conference (VTC 2005-Spring), Stockholm, Sweden*, volume 5, pages 3048–3052, June 2005.

[Bin90] John A. C. Bingham. Multicarrier modulation for data transmission: An idea whose time has come. *IEEE Communications Magazine*, 28:5–8, May 1990.

[BNG06] Faouzi Bader, Labed Nadjet, and Ismael Gutierrez. Intercell interference investigation in a MC-CDMA system with iterative demapping. In *Proceedings* 64^{th} *IEEE Vehicular Technology Conference (VTC 2006 - Fall), Montreal, Canada*, September 2006.

[Bos04] Martin Bossert. *Channel Coding for Telecommunications*. John Wiley and Sons, 2004.

[Bos05] Martin Bossert. On coding for OFDM and the broadcast channel. In *Proceedings* 5^{th} *International Workshop on Multi-Carrier Spread-Spectrum (MC-SS 2005), Oberpaffenhofen, Germany*, pages 29–44, September 2005.

[BSB04] Bernd Baumgartner, Vladimir Sidorenko, and Martin Bossert. Multicarrier spread spectrum: A coding perspective. In *Proceedings IEEE 8th International Symposium on Spread Spectrum Techniques and Applications (ISSSTA 2004), Sydney, Australia*, September 2004.

[CHL07] Mathieu Chacun, Maryline Helard, and Rodolphe Legouable. Iterative intercell interference cancellation for DL MC-CDMA systems. In *Proceedings* 6^{th} *International Workshop on Multi-Carrier Spread-Spectrum (MC-SS 2007), Herrsching, Germany*, pages 277–286, May 2007.

[Cov72] Thomas M. Cover. Broadcast channels. *IEEE Transactions on Information Theory*, IT-18:2–14, January 1972.

[DAB00] European Telecommunications Standard Institute (ETSI). *Radio Broadcasting Systems; Digital Audio Broadcasting (DAB) to mobile, portable and fixed receivers*, April 2000. EN 300 401 V1.3.1.

[Dam06] Armin Dammann. *On Antenna Diversity Techniques for OFDM Systems*. PhD thesis, Universität Ulm, Germany, June 2006. VDI Verlag Düsseldorf, Series 10, No. 766, ISBN 3-18-376610-8.

[DASR06] Armin Dammann, Serkan Ayaz, Stephan Sand, and Ronald Raulefs. On iterative detection, demodulation, and decoding for OFDM-CDM. In *Proceedings International Symposium on Turbo Codes & Related Topics, (ISTC 2006)*, Munich, Germany, April 2006.

[DK01a] Armin Dammann and Stefan Kaiser. Performance of low complex antenna diversity techniques for mobile OFDM systems. In *Proceedings* 3^{rd} *International Workshop on Multi-Carrier Spread Spectrum (MC-SS 2001), Oberpfaffenhofen, Germany*, pages 53–64, September 2001.

[DK01b] Armin Dammann and Stefan Kaiser. Standard conformable antenna diversity techniques for OFDM and its application to the DVB-T system. In *Proceedings IEEE Global Telecommunications Conference (GLOBECOM 2001), San Antonio, TX, USA*, pages 3100–3105, November 2001.

[DL05] Xenofon G. Doukopoulos and Rodolphe Legouable. Impact of the intercell interference in DL MC-CDMA systems. In *Proceedings* 5^{th} *International Workshop on Multi-Carrier Spread-Spectrum (MC-SS 2005), Oberpaffenhofen, Germany*, pages 101–109, September 2005.

[DL07] Xenofon G. Doukopoulos and Rodolphe Legouable. Intercell interference cancellation for MC-CDMA systems. In *Proceedings* 65^{th} *IEEE Vehicular Technology Conference (VTC 2007 - Spring), Dublin, Ireland*, April 2007.

[DSR98] Dariush Divsalar, Marvin K. Simon, and Dan Raphaeli. Improved parallel interference cancellation for CDMA. *IEEE Transactions on Communications*, 46(2):258–268, February 1998.

[DVB04] European Telecommunications Standard Institute (ETSI). *Digital Video Broadcasting (DVB); Framing structure, channel coding and modulation for digital terrestrial television*, July 2004. EN 300 744 V1.2.1.

[ETS] http://www.etsi.org.

[FG98] Gerard J. Foschini and Michael J. Gans. On limits of wireless communications in a fading environment when using multiple antennas. *Wireless Personal Communications*, 6(3):311–335, March 1998.

[FK03] Khaled Fazel and Stefan Kaiser. *Multi-Carrier and Spread Spectrum Systems*. John Wiley and Sons, 2003.

[FMM04] Nan Feng, Siun-Chuon Mau, and Narayan B. Mandayam. Pricing and power control for joint network-centric and user-centric radio resource management. *IEEE Transactions on Communications*, 52(9):1547–1557, 2004.

[FP93] Khaled Fazel and Lutz Papke. On the performance of concolutionally-coded CDMA/OFDM for mobile communications systems. In *Proceedings IEEE International Symposium on Personal, Indoor and Mobile Radio Communications (PIMRC 1993), Yokohama, Japan*, pages 468–472, September 1993.

[Hag04] Joachim Hagenauer. The EXIT chart — introduction to extrinsic information transfer. In *Proceedings European Signal Processing Conference (EUSIPCO 2004), Vienna, Austria*, September 2004.

[Hal83] Samuel W. Halpern. Reuse partitioning in cellular systems. In *Proceedings* 33^{rd} *IEEE Vehicular Technology Conference, Toronto, Canada*, pages 322–327, May 1983.

[Hay88] Simon Haykin. *Digital Communications*. John Wiley and Sons, 1988.

[Hoe92] Peter Hoeher. A statistical discrete-time model for the WSSUS multipath channel. *IEEE Transactions on Vehicular Technology*, 41:461–468, November 1992.

[HOP96b] Joachim Hagenauer, Elke Offer, and Lutz Papke. Iterative decoding of binary block and convolutional codes. *IEEE Transactions on Information Theory*, 42(2):429–445, March 1996.

[HT04] Harri Holma and Antti Toskala. *WCDMA for UMTS*. John Wiley and Sons, 2004.

[IEE03] ANSI/IEEE. *IEEE 802.11: Wireless LAN Medium Access Control (MAC) and Physical Layer (PHY) Specifications*, June 2003. 1999 Edition (R2003).

[IEE04] IEEE 802.11-03/940r2. IEEE P802.11 wireless LANs, TGn channel models, January 2004.

[IFN02] Manabu Inoue, Takeo Fujii, and Masao Nakagawa. Space time transmit site diversity for OFDM multi base station system. In *Proceedings IEEE Mobile and Wireless Communication Networks (MWCN 2002), Stockholm, Sweden*, pages 40–34, September 2002.

[ISTa] IST-2002-507039 4More Project. http://www.ist-4more.org.

[ISTb] IST-2004-507581 WINNER Project. http://www.ist-winner.org.

[ISTc] IST-4-027756 WINNER II Project. http://www.ist-winner.org.

[Kai95] Stefan Kaiser. Analytical performance evaluation of OFDM-CDMA mobile radio systems. In *Proceedings European Personal and Mobile Communications Conference (EPMCC'95), Bologna, Italy*, pages 215–220, November 1995.

[KFV06] M. Kemal Karakayali, Gerard J. Foschini, and Reinaldo A. Valenzuela. Network coordination for spectrally efficient communications in cellular systems. *IEEE Transactions on Wireless Communications*, 13:56–61, 2006.

[KH97] Stefan Kaiser and Joachim Hagenauer. Multi-carrier CDMA with iterative decoding and soft-interference cancellation. In *Proceedings IEEE Global Telecommunications Conference (GLOBECOM 97), Phoenix, USA*, pages 6–10, November 1997.

[KKH05] Jongnam Kim, Hoon Kim, and Youngnam Han. New preamble structures for synchronization and cell searching in OFDM systems. In *Proceedings IEEE Vehicular Technology Conference (VTC 2005 - Fall), Dallas, USA*, September 2005.

[KN96] Irene Katzela and Mahmoud Naghshineh. Channel assignment schemes for cellular mobile telecommunication systems: A comprehensive summary. *IEEE Personal Communications Magazine*, 3, 1996.

[LCM84] Shu Lin, Daniel J. Costello Jr., and Michael J. Miller. Automatic-repeat-request error-control schemes. *IEEE Communications Magazine*, 22(12):5–17, December 1984.

[Lee97] Robert A. Leese. A unified approach to the assignment of radio channels on a regular hexagonal grid. *IEEE Transactions on Vehicular Technology*, 46(4), November 1997.

[LG94] Alberto Leon-Garcia. *Probability and Random Processes for Electrical Engineering*. Addison Wesley, 2nd edition, 1994.

[NBZ97] Ramon Nogueroles, Martin Bossert, and Victor Zyablov. Capacity of MC-FDMA in mobile communications. In *Proceedings IEEE International Symposium on Personal, Indoor and Mobile Radio Communications (PIMRC 1997), Helsinki, Finland*, pages 110–114, September 1997.

[NSR+98] M. Nunes, J. Santos, A. Rodrigues, J. Punt, H. Nikokaar, and R. Prasad. Effects of downlink intercell interference on MC-CDMA system performance. In *Proceedings IEEE International Symposium on Personal, Indoor and Mobile Radio Communications (PIMRC 1998), Boston, USA*, volume 3, pages 1050–1054, September 1998.

[NTT07] NTT DoCoMo, Press Release, February 9, 2007. NTT DoCoMo achieves world's first 5Gbps packet transmission in 4G field experiment, 2007. http://www.nttdocomo.com/pr/2007/001319.html.

[Pap91] Athanasios Papoulis. *Probability, Random Variable and Stochastic Processes*. McGraw-Hill, 1991.

[Par92] J. David Parsons. *The Mobile Radio Propagation Channel*. John Wiley and Sons, 1992.

[Pro95] John G. Proakis. *Digital Communications*. McGraw-Hill, 3rd edition, 1995.

[RLJ00] Lars K. Rasmussen, Teng J. Lim, and Ann-Louise Johansson. A matrix-algebraic approach to successive interference cancellation in CDMA. *IEEE Transactions on Communications*, 48(1):145–151, January 2000.

[RVH95] Patrick Robertson, Emmanuelle Villebrun, and Peter Hoeher. A comparison of optimal and sub-optimal MAP decoding algorithms operating in the log domain. In *Proceedings IEEE International Conference on Communications (ICC 1995), Seattle, USA*, 1995.

[Sch06] Henrik Schulze. A comparison between Alamouti transmit diversity and (cyclic) delay diversity for a DRM+ system. In *Proceedings International OFDM Workshop (InOWo 2006), Hamburg, Germany*, August 2006.

[SK98] Hikemt Sari and Georges Karam. Orthogonal frequency-division multiple access and its application to CATV networks. *European Transactions on Telecommunications*, 9(6):507–516, November–December 1998.

[Stü02] Gordon L. Stüber. *Principles of Mobile Communication*. Kluwer Academic Publishers, 2nd edition, 2002.

[tB00] Stephan ten Brink. Designing iterative decoding schemes with the extrinsic information transfer chart. *AEÜ International Journal of Electronics Communications*, 54(6):389–398, 2000.

[TC03] Zhi Tian and Kuo-Chu Chang. Multistation data fusion for CDMA wireless communications. *Journal on Optical Engineering*, 42:1572–1582, June 2003.

[THS06] Hidekazu Taoka, Kenichi Higuchi, and Mamoru Sawahashi. Experiments on space diversity effect in MIMO channel transmission with maximum data rate of 1 Gbps in downlink OFDM radio access. *European Transactions on Telecommunications*, 17(6):611–622, December 2006.

[TJC99] Vahid Tarokh, Hamid Jafarkhani, and A. Robert Calderbank. Space-time block codes from orthogonal designs. *IEEE Transactions on Information Theory*, 45(5):1456–1467, July 1999.

[TSC98] Vahid Tarokh, Nambi Seshadri, and A. Robert Calderbank. Space-time codes for high data rate wireless communication: Performance criterion and code construction. *IEEE Transactions on Information Theory*, 44(2):744–764, March 1998.

[TV05] David Tse and Pramod Viswanath. *Fundamentals of Wireless Communication*. Cambridge University Press, 2005.

[UMT98] European Telecommunications Standard Institute ETSI. *Selection procedures for the choice of radio transmission technologies of the UMTS*, April 1998. TR 101 112 V3.2.0.

[Ver98] Sergio Verdu. *Multiuser Detection*. Cambridge University Press, 1998.

[vNP00] Richard van Nee and Ramjee Prasead. *OFDM for Wireless Multimedia Communications*. Artech House Publishers, 2000.

[VVZ94] Andrew J. Viterbi, Audrey M. Viterbi, and Ephraim Zehavi. Other-cell interference in cellular power-controlled CDMA. *IEEE Transactions on Communications*, 42(2/3/4):1501–1504, February/March/April 1994.

[WE71] Stephan B. Weinstein and Paul M. Ebert. Data transmission by frequency division multiplexing using the discrete fourier transform. *IEEE Transactions on Communications*, COM-19(15):628–634, October 1971.

[WG00] Zhendao Wang and Georgios B. Giannakis. Wireless multicarrier communications - where Fourier meets Shannon. *IEEE Signal Processing Magazine*, pages 29–48, May 2000.

[Wit93] Armin Wittneben. A new bandwidth efficient transmit antenna modulation diversity scheme for linear digital modulation. In *Proceedings IEEE International Conference on Communications (ICC 1993), Geneva, Switzerland*, pages 1630–1634, May 1993.

[YLF93] Nathan Yee, Jean-Paul Linnartz, and Gerhard Fettweis. Multi-carrier CDMA for indoor wireless radio networks. In *Proceedings IEEE International Symposium on Personal, Indoor and Mobile Radio Communications (PIMRC 1993), Yokohama, Japan*, pages 109–113, September 1993.

Publications of the Author

Publications Containing Parts of the Thesis

Journals

[1] Simon Plass. On intercell interference and its cancellation in cellular multicarrier CDMA systems. *EURASIP Journal on Wireless Communications and Networking - Special Issue on Multicarrier Systems*, 2008. 11 pages, Article ID 173645, doi:10.1155/2008/173645.

[2] Simon Plass, Ronald Raulefs, and Armin Dammann. Transmit diversity at the cell border by using smart base stations. *EURASIP Journal on Wireless Communications and Networking - Special Issue on Smart Antennas for Next-Generation Wireless Systems*, 2007. ?? pages, Article ID ??, doi:10.1155/2007/??

[3] Simon Plass, Stephan Sand, Mikael Sternad, and Arne Svensson. High spectral efficient and flexible next generation mobile communications. *Journal on Wireless Personal Communications*, 2007. 11 pages, doi:10.1007/s11277-007-9392-y.

[4] Simon Plass. Hybrid partitioned cellular downlink structure for MC-CDMA and OFDMA. *IEE Electronics Letters*, 42(4):226–228, February 2006.

Conferences

[5] Simon Plass and Armin Dammann. Analysis of iterative soft inter-cell interference cancellation in cellular MC-CDMA. In *Proceedings ITG Conference on Source and Channel Coding (SCC 2008), Ulm, Germany*, January 2008.

[6] Simon Plass and Armin Dammann. Adaptive cellular cyclic delay diversity for multi-carrier spread spectrum systems. In *Proceedings IEEE Consumer Communications & Networking Conference (CCNC 2008), Las Vegas, USA*, January 2008.

[7] Simon Plass and Stephan Sand. Extrinsic information transfer in cellular MC-CDMA for inter-cell interference cancellation. In *Proceedings Asilomar Conference on Signals, Systems and Computers (Asilomar 2007), Pacific Grove, CA, USA*, November 2007.

[8] Stephan Sand, Simon Plass, and Armin Dammann. EXIT chart analysis of iterative receivers for space-time coded OFDM systems. In *Proceedings* 66^{th} *IEEE Vehicular Technology Conference (VTC 2007 - Fall), Baltimore, USA*, October 2007.

[9] Simon Plass. Investigations on soft inter-cell interference cancellation in OFDM-CDM systems. In *Proceedings International OFDM Workshop (InOWo 2007), Hamburg, Germany*, August 2007.

[10] Simon Plass and Ronald Raulefs. The cellular Alamouti technique - Increasing transmit diversity at the cell border. In *Proceedings IEEE AP-S International Symposium 2007, Honolulu, USA*, June 2007.

[11] Simon Plass and Ronald Raulefs. The cellular Alamouti technique. In *Proceedings* 6^{th} *International Workshop on Multi-Carrier Spread-Spectrum (MC-SS 2007), Herrsching, Germany*, pages 267–275, May 2007.

[12] Simon Plass, Xenofon G. Doukopoulos, and Rodolphe Legouable. On MC-CDMA link-level inter-cell interference. In *Proceedings* 65^{th} *IEEE Vehicular Technology Conference (VTC 2007 - Spring), Dublin, Ireland*, April 2007.

[13] Simon Plass and Armin Dammann. Cellular cyclic delay diversity for next generation mobile systems. In *Proceedings* 64^{th} *IEEE Vehicular Technology Conference (VTC 2006 - Fall), Montreal, Canada*, September 2006.

[14] Simon Plass and Armin Dammann. Smart base stations using cyclic delay diversity in a cellular OFDMA environment. In *Proceedings International OFDM Workshop (InOWo 2006), Hamburg, Germany*, pages 165–169, August 2006.

[15] Simon Plass and Armin Dammann. A partitioned cellular environment for MC-CDMA and OFDMA. In *Proceedings* 15^{th} *Wireless World Research Forum (WWRF), Paris, France*, December 2005.

[16] Simon Plass and Stefan Kaiser. MC-CMDA versus OFDMA in cellular environments. In *Proceedings European Signal Processing Conference (EUSIPCO 2005), Antalya, Turkey*, September 2005. invited paper.

[17] Simon Plass and Armin Dammann. On the error performance of sectorized cellular systems for MC-CDMA and OFDMA. In *Proceedings IEEE International Symposium on Personal, Indoor and Mobile Radio Communications (PIMRC 2005), Berlin, Germany*, September 2005.

[18] Simon Plass and Armin Dammann. Radio resource management for MC-CDMA over correlated Rayleigh fading channels. In *Proceedings* 5^{th} *International Workshop on Multi-Carrier Spread-Spectrum (MC-SS 2005), Oberpaffenhofen, Germany*, pages 119–126, September 2005.

[19] Simon Plass, Armin Dammann, and Stefan Kaiser. Error performance for MC-CDMA and OFDMA in a downlink multi-cell scenario. In *Proceedings IST Mobile & Wireless Communications Summit (IST Summit 2005), Dresden, Germany*, June 2005.

[20] Simon Plass, Armin Dammann, and Stefan Kaiser. Analysis of coded OFDMA in a downlink multi-cell scenario. In *Proceedings International OFDM Workshop (InOWo 2004), Dresden, Germany*, pages 22–26, September 2004.

[21] Simon Plass, Stephan Sand, and Gunther Auer. Modeling and analysis of a cellular MC-CDMA downlink system. In *Proceedings IEEE International Symposium on Personal, Indoor and Mobile Radio Communications (PIMRC 2004), Barcelona, Spain*, volume 1, pages 160–164, September 2004.

Other Publications

Books

[22] Simon Plass, Armin Dammann, Stefan Kaiser, and Khaled Fazel. *Multi-Carrier and Spread Spectrum 2007*. Springer, 2007. ISBN 978-1-4020-6128-8.

Journals

[23] Simon Plass, Gerd Richter, and A. J. Han Vinck. Coding schemes for crisscross error patterns. *Journal on Wireless Personal Communications*, 2007. 11 pages, doi:10.1007/s11277-007-9389-6.

[24] Christian Mensing and Simon Plass. Positioning based on factor graphs. *EURASIP Journal on Advances in Signal Processing*, 2007. 11 pages, Article ID 41348, doi:10.1155/2007/41348.

Conferences

[25] Armin Dammann, Ronald Raulefs, and Simon Plass. Soft cyclic delay diversity and its performance for DVB-T in Ricean channels. In *Proceedings IEEE Global Telecommunications Conference (GLOBECOM 2007), Washington, DC, USA*, November 2007.

[26] Simon Plass and Armin Dammann. Cyclic delay diversity - A simple transmit diversity technique for broadcast systems. In *Proceedings IEEE Broadcast Symposium 2007, Washington, D.C., USA*, November 2007.

[27] Simon Plass, Armin Dammann, Gerd Richter, and Martin Bossert. Resulting channel characteristics from time-varying cyclic delay diversity in OFDM. In *Proceedings* 66^{th} *IEEE Vehicular Technology Conference (VTC 2007 - Fall), Baltimore, USA*, October 2007.

[28] Simon Plass, Armin Dammann, and Tommy Svensson. Block-Equidistant resource mapping in OFDMA, MC-CDMA, and SS-MC-MA. In *Proceedings International OFDM Workshop (InOWo 2007), Hamburg, Germany*, August 2007.

[29] Armin Dammann, Ronald Raulefs, and Simon Plass. Performance of cyclic delay diversity in Ricean channels. In *Proceedings* 6^{th} *International Workshop on Multi-Carrier Spread-Spectrum (MC-SS 2007), Herrsching, Germany*, pages 217–226, May 2007.

[30] Christian Mensing, Simon Plass, and Armin Dammann. Positioning with generalized multi-carrier communications signals. In *Proceedings* 6^{th} *International Workshop on Multi-Carrier Spread-Spectrum (MC-SS 2007), Herrsching, Germany*, pages 287–296, May 2007.

[31] Simon Plass, Stephan Sand, Mikael Sternad, and Arne Svensson. High spectral efficient and flexible next generation mobile communications. In *Proceedings of the* 4^{th} *and Final COST 289 Workshop - Spectrum and Power Efficient Broadband Communications, Gothenburg, Sweden*, April 2007.

[32] Simon Plass, Gerd Richter, and A. J. Han Vinck. Coding schemes for crisscross error patterns. In *Proceedings of the* 4^{th} *and Final COST 289 Workshop - Spectrum and Power Efficient Broadband Communications, Gothenburg, Sweden*, April 2007.

[33] Christian Mensing, Simon Plass, and Armin Dammann. Synchronization algorithms for positioning with OFDM communications signals. In *Proceedings of the Workshop on Positioning, Navigation, and Communication (WPNC 2007), Hannover, Germany*, March 2007.

[34] Armin Dammann and Simon Plass. Cyclic delay diversity: Effective channel properties and applications. In *Proceedings* 17^{th} *WWRF Meeting, Heidelberg, Germany*, November 2006.

[35] Simon Plass, Xenofon G. Doukopoulos, and Rodolphe Legouable. Investigations on link-level inter-cell interference in OFDMA systems. In *Proceedings* 13^{th} *Annual Symposium on Communications and Vehicular Technology in the Benelux (SCVT 2006), Liege, Belgium*, pages 49–52, November 2006.

[36] Christian Mensing and Simon Plass. TDoA positioning based on factor graphs. In *Proceedings of the IEEE International Symposium on Personal, Indoor and Mobile Radio Communications (PIMRC 2006), Helsinki, Finland*, September 2006.

[37] Christian Mensing and Simon Plass. Location determination with factor graphs for TDoA. In *Proceedings of the NEWCOM-ACoRN Joint Workshop (NAW 2006), Vienna, Austria*, September 2006.

[38] Christian Mensing and Simon Plass. Positioning algorithms for cellular networks using TDOA. In *Proceedings of the IEEE International Conference on Acoustics, Speech, and Signal Processing (ICASSP 2006), Toulouse, France*, volume 4, pages 513–516, May 2006.

[39] Ingmar Groh, Simon Plass, and Stephan Sand. Capacity approximation for uncorrelated MIMO channels using random matrix methods. In *Proceedings Second International Symposium on Communications, Control and Signal Processing, (ISCCSP 2006), Marrakech, Morocco*, March 2006.

[40] Simon Plass, Armin Dammann, and Stefan Kaiser. On modeling and analysis of a coded OFDMA downlink in a multi-cell environment. In *Proceedings International Seminar on Spectrum and Power Efficient Broadband Communications (COST 289), Budapest, Hungary*, July 2004.

[41] Gerd Richter and Simon Plass. Fast decoding of rank-codes with rank errors and column erasures. In *Proceedings IEEE International Symposium on Information Theory (ISIT 2004), Chicago, USA*, pages 398–398, June 2004.

[42] Gerd Richter and Simon Plass. Error and erasure of rank-codes with a modified Berlekamp-Massey algorithm. In *Proceedings ITG Conference on Source and Channel Coding (SCC 2004), Erlangen, Germany*, pages 203–211, January 2004.